REPORT NUMBER
SAI02379-713LJ
LAPS-51
May 1979

LABORATORY FOR APPLIED PLASMA STUDIES

GAS RELEASE AND CONDUCTIVITY MODIFICATION STUDIES

By

Lewis M. Linson and David C. Baxter

FINAL REPORT
CONTRACT NO. NAS5-24121

SCIENCE APPLICATIONS INCORPORATED

TABLE OF CONTENTS

GAS RELEASE AND CONDUCTIVITY MODIFICATION STUDIES

Lewis M. Linson and David C. Baxter

Science Applications, Inc.
La Jolla, California 92038

ABSTRACT

The behavior of gas clouds produced by releases from orbital velocity in either a point release or venting mode is described by the modification of snowplow equations valid in an intermediate altitude regime. Quantitative estimates are produced for the time dependence of the radius of the cloud, the average internal energy, the translational velocity, and the distance traveled. The dependence of these quantities on the assumed density profile, the internal energy of the gas, and the ratio of specific heats is examined. The new feature is the inclusion of the effect of the large orbital velocity. The resulting gas cloud models are used to calculate the characteristics of the field-line-integrated Pedersen conductivity enhancements that would be produced by the release of barium thermite at orbital velocity in either the point release or venting modes as a function of release altitude and chemical payload weight.

I. INTRODUCTION

A number of experiments[1,2] have been suggested for the Spacelab that require the release of large amounts of gas into the ionosphere. Examples of such experiments are the:

- Generation of acoustic gravity waves from a known source of momentum and energy;
- Enhancement of the ionospheric electron concentration and modification of the ionospheric conductivity by the deployment of easily ionizable vapors such as barium or cesium;
- Dispersement of chemically reactive gases, such as H_2 or H_2O, in order to affect the neutral and ionization chemistry and create holes in the F-region of the ionosphere;
- Creation of large-scale neutral winds by transferring momentum to the ambient atmosphere;
- Testing of Alfvén's critical velocity hypothesis regarding the anomalous ionization of neutrals moving at high velocity across a magnetized plasma.

These experiments and others like them require the release of large amounts of gas in order to either disperse material, transfer momentum, or input energy. The experiments can be divided into two classes depending on the suggested method of deployment--either as a point release or in a venting mode. We define a point release as a rapid or explosive release of gas or material that takes place in a time less than a second. In this case, the region of space into which the material is dumped is confined and the expansion of the gas can be treated as being spherical. Other experiments require the deployment of gas in a venting mode lasting from five to ten or more seconds. The released gas is then spread out in a trail and it expands cylindrically.

If conducted from Spacelab the released gas initially will have a large translational velocity equivalent to a hypersonic Mach 10 flow. The large kinetic energy associated with the initial translational velocity is a new feature that has not been treated previously. This feature dominates the interaction with the ambient atmosphere leading to rather striking results that affect the properties of the release. In order to carry out the objectives of the experiments, one needs to be able to describe various aspects of the released gas such as what happens to the momentum and energy, how fast the cloud expands, how hot the expanding cloud becomes, and how far it travels.

This report considers three aspects of these experiments in detail. First, we review the properties of the gas cloud expansion that results from a point release that was obtained from a previous study.[3,4] Second, we develop a model that describes the expansion of gas released in the venting mode. Third, we apply the results of the above two studies in order to calculate the enhancement in conductivity that can be produced by the release of barium vapor in sunlight as a function of altitude and the amount of release vapor. The major part of this report is concerned with the technical details of these calculations.

We have developed models of the dynamic response of gas clouds, released in both the point release and venting modes, when they interact with the ambient rarefied atmosphere at the hypersonic orbital velocity. These models are based on a number of simplifying assumptions first introduced by Stuart[5] in order to describe the evolution of a stationary point explosion in the upper atmosphere. The principal assumptions relate to the form of the velocity distribution within the cloud and involve a self-similar density distribution during the cloud expansion. We have added the effect of

the translational velocity at release to Stuart's model and have treated the different geometries and time-dependencies of the released gas for the two release modes.

The models apply to an intermediate altitude regime. This regime is identified by comparing an important characteristic cloud size with the molecular mean-free-path, λ. For a spherical point release, this size is called the equal-mass-radius, a_o, and is defined as the radius of a spherical volume of ambient atmosphere containing a mass equal to the mass of released gas, M_o. When a_o is comparable to λ, neither continuum dynamics nor kinetic theory is appropriate for describing the interaction of the gas cloud. At lower altitudes, where λ is much smaller than a_o, continuum dynamics or fluid mechanics might be applicable. Flow of the ambient atmosphere around the gas cloud and the effects of shocks and waves created in the ambient atmosphere by the gas cloud would be important. On the other hand, at higher altitudes where the mean-free path is much larger than a_o, a kinetic theory approach is required. In this case the majority of the ambient molecules would pass right through the roughly spherical

gas cloud which is initially traveling at the orbital velocity while only a fraction of them would strike one of the gas cloud molecules, scattering it out of the cloud, thus producing a broad diffuse wake. The distinguishing feature of our model is the assumption that in the intermediate altitude regime the ambient atmosphere interacts strongly with the gas cloud and is carried with it, becoming a part of the cloud itself.

Bernhardt[6] recently completed a similar study using a kinetic approach appropriate to the high-altitude regime. He used the same criteria for defining the high-altitude regime, $a_o < 3\lambda$, as we adopt in this report. Because the physical assumptions appropriate to the two regimes are different, the model calculations produce qualitatively different results. As one example of this difference, the distance that the bulk of an initially spherically gas cloud travels is independent of the amount of gas released in the high-altitude regime (it scales only with λ) but in the intermediate-altitude regime this distance scales with a_o and thus depends on the mass of released gas.

The parameters that characterize the properties of the gas cloud in which we are interested are: the

scale size, R, of the cloud; the expansion velocity, $\dot{R}$, of the outer edge of the cloud; the translational velocity, V, of the released gas; an equivalent "temperature," T, determined by the average internal energy per particle, and the distance, L, that the released gas has traveled with respect to the ambient atmosphere. In the point release case, these parameters are given as functions of time since release. The principal difference between the point-release case and the venting-mode case is that in the frame of the venting canister there is a steady-state cylindrically-symmetric distribution of gas downstream of the canister.

In Sec. II we discuss several topics related to the snowplow model as applied to point releases. In Sec. II-A we describe the basic assumptions and equations of the snowplow model. In Sec. II-B we briefly review and summarize the results for the point release of a spherical gas cloud at orbital velocity which is treated comprehensively in Ref. 3. We shall make use of the cloud size as a function of time, R(t), in other sections of this report and we shall compare the qualitative behavior of the gas cloud for this case with similar behavior for the venting-mode case to be developed in more detail in later sections.

The neutral gas cloud and wake expansion models are based on an assumption that the density distribution remains self-similar, i.e., that the cloud maintains its density distribution during the expansion. One result of our models is that different density distributions do not result in qualitative changes in the nature of the solutions. In Sec. II-C we modify the Stuart[5] model to include the fact that at late times the gas cloud which initially follows a Stuart snowplow expansion eventually evolves into a Gaussian shape expanding by diffusion. We treat the effect of diffusion as if it were superimposed on the expansion process modeled by the self-similar snowplow expansion. The result of this analysis is that a cloud with an initial constant density profile rapidly evolves into a Gaussian-like shape and that the Gaussian scale length of the Gaussian distribution has a time dependence almost identical to the cloud radius described from the snowplow model.

In Sec. III we describe the venting-mode model and the equations that determine the cloud parameters. This quantitative model conserves the mass, momentum, and energy of the expanding and moving gas cloud wake consisting

of the released gas and swept-up ambient atmosphere. The assumptions on which the model is based and the limitations of the model are discussed. Our model applies only to the downstream portion of the wake and does not provide a description valid in the transition zone between the spherical distribution near the venting canister and the cylindrical distribution farther downstream. The appropirate conservation equations are derived. The characteristics of the vented gas cloud are determined by the model and a specification of the parameters associated with the released gas; $\dot{M}_o$, the rate at which mass exits the canister in kg/s; $\dot{E}_o$, the rate at which energy exits the canister in J/s; and γ, the ratio of specific heats.

In Sec. IV the results of the venting model are described. The wake-model equations are integrated numerically and an accurate analytic approximation is derived. In particular, the radius of the wake, the radial expansion velocity, the axial velocity of the gas in the wake, the temperature, and the distance that the gas has traveled with respect to the atmosphere are obtained. The dependence of the solutions on the various input parameters is illustrated in a series of

figures. It is found that the analytic expression provides a good description of the scaling of these solutions with the input parameters. The wake-model, and thus the solutions, becomes more valid far downstream at large radius in the wake; the model is less valid at small R. For any particular set of the input parameters, the wake-model allows a family of solutions corresponding to different assumed initial values of the radial expansion velocity, $\dot{R}_o$, specified at a small value of radius, R_o. The approach of the various numerical solutions to the analytic curve at large R is also illustrated by appropriate sets of figures. As an example of a quantitative result, it is found that far downstream all solutions have the behavior $R(x) \sim Kx^{\frac{1}{2}}$, where the constant K depends on the values of the input parameters.

In Sec. V we apply the results of our theoretical modeling of the expansion of the neutral gas clouds to the calculation of the change in Pedersen conductivity that results when the neutral gas being released is neutral barium atom vapor. Much of the motivation for the calculations reported here is based on previous modeling of large barium ion clouds released in the ionosphere from rockets. In particular, the approach

used here relies heavily on detailed data analyses[7] of the Spruce ion cloud, a barium release experiment conducted on 1 February 1971 at 2352 UT at an altitude of about 190 km from Eglin AFB in Florida. The data consist of both optical and radar data obtained with an incoherent scatter radar, an HF long-pulse radar, and by radio-wave propagation through the ion clouds. These data provide information on the electron concentration and distribution and scale size of the ion cloud. We combine our recent work on the expansion of neutral clouds released from orbital velocity in both the point release and venting modes with detailed ion cloud modeling performed on the Spruce ion cloud in order to calculate the height-integrated Pedersen conductivity that can be produced by the release of various amounts of vapor at a range of altitudes.

In Sec. V-A we consider the deposition of barium ions from the neutral barium atom vapor. Based on the results of Sec. III-C, we assume that the density distribution in the barium cloud during the time of ion deposition is essentially a Gaussian distribution. We make extensive use of earlier work on the deposition of ionization from barium releases conducted from rockets

in order to determine parameters of the barium ion cloud in terms of parameters associated with the neutral cloud. The procedure that we apply takes into account the competing processes of barium oxidation by ambient molecular oxygen and photoionization by sunlight. These effects result in an altitude-dependent inventory of available barium ions from a given amount of barium vapor and in an effective ionization time constant associated with the loss of neutral barium atoms. The model described here also includes the effect of the time delay before photoionization begins when the initial density is high and impedes the transport of the metastable-exciting radiation to the center of the cloud. The choice of parameterizations is based on the detailed analysis of the Spruce ion cloud.

The important parameters for carrying out conductivity modification experiments are the field-line-integrated Pedersen conductivity and the transverse scale size of the ion cloud perpendicular to the magnetic field. The scaling of these two parameters with altitude and amount of gas released is assumed to vary as the radius of the neutral cloud at an appropriate time. The results of the analysis are shown in

Sec. V-B in three pairs of figures, each pair corresponding to one of the following three cases: a point release from a rocket, from Spacelab, and a vented release from Spacelab. The figures show contours of constant perpendicular scale size of the ion cloud and constant Pedersen conductivity in the altitude versus chemical-payload-weight plane. As a typical example, a 48-kg barium release from a rocket at 190 km altitude will produce a field-line-integrated Pedersen conductivity of approximately 30 mho, several times the ambient ionospheric conductivity, and will have a transverse scale size just less than 3 km. If the same chemical payload is released at orbital velocity, the resulting conductivity is lower by a factor of 5 from that produced by a release from a rocket and the transverse size of the ion cloud is increased by a factor of approximately 2.3.

II. REVIEW OF SNOWPLOW MODELS

The expansion of neutral gas clouds from point releases in the intermediate altitude regime can be described by snowplow equations. Point releases at orbital velocity are described by a model that represents an extension of Stuart's[5] original model. The venting model described in detail in Sec. III is based on a modification of Stuart's model that takes into consideration both the orbital velocity and the steady-state cylindrical geometry. We briefly review the snowplow model and summarize the results for point releases. These results will be useful for comparing with the results of the venting model and will be used in Sec. V where we calculate the deposition of ionization from a knowledge of the time variation of the cloud size, R(t).

A. Basic assumptions and equations

The central assumptions of Stuart's model are that a spherical cloud of gas, consisting of released gas plus swept-up ambient atmosphere, retains a self-similar or shape-preserving density profile, that the velocity of the gas is radial, and that the velocity increases linearly with radius from the center of the cloud. In the case of release at orbital velocity, the

above assumptions are modified. We assume that the expanding gas cloud remains spherical in shape and that its center moves with a velocity $\vec{u}(t)$. We also assume that the gas cloud completely picks up the ambient air by incorporating all of the atmosphere that crosses its boundary into the cloud. The cloud does not disturb the ambient atmosphere exterior to the cloud and no ambient molecules can pass through the cloud unaffected. The appropriate equations conserve the mass, momentum and energy of the expanding and moving gas cloud consisting of the released gas and swept-up ambient air. The qualitative results of the model are believed to be reliable during the early phase of the cloud's dynamics prior to times when diffusion is the dominant process. A detailed analysis resulting from these assumptions is described in Ref. 3.

In the Stuart snowplow model and its extension described above, all lengths are found to scale with a characteristic length called the equal-mass-radius, a_o. This length is the radius of a spherical volume of ambient atmosphere with mass equal to the mass of the released gas, M_o. In terms of the ambient atmospheric density, ρ_a, the equal-mass-radius is defined by $a_o = (3M_o/4\pi\rho_a)^{1/3}$.

This model appears to be appropriate when $3 < a_o/\lambda < 30$ where λ is the ambient mean-free-path between collisions. At higher altitudes where $a_o < 3\lambda$ a kinetic treatment would be necessary. At lower altitudes where $a_o > 30\lambda$, it is difficult to consider the released and ambient species as being well-mixed, and other gasdynamic phenomena neglected in the snowplow treatment, such as shock formation and wave generation, would be important.

We summarize the equations that lead to a specification of the snowplow model. The similarity condition for the mass density, $\rho(\vec{r}, t)$, becomes

$$\rho(\vec{r}, t) = [M(t)/R^3(t)]\ f(\vec{\xi}) \qquad (1)$$

where M(t) is the total mass of the cloud including swept-up ambient atmosphere and R(t) is the radius of the cloud. The dimensionless space variable $\vec{\xi}$ is given by

$$\vec{\xi} = [\vec{r} - \vec{x}(t)]/R(t) \qquad (2)$$

where $\vec{x}(t)$ is the three-dimensional position of the center-of-mass of the cloud and $\vec{r}$ is any point in three-dimensional space. Equation (1) describes a gas cloud that retains its density profile while

expanding and translating. The shape function $f(\vec{\xi})$ has the properties

$$\int f(\vec{\xi}) d^3\vec{\xi} = 1 \quad ; \tag{3}$$

$$\int \vec{\xi} f(\vec{\xi}) d^3\vec{\xi} = 0 \quad . \tag{4}$$

The second moment is a time-independent (but shape-dependent) constant α;

$$\alpha = \int \xi^2 f(\vec{\xi}) d^3\vec{\xi} \quad . \tag{5}$$

For a constant density profile, $f(\vec{\xi}) = 3/4\pi$ and $\alpha = 0.6$. For a spherical shell with all of the mass concentrated at the radius R(t), $f(\vec{\xi}) = \delta(|\vec{\xi}| - 1)/4\pi$ and $\alpha = 1.0$.

The gas velocity at any point is assumed to be given by

$$\vec{v}(\vec{r}, t) = \vec{u}(t) + \dot{R}(t)\vec{\xi}(\vec{r}, t) \tag{6}$$

where

$$\vec{u}(t) = \frac{d\vec{x}}{dt} = \dot{\vec{x}} \tag{7}$$

and the dot represents differentiation with respect to time. Thus the hydrodynamic derivative is given by

$$\frac{D}{Dt} = \left(\frac{\partial}{\partial t}\right)_{\vec{r}} + \vec{v} \cdot \nabla = \left(\frac{\partial}{\partial t}\right)_{\vec{\xi}} \tag{8}$$

because a point moving such that $\vec{\xi}$ is constant moves with the local "fluid" velocity.

The conservation equation for mass is written

$$\frac{D\rho}{Dt} + \rho\nabla \cdot \vec{v} = D_n\nabla^2\rho + S(\vec{r}, t) \qquad (9)$$

where S is a mass source function due to sweeping up of the ambient atmospheric mass and D_n is a diffusion coefficient. Snowplow models set $D_n = 0$ in order not to violate the density similarity assumption. We will discuss the effect of diffusion on changing density profiles in Sec. II-C below. Due to the density similarity assumption, the mass source term must be given by

$$S(\vec{r}, t) = (\dot{M}/M)\rho(\vec{r}, t) \qquad (10)$$

where $\dot{M}$ is the rate at which ambient atmospheric mass is swept up as the cl ud expands and translates. For spherical clouds wit.. ut translation

$$\dot{M} = 4\pi R^2 \rho_a \dot{R} \quad . \qquad (11)$$

With translation, a more complicated expression, dependent upon model assumptions, is necessary. In general, with translation, the volume of swept-up atmosphere, $V' = (M - M_o)/\rho_a$, is greater than the

volume of the gas cloud, $V = 4\pi R^3/3$.

The momentum equation is written

$$\rho(\vec{r}, t) \frac{D\vec{v}}{Dt} + S(\vec{r}, t) \vec{v}(\vec{r}, t) = -\nabla p(\vec{r}, t) \qquad (12)$$

where p is the pressure in the cloud and the mass source term accounts for the momentum of the picked-up atmosphere. The internal energy density of the gas is given by $p/(\gamma - 1)$ where γ is the ratio of specific heats. The total internal energy of the cloud is

$$U = \int_V \frac{p(\vec{r}, t)}{\gamma - 1} d^3\vec{r} \qquad (13)$$

where the integral is taken over the volume of the cloud. Following procedures similar to those applied by Stuart as discussed in Ref. 3, the equations governing the translation and radial expansion in the cloud can be brought to the forms

$$\frac{d}{dt}(M\vec{u}) = 0 \quad , \qquad (14)$$

$$\alpha R \frac{d}{dt}(M\dot{R}) = 3(\gamma - 1)U - 3p_s V \qquad (15)$$

where α is the second moment of f and p_s is the limit of the cloud pressure approaching the surface from within and has been assumed to be spherically symmetric. Note that $M\vec{u}$ is the total momentum of the cloud and that both M and $\vec{u}$ are functions of time.

Equation (15) shows that the expansion of the cloud is driven by $(\gamma - 1)$ times its internal energy, proportional to the cloud pressure, and is retarded by the pressure at the surface of the cloud. In our model, we take p_s to be the atmospheric pressure p_a. These equations represent a quantitative description of the basic snowplow model. Reference 3 contains discussions of the treatment of these equations, their relationship to other author's work, the effects of various treatments of the pressure at the surface of the cloud, extensions of the derivations outlined here to incorporate different values of the molecular mass and γ for the released gas and atmospheric gas.

We can replace the internal energy U, defined by Eq. (13), in Eq. (15) by using conservation of total energy,

$$E = U + K = E_o + \frac{M - M_o}{\rho_a} \frac{p_a}{\gamma - 1} \quad , \qquad (16)$$

where K is the kinetic energy given by

$$K = \frac{1}{2}\int_V \rho \vec{v}^2 d^3r = \frac{M}{2}\left(u^2 + \alpha \dot{R}^2\right) \quad , \tag{17}$$

E_o is the total initial energy of the cloud, $(M - M_o)/\rho_a = V'$ is the volume of the swept-up atmospheric gas, and $p_a/(\gamma - 1)$ is the internal energy density of the ambient atmosphere. Because we are including the possibility of a nonzero translational velocity for the cloud, the volume, V', of swept-up atmosphere may be greater than the volume, V, of the cloud itself.

The initial energy of the cloud, E_o, derives from the translational velocity of the release vehicle and from the chemical and/or thermal energy of the exploding gas. The chemical energy, initially released as heat, is transformed into kinetic energy of expansion in a time scale which is short compared to that of the other processes in this model. Thus

$$E_o = \frac{M_o}{2}\left(u_o^2 + \alpha \dot{R}_o^2\right) \tag{18}$$

where M_o is the initial released mass, u_o is the initial translational velocity, and $\dot{R}_o$ is the initial expansion velocity.

Equation (15) becomes:

$$\alpha R \frac{d}{dt}(MR) = 3(\gamma - 1)\left[E_o - K + (V' - V)\frac{p_a}{\gamma - 1}\right]. \quad (19)$$

Ambient atmosphere has been swept up and compressed by the cloud and the term $(V' - V)p_a/(\gamma - 1)$ is the portion of the swept-up atmospheric thermal energy that is available to drive the expansion of the cloud. If there is no translation, then $V' \equiv (M - M_o)/\rho_a = V$, the ambient atmosphere is not compressed and its internal energy does not contribute to the expansion of the cloud. At late times $(V' - V)p_a/(\gamma - 1)$ approaches a constant, thus contributing to Eq. (19) in the same manner as E_o.

B. Results for point releases from rockets and Spacelab

Equations (19) and (14) together with an equation for dM/dt, such as Eq. (11), can be integrated numerically to produce the translational motion, expansion, and mass accretion of the gas cloud. Reference 3 contains the results of such integrations for various values of the input quantities E_o, γ, α, and $\dot{R}_o$. Here we show only typical results in order to illustrate the nature of the solutions and present analytic expressions that approximate the behavior of R(t) for $R \gg a_o$ and have the correct asymptotic behavior as $t \to \infty$.

Figure 1 shows several examples of R(t) obtained by numerically integrating the equations. Both the radius and the time are scaled by the equal-mass-radius. The time scale has been drawn under the assumption that $\dot{R}_o$ = 1 km/s for all cases. The heavy solid curve is the nominal case with $\gamma = 1.4$ and $\alpha = 0.6$ corresponding to a uniform density profile. The dashed curve shows the influence of the assumption of an extreme density profile, that of a spherical shell with all the mass concentrated at the outer edge characterized by $\alpha = 1$. It does not expand as fast as the constant density profile because the available energy drives all particles at the same velocity. Likewise, the outer edge of a gas cloud with a density profile more peaked at the center with $\alpha < 0.6$ would expand more rapidly than shown by the solid curve.

The four thin solid curves show the effect of various values of γ. As γ decreases, the number of degrees of freedom increases and a larger fraction of the energy is stored as internal energy per particle and less is available for kinetic energy of expansion. The curve labeled $\gamma = \infty$ corresponds to the assumption that none of the available energy is stored as internal energy. Regardless of the

value of γ associated with the released gas, as $R >> 1$ the cloud radius approaches a curve corresponding to the value of γ of the ambient atmosphere (as shown in Ref. 3) because the majority of the gas clouds' particles are atmospheric particles.

The dotted curve represents the original Stuart snowplow without the effect of translational velocity. This curve corresponds to a release from a rocket in which the translational velocity is small compared to the initial expansion velocity $\dot{R}_o$. All of the curves initially have the behavior $R = \dot{R}_o t$. The snowplow without translation begins to decrease its rate of expansion as $R \rightarrow a_o$ and the cloud has picked up an atmospheric mass comparable to the mass of released gas.

The case of release at orbital velocity is qualitatively different. Figure 1 shows that $\dot{R}$ increases from its initial value before $R = a_o$ and reaches a maximum at around $R = a_o$ before decreasing. The explanation for this behavior depends upon the fact that the velocity of the atmosphere relative to the shuttle corresponds to a large kinetic energy per particle amounting to 5.1 eV for oxygen atoms. This energy input rapidly exceeds the original chemical energy, $\alpha M_o \dot{R}_o^2/2$, before the swept-up

mass approaches M_o or $R \sim a_o$. The result is an increase in the internal energy of the cloud leading to its rapid expansion. This rapid expansion leads to a rapid rate of sweeping up of atmospheric mass. The translational velocity of the gas cloud drops rapidly with a resultant significant reduction in the rate of energy input to the cloud.

Figure 2 shows the typical behavior of a 100 kg gas release at orbital velocity at 200 km altitude. The time and length scales are given in seconds and kilometers, respectively, based on the derived value of 3.65 km for the equal-mass-radius. The dashed curve for the cloud radius is the same as the heavy solid curve in Fig. 1. The solid curve labeled temperature corresponds to the average internal energy per particle with an assumed mass of 20 atomic masses. The curve shows the initially cold expanding gas rapidly heating due to the atmospheric energy input reaching a maximum of 5600°C by 2 s after release. This rapid heating leads to the rapid expansion and subsequent cooling of the gas cloud. The temperature asymptotically approaches the ambient atmospheric temperature. The distance traveled is $L = \int_0^t u(t')dt'$ and is shown by the

broken curve. The cloud at first coasts at orbital velocity but rapidly decelerates when $R \sim a_o$ reaching 2/3 of its asymptotic travel distance within 3 s. Note that by 4.5 s after release the cloud diameter exceeds the distance traveled while the cloud is still expanding rapidly and its forward motion has nearly stopped. The fact that the cloud size rapidly exceeds the distance traveled suggests that the model assumption of a spherical cloud shape is justified because any asymmetry that may be introduced by the translational velocity rapidly becomes less important.

Indeed, the fact that after a few seconds the gas release at orbital velocity appears to behave as a stationary point release of greater initial energy can be used to obtain an accurate approximation to R(t). In our model, when $u(t) < \dot{R}(t)$ or $M\dot{R} > M_o u_o$, we take $\dot{M} = 4\pi R^2 \rho_a \dot{R}$ and then $V' - V = \Delta V$ ceases to grow and M(t) may be written

$$M(t) = M_o + \frac{4}{3}\pi \rho_a R^3 + \Delta V \rho_a \qquad (20)$$

where the last term is a constant generally smaller than the first and much smaller than the second. The total energy available for driving the late-time

expansion may be written

$$E_T = E_o + \Delta V \frac{\rho_a}{\gamma - 1} \tag{21}$$

where E_o is given by Eq. (18). The last term can be shown to be smaller than the first by writing it as $(3\Delta V/4\pi a_o^3)\left[M_o C_a^2/\gamma(\gamma - 1)\right]$ where C_a is the atmospheric sound speed.

Thus, for $M\dot{R}$ greater than $M_o u_o$, Eq. (19) can be written

$$\alpha R \frac{d}{dt}(M\dot{R}) = 3(\gamma - 1)(E_T - K) \tag{22}$$

where E_T is a constant given by Eq. (21) and K is the kinetic energy given by Eq. (17). As $t \to \infty$, $u(t) \to 0$, $M(t) \to M_o R^3/a_o^3$, and $K \to \frac{1}{2}\alpha M\dot{R}^2$. If we define a non-dimensional time by

$$s = \dot{R}_o t/a_o \tag{23}$$

where $\dot{R}_o$ is the initial expansion velocity, we find that for large s, the solution of Eq. (22) has the asymptotic form

$$R \to a_o C s^{0.4} \quad \text{as} \quad s \to \infty \tag{24}$$

where

$$C = \left[\frac{25(\gamma - 1)}{4\gamma}\right]^{1/5} \left(\frac{2E_T}{\alpha M_o \dot{R}_o^2}\right)^{1/5} . \qquad (25)$$

The first term has the numerical values 1.123 and 1.201 for $\gamma = 1.4$ and 5/3, respectively. If we neglect the small term proportional to ΔV in Eq. (21), then the coefficient C can be written

$$C = \left[\frac{25(\gamma - 1)}{4\gamma}\right]^{1/5} \left(1 + \frac{u_o^2}{\alpha \dot{R}_o^2}\right)^{1/5} . \qquad (26)$$

By direct comparison with the numerical integration of Eq. (19) from $s = 0$, we have found that an analytic expression of the form

$$R(t) = a_o C\left[\left(\frac{\dot{R}_o t}{a_o}\right)^{0.8} - 0.44\right]^{1/2} \qquad (27)$$

provides an excellent approximation to R(t) for $R \geq a_o$ with C defined by Eq. (26) for both the stationary and orbital release cases with $u_o = 0$ and 7.8 km/s, respectively. We shall make use of the expression in Eq. (27) for R(t) later in this report.

C. Snowplow model with diffusion

At late-time, gas clouds released in the atmosphere have a Gaussian density profile and expand by diffusion. In this section we explore how rapidly the density profile of a spherical point release can change in profile from the self-similar profile assumed in the snowplow model to the Gaussian profile at late time. We find that this change can take place surprisingly rapidly.

In this work we modify the snowplow model to include the fact that at late time the gas cloud can be modeled by a Gaussian density profile diffusing into the ambient atmosphere. The r' .lt is a model which initially follows a snowplow expansion and evolves into a Gaussian diffusing cloud. Obviously, we must relax one of the central assumptions of the snowplow model, specifically that the cloud retains a shape-preserving density profile. We will treat the effect of diffusion as if it were superimposed on the expansion process modeled by the self-similar snowplow expansion. In a self-similar expansion the size of the cloud is given by R(t), a time-dependent scale length of the cloud. If the self-similar shape were a spherical constant-density profile, for example, we would take R(t) to be equal to the radius of the sphere.

We use this same R(t) to scale the continuity equation for mass, Eq. (9), but now we retain the diffusion term. We restrict this discussion to the stationary point release case for which $\vec{\xi}(\vec{r}, t) = \vec{r}/R(t)$, the fluid velocity of the gas is $\vec{v} = \vec{r}\dot{R}/R$, and R(t) is the characteristic scale length of the expanding cloud if there were no diffusion. The last term on the right-hand side of Eq. (9) includes the effect of sweeping up ambient mass according to Stuart's original model and is given by Eq. (10).

By making a suitable change of space and time variables we can define a function $f[\vec{\xi}(r, t), \tau_D(t)]$ which is analogous to the shape function of the self-similar model. If we define τ_D by

$$\tau_D = \int_{t_D}^{t} \frac{4D_n dt'}{R^2(t')} \quad ; \tag{28}$$

implying that diffusion begins at $t = t_D$, then the density can be written

$$\rho(\vec{r}, t) = \left[M(t)/R^3(t)\right] \; f\left[\vec{\xi}(\vec{r}, t), \tau_D(t)\right] \quad . \tag{29}$$

With these substitutions Eq. (9) can be simply written

$$\frac{\partial f}{\partial \tau_D} = \frac{1}{4} \nabla_\xi^2 f \qquad (29)$$

where we have used the following:

$$\vec{\nabla} \cdot \vec{v} = 3\dot{R}/R \quad ;$$

$$\frac{\partial \rho}{\partial t} = \frac{\dot{M}}{R^3} f - 3 \frac{\dot{M}P}{R^4} f + \frac{M}{R^3} \frac{\partial \vec{\xi}}{\partial t} \cdot \nabla_\xi f + \frac{M}{R^3} \frac{\partial \tau_D}{\partial t} \frac{\partial f}{\partial \tau_D} \quad ;$$

$$\nabla \rho = \frac{M}{R^4} \nabla_\xi f \quad ;$$

$$\nabla^2 \rho = \frac{M}{R^5} \nabla_\xi^2 f \quad ;$$

$$\frac{\partial \vec{\xi}}{\partial t} = - \dot{R} \vec{r}/R^2 \quad ;$$

$$\frac{\partial \tau_D}{\partial t} = \frac{4D_n}{R^2(t)} \quad .$$

Equation (29) is the diffusion equation for $f(\vec{\xi}, \tau)$, which has the solution

$$f(\vec{\xi}, \tau_D) = \int d^3\vec{\xi}' f(\vec{\xi}', 0) \frac{\exp\left[- (\vec{\xi} - \vec{\xi}')^2/\tau_D\right]}{(\pi \tau_D)^{3/2}} \qquad (30)$$

In terms of this function we may write the density at any time $t > t_D$ as

$$\rho(\vec{r},\ t) = \frac{M(t)}{R^3(t)}\ \frac{1}{M_D} \int d^3\vec{r}'\rho(\vec{r}',t_D)\ \frac{\exp\left[-\left(\frac{\vec{r}}{R} - \frac{\vec{r}'}{R_D}\right)^2/\tau_D(t)\right]}{\left[\pi\tau_D(t)\right]^{3/2}}$$

where $R_D = R(t_D)$ and $M_D = M(t_D)$. For $\tau_D << 1$ we have the limit of little diffusion and the density reduces to that given by the self-similar model,

$$\rho(r,\ t) = \frac{M}{M_D}\ \frac{R_D^3}{R^3}\ \rho\left(r\ \frac{R_D}{R}\ ,\ t_D\right)$$

or

$$\rho(r,\ t) = \frac{M}{R^3}\ f(r/R,\ 0) \quad .$$

At long times after diffusion has been turned on, the similarity function f approaches a Gaussian distribution with an expanding radius and constant volume:

$$f(\xi,\ \tau_D) \rightarrow (\pi\tau_D)^{-3/2}\exp(-\xi^2/\tau_D) \qquad (31)$$

as $\tau_D \rightarrow \infty$.

In order to illustrate the effect that diffusion in ξ has on an assumed density distribution, we have applied Eq. (30) to two specific examples. The first is a uniform density out to a finite expanding radius; we refer to this profile as a flat-top distribution. The second is

an expanding spherical shell with all the mass concentrated at the surface of the shell. For the flat-top distribution

$$f(\xi, 0) = 3/4\pi \quad ; \quad \xi < 1$$

$$f(\xi, 0) = 0 \quad ; \quad \xi > 1 \ ;$$

and for the spherical shell

$$f(\xi, 0) = \delta(\xi - 1)/4\pi \ .$$

The normalization has been chosen so that each contains a unit volume.

We have found that the profile approaches a Gaussian profile more rapidly if the Gaussian with which it is compared has a Gaussian radius of the form $(\beta + \tau_D)^{1/2}$, i.e.,

$$f(\xi, \tau_D) \rightarrow \left[\pi(\beta + \tau_D)\right]^{-3/2} \exp\left[-\xi^2/(\beta + \tau_D)\right] \ . \quad (32)$$

In order to illustrate the change of the flat-top and spherical-shell distributions toward the Gaussian form given in Eq. (32) at various values of τ_D, we have renormalized both the radius and density by defining

$$z = \xi/[0.693\ (\beta + \tau_D)]^{\frac{1}{2}} \ ,$$

$$g(z, \tau_D) = \left[\pi(\beta + \tau_D)\right]^{3/2} f(\xi, \tau_D) \ . \quad (33)$$

The limiting value of $g(z, \tau_D)$ for large τ_D is $\exp(- 0.693\ z^2)$. The scale factor 0.693 is chosen so that $g(1, \infty)$ is 0.5

Figures 3 and 4 show $g(z, \tau_D)$ for various values of τ_D for the flat-top and spherical shell initial distributions respectively. The value of β in the scalings given by Eq. (33) are different for the two cases. It is appropriate that β be unequal to zero because in both cases the initial shapes have finite spatial extent. We have chosen β so that $g(1, 1)$ is approximately equal to one half; for the flat-top $\beta = 0.5$ and for the spherical shell $\beta = 0.75$. The larger value of β for the spherical shell results from the fact that all of the mass is initially at $\xi = 1$ for the shell while the mass is distributed over $\xi \leq 1$ for the flat-top.

The vertical dashed lines in Figures 3 and 4 indicate the position of the initial radius in the newly-scaled radial coordinate z. For τ_D greater than one, the scaled position of the initial radius continues to move to the left and approaches $z = 1.2\ \tau_D^{-\frac{1}{2}}$ as $\tau_D \to \infty$ indicating the increase in size of the cloud due to diffusion as shown by the $\tau_D = \infty$ curve. For the flat-top in Figure 3, the horizontal dashed lines indicate the height of the original flat-top in the newly-scaled density with amplitude $[\pi(\beta + \tau_D)]^{3/2} f(\xi, 0)$.

Examination of Figures 3 and 4 indicates that the density distributions are approaching Gaussian-like shapes for $\tau_D > 0.2$ and 0.75 for the two cases, respectively, and have essentially the asymptotic shape given in Eq. (33) for $\tau_D > 0.4$ and 1.0 respectively. We will discuss specific evaluations of τ_D below.

The approximation of $f(\xi, \tau_D)$ by its limiting form $\left[\pi(\beta + \tau_D)\right]^{-\frac{1}{2}} \times \exp\left[-\xi^2/(\beta + \tau_D)\right]$ is equivalent to approximating the density distribution of the cloud by a Gaussian density profile

$$\rho(r, t) \simeq M(t) \left[\pi a^2(t)\right]^{-3/2} \exp\left[-r^2/a^2(t)\right] \qquad (34)$$

with a time-dependent Gaussian radius, a(t), given by

$$a^2(t) = R^2(t) \left[\beta + \tau_D(t)\right] \qquad (35)$$

where τ_D is given by Eq. (28). Although the actual shape at early time is not Gaussian, in the case of the flat-top distribution we find that the distance at which the density is 1/e of its value at r = 0 is within a few percent of R(t) for $\tau_D(t) < 0.5$ and of course is indistinguishable from a(t) given by Eq. (35) for $\tau_D > 0.5$.

In the preceding, we have discussed a procedure for introducing diffusion within the framework of a snowplow model. The effect of diffusion is to transform an initial self-similar profile for the density into a Gaussian profile. The treatment so far does not depend on the the time-dependence of R(t) which we take to be determined by the snowplow model without diffusion.

With a normalized time defined by Eq. (23), we define a function $\phi(s)$ such that

$$R(t) = a_o \phi(s) \ . \qquad (36)$$

With u = 0 we have $\Delta V = V' - V = 0$ and the original Stuart snowplow equation has the form of Eq. (22) with $E_T = \alpha M_o \dot{R}_o^2/2$ and $K = \alpha M \dot{R}^2/2$. Our normalizations for ϕ and s are different from those of Stuart; with our normalizations ϕ satisfies the differential equation

$$\phi \frac{d}{ds}\left[(1 + \phi^3) \frac{d\phi}{ds}\right] = \frac{3(\gamma - 1)}{2}\left[1 - (1 + \phi^3)\,(d\phi/ds)^2\right].$$

The solution of this equation has the following properties for large and small s:

$$\phi(s) \to s \qquad \text{for } s \ll 1$$

$$\phi(s) \to \left(6.25\,\frac{\gamma - 1}{\gamma}\right)^{0.2} s^{0.4} \qquad \text{for } s \gg 1 \quad .$$

At early time the cloud expands with the initial expansion velocity $\dot{R}_o$ while at later time the cloud radius is predicted to expand as $t^{0.4}$. At very late time when the snowplow description is no longer appropriate, the cloud expands as $t^{0.5}$ due to diffusion. It is apparent that once the appropriate value of γ of the released gas is specified, the snowplow model for the expansion of a gas cloud determines the time-dependence of the radius R(t) of the cloud in terms of the two key parameters a_o and $\dot{R}_o$.

Once the functional dependence of $\phi(s)$ is known, then we may define a normalized diffusion function $\bar{\tau}(s)$ by

$$\bar{\tau}(s) = \int_1^s \frac{ds'}{\phi^2(s')} \quad . \tag{37}$$

The diffusion parameter τ_D defined in Eq. (28) can be expressed in terms of $\bar{\tau}(s)$ as

$$\tau_D(t) = \frac{4D_n}{a_o \dot{R}_o} \left[\bar{\tau}(s) - \bar{\tau}(s_D)\right] \qquad (38)$$

where $s = \dot{R}_o\, t/a_o$ and the diffusion is assumed to commence at $t = t_D$. For a gas with $\gamma = 5/3$ which is appropriate for barium atom vapor, we show the resulting normalized diffusion function $\bar{\tau}(s)$ in Fig. 5. The solid curve is the correct value of $\bar{\tau}(s)$ only as long as $\phi(s)$ is given by the snowplow model. If the snowplow model were to be turned off at a specific value of s, then ϕ^2 in the denominator would be a constant and ϕ would increase linearly with s. Examples are shown by the dashed curves in Fig. 5 if the snowplow were stopped at s = 18 and 46.

As an example of the time scale in which the profile can change from a flat-top distribution to a substantially Gaussian shape when $\tau_D = 0.2$, we use parameters associated with a 48 kg barium release (called Spruce) at 190 km altitude. For this cloud, detailed modeling[7] has shown that $D_n = 0.052$ km^2/s, $a_o = 1.26$ km, and $\dot{R}_o = 1.15$ km/s so that the numerical value of the coefficient of the brackets in Eq. (38) is 0.144. Thus τ_D has the value 0.2 when $\bar{\tau}(s) - \bar{\tau}(s_D) = 1.4$. Figure 5 shows that if we take s_D as small as 1, τ_D could reach 0.2 as rapidly as

$t = sa_o/\dot{R}_o = 4.4$ s with $s \sim 4$. Our detailed analysis[7] of the observed profile of the neutral cloud has indicated that it is in substantial agreement with the scale size and profile obtained by adding diffusion to a snowplow description of the expansion in radius of the neutral cloud.

III. VENTING MODEL AND EQUATIONS

In this section we describe a quantitative model that conserves the mass, momentum, and energy of the expanding and flowing gas in the wake downstream of a canister traveling at orbital velocity and venting gas. In the frame of reference moving with the canister, the flow is in steady-state. In accordance with snowplow models, we assume that all of the ambient air that encounters the wake and crosses its boundary becomes incorporated into it. The wake does not disturb the ambient atmosphere exterior to it. The quantitative results of this model are believed to be reliable beyond one wake radius downstream of the canister and prior to times when diffusion is the dominant process. The reasonableness and implications of these assumptions are discussed below.

In the point release problem treated previously we found that all lengths scale with a characteristic length, the equal-mass radius, a_o. Likewise, in the steady-state wake problem all lengths scale with a different characteristic length a.

This length is defined as the radius of a cylindrical volume of ambient atmosphere that contains a mass per unit axial length equal to $\dot{M}_o/V_a$, i.e.,

$$a = (\dot{M}_o/\pi V_a \rho_a)^{\frac{1}{2}} \quad . \tag{39}$$

where $\dot{M}_o$ is the rate at which mass is being released from the source. It is also the radius of a disk moving at the source (shuttle) velocity, V_a, in the ambient atmosphere through which the ambient mass flux is equal to $\dot{M}_o$.

As in the previous section, we take this venting model to be most appropriate in an intermediate altitude regime defined by $3 < a/\lambda < 30$ where λ is the ambient mean-free-path between collisions. At higher and lower altitudes the assumptions of the model are less justified and require different approaches.

Figure 6 shows the altitude variation of the number density, n, mass density, ρ_a, and mean free path, λ, of the ambient atmosphere based on the CIRA 1972 model atmosphere. The solid curves correspond to a moderate exospheric temperature $T_{ex} = 1200^{o}$. The mean-free-path $\lambda = (n\sigma)^{-1}$ is derived from an assumed typical collision cross section $\sigma = 5 \times 10^{-19}$ m^2 independent of species

or temperature. The variation of the atmospheric density for more extreme values of the exospheric temperature, 700° and 2000°, is shown by the dashed curves.

Figure 7 shows contours of constant characteristic length a in the altitude versus mass-venting-rate plane. Because the horizontal axis is logarithmic and $a \propto \dot{M}_o^{\frac{1}{2}}$, all of the solid curves for $T_{ex} = 1200^{\circ}$ have the same shape and are displaced horizontally from each other by an appropriate amount. The two dashed curves drawn for $a = 1$ km indicate the shapes of the contours for $T_{ex} = 700^{\circ}$ and 1200°, respectively. These curves can be used to estimate the value of a for different model atmospheres.

Figure 8 shows contours of constant values of a/λ in the same altitude versus mass-venting-rate plane. Again, the solid curves all have the same shape and represent appropriate horizontal displacements. We note that the intermediate altitude regime, $3 < a/\lambda < 30$, covers a broad range of mass-rates and altitudes of interest for the experiments proposed for Spacelab. In this intermediate regime, ambient atmosphere is picked up and mixed with the gas cloud, and neither the high-altitude kinetic approach nor the low-altitude continuum fluid dynamics approach is valid.

Following the approach of our previous work outlined in the previous section, we have further modified the treatment of Stuart[5] and assumed a self-similar expansion of the cloud as a wake behind the source. We assume that the density of the wake is given by

$$\rho(r, x) = f(\xi)\dot{M}(x)/R^2(x)V(x) \qquad (40)$$

where x is the axial distance in the direction downstream of the source, r is the radial distance from the x-axis, $R(x)$ is the radial extent of the wake at a distance x downstream, $\xi = r/R(x)$, $f(\xi)$ is the dimensionless self-similar radial density profile, $\dot{M}$ is the mass flux in the wake through the disc of radius $R(x)$ centered on the x-axis, and $V(x)$ is the x-component of the fluid velocity at axial distance x.

As in the point release problem, an ad hoc assumption is required about the fluid velocity flow field. We have assumed that the x-component of the velocity, $V(x)$ is independent of radial distance and that the radial velocity component is given by

$$V_r = V(x) \frac{r}{R(x)} \frac{dR}{dx} \quad . \qquad (41)$$

Equation (41) insures that the velocity at the surface of the steady-state wake is parallel to the surface.

This model assumes that the only interaction between the gas cloud wake and the ambient atmosphere is the sweeping up of all the ambient atmosphere encountered by the cloud. Shocks and diversion of fluid flow in the surrounding atmosphere external to the cloud are neglected in this model. We also neglect the effects of ionization and condensation within the wake.

The imposition of contraints on the velocity as in Eq. (41) and on the density profile in Eq. (40) is somewhat artificial as they have been imposed to make the problem mathematically tractable. These constraints lead to some inconsistencies between the model and the actual wake of a steady-state release. As with all mathematical models, it is hoped that the necessary inconsistencies are small enough that they do not destroy the value of the model. In this case, the model assumption about the velocity in Eq. (41) obviously cannot be satisfied near the point of release for nearly all modes of gas release. In fact, as we shall see later, Eq. (41) cannot be valid near the point of release for any configuration because of conservation of mass, momentum, and energy.

The equations for local conservation of mass and momentum are

$$\frac{\partial}{\partial t}(\rho) + \vec{\nabla} \cdot (\rho \vec{V}) = S(x, r) \qquad (42)$$

and

$$\frac{\partial}{\partial t}(\rho \vec{V}) + \vec{\nabla} \cdot (\rho \vec{V}\vec{V}) + \vec{\nabla} p = \vec{t}(x, r) \quad . \qquad (43)$$

In Eq. (42), $S(x, r)$ is the mass source function due to the sweeping of atmospheric mass and the mass injection from the shuttle source. In Eq. (43), p is the gas pressure within the wake and $\vec{t}(x, r)$ is the momentum source due to the swept-up ambient atmosphere having velocity V_a in the x-direction in the rest frame of the shuttle.

The velocity vector $\vec{V}$, defined above, is the fluid flow velocity in the rest frame of the shuttle and is not the velocity of the released gas with respect to the atmosphere as in the previous section. The corresponding conservation equation for energy is

$$\frac{\partial}{\partial t}\left(u + \frac{1}{2}\rho V^2\right) + \vec{\nabla} \cdot \left[\vec{V}\left(u + \frac{1}{2}\rho V^2 + p\right)\right] = Q(x, r) \qquad (44)$$

where

$$u = \frac{p}{\gamma - 1} \tag{45}$$

is the internal energy density, γ is the ratio of specific heats, and $Q(x, r)$ is the energy source term due to the swept-up ambient mass with velocity V_a and the energy injected with the mass from the shuttle source.

Because we are solving for a steady-state solution, the time derivatives do not contribute in Eqs. (42), (43), and (44). The global equations for conservation of mass, x-component of momentum, and energy are obtained by integrating these equations over the volume of the wake envelope bounded downstream by a plane of constant x as shown by the dotted line in the sketch below. The result is

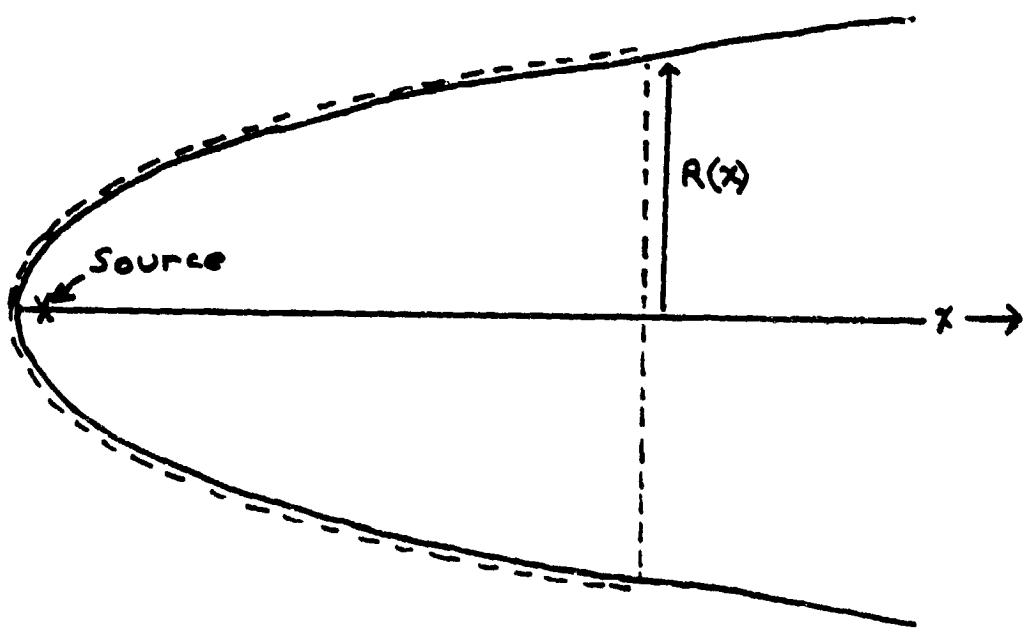

$$\dot{M}(x) = \dot{M}_o + V_a \rho_a \pi R^2(x) = \dot{M}_o(1 + R^2/a^2) \ , \quad (46)$$

$$\dot{M}(x)V(x) - \rho_a V_a^2 \pi R^2(x) - \pi R^2 p_a + \int_0^R p(x, r) 2\pi r dr = 0 \ , \quad (47)$$

$$-(u_a + \tfrac{1}{2}\rho_a V_a^2 + p_a)V_a \pi R^2 + V(x) \int_0^R \left(u + \tfrac{1}{2}\rho |\vec{V}|^2 + p\right) 2\pi r dr = \dot{E}_o \quad (48)$$

where u_a and p_a are the internal energy density and pressure of the ambient atmosphere and $\dot{E}_o$ is the rate at which the source is injecting energy along with the mass injection $\dot{M}_o$.

The ambient temperature T_a is related to p_a and u_a by

$$p_a = \frac{kT_a}{m_a} \rho_a = (\gamma_a - 1) u_a \quad (49)$$

where k is Boltzman's constant and m_a is the mass of the ambient particles. Thus, $u_a + p_a$ in Eq. (48) can be written

$$u_a + p_a = \frac{\gamma_a}{\gamma_a - 1} \frac{kT_a}{m_a} \rho_a \ .$$

By using the definition of the characteristic length, $a^2 = \dot{M}_o/\pi\rho_a V_a$, Eq. (45) to relate p and u, Eqs. (40) and (41) for the radial dependence of ρ and $\vec{V}$, and defining

$$\frac{dU}{dx} = \int_0^R u(x, r)\, 2\pi r dr, \tag{50}$$

Eqs. (47) and (48) can be written

$$\dot{M}V - \dot{M}_o \frac{R^2}{a^2}\left(V_a + \frac{kT_a}{V_a m_a}\right) + (\gamma - 1)\frac{dU}{dx} = 0\ , \tag{51}$$

$$-\dot{M}_o \frac{R^2}{a^2}\left(\frac{V_a^2}{2} + \frac{\gamma_a}{\gamma_a - 1}\frac{kT_a}{m_a}\right) + \gamma V \frac{dU}{dx} + \frac{1}{2}\dot{M}(V^2 + \alpha\dot{R}^2) = \dot{E}_o. \tag{52}$$

where

$$\alpha = \int_0^1 f(\xi)\xi^2 2\pi\xi d\xi \tag{53}$$

is a dimensionless invariant determined by the self-similar radial density profile and

$$\dot{R} = V\frac{dR}{dx}\ . \tag{54}$$

The radial component of the momentum conservation Eq. (43) is treated analogously to the virial treatment of Stuart.[5] By taking the dot product with $\vec{r}$ on both sides of Eq. (43), where $\vec{r}$ is the component of position perpendicular to the x-axis, integrating over the volume shown in the previous sketch, and differentiating with respect to x, one obtains.

$$\alpha R \frac{d}{dx} (\dot{M}\dot{R}) = 2 (\gamma - 1) \frac{dU}{dx} - \pi R^2 p_a \qquad (55)$$

The set of Eqs. (46), (51), (52), and (55) determines the four quantities R, $\dot{M}$, V, and dU/dx and constitute the venting model.

IV. RESULTS OF THE VENTING MODEL

In this section we illustrate the properties of the solution of the equations derived in the previous section. We restrict our discussion to the special case $\gamma_a = \gamma_g = \gamma$ and will not distinguish between the mass of the gas species, m_g, and the mass of ambient species, m_a, by setting them both equal to 20 atomic mass units as representative of a mean molecular weight in the thermosphere. The choice of the molecular mass has no impact on the dynamics when $\gamma_a = \gamma_g$ but enters only when determining an average "temperature" defined as

$$T = (\gamma - 1) \frac{m_a V}{k\dot{M}} \frac{dU}{dx} \quad . \tag{56}$$

A. Analytic characteristics of the solution

In order to examine the nature of the solution of the venting model equations, we first note that the ambient energy density and internal energy appear in the same combination in Eqs. (51) and (55). Hence, we define

$$U' = (\gamma-1) \frac{dU}{dx} - \pi R^2 p_a \, . \tag{57}$$

By using this definition of U' to eliminate dU/dx from Eq. (52) and rearranging terms, the energy equation may

be written

$$\frac{\gamma}{\gamma-1} VU' = \dot{E}_o + \frac{\gamma}{\gamma-1} \frac{\dot{M}_o}{V_a} \frac{kT_a}{m_a} \left(\frac{R}{a}\right)^2 (V_a - V)$$

$$+ \frac{1}{2} \left[\dot{M}_o V_a^2 \left(\frac{R}{a}\right)^2 - \dot{M}V^2\right] - \frac{1}{2} \alpha \dot{M} \dot{R}^2 . \qquad (58)$$

As $R \to \infty$, $V \to V_a$ and the second term on the RHS approaches a constant, contributing to the energy balance in the same manner as $\dot{E}_o$. This terms arises from the compression of the ambient atmosphere as it is swept up and serves as a source of energy to drive the radial expansion. Each of the terms in the square brackets increases as R^2 as $R \to \infty$ and the leading terms exactly cancel leaving a constant as the dominant contribution of this term to the energy equation in this limit.

The structure of Eqs. (51) and (55) is considerably simplified if we define new normalized independent and dependent variables

$$y = R^2/a^2 ; \qquad (59)$$

$$q = \dot{M}V/\dot{M}_o V_a ; \qquad (60)$$

$$\chi = \alpha \dot{M}^2 \dot{R}^2 / \dot{M}_o^2 V_a^2 ; \qquad (61)$$

$$\Delta = U'/\dot{M}_o V_a . \qquad (62)$$

Equations (51) and (55) can now be written

$$q = y - \Delta, \tag{63}$$

$$y \frac{d\Delta}{dy} = 2q\Delta, \tag{64}$$

respectively. Unfortunately, the energy equation does not simplify greatly. However, by multiplying Eq. (58) by $\dot{M}$, using Eq. (46), defining the constants c and b,

$$c = \frac{2\dot{E}_o}{\dot{M}_o V_a^2} \quad , \quad b = \frac{kT_a}{m_a V_a^2} \quad , \tag{65}$$

and using Eq. (63) appropriately, the energy equation (58) can be written uniquely with no terms of the form q^2, y^2, or qy;

$$\frac{2}{\gamma-1} q\Delta = c + (1+c)y + \frac{2\gamma b}{\gamma-1} y(1+\Delta) + \Delta^2 - \chi \quad . \tag{66}$$

The three equations (63), (64), and (66) determine the three functions q, Δ, and χ as functions of y (and thus R). The equations in this form do not contain $\dot{R}$ explicitly and the dynamics do not depend explicitly on the value of α. In terms of these normalized functions, the axial velocity, V, and temperature, T, defined by Eq. (56), are given by

$$V = V_a \frac{q}{1+y} = V_a \frac{y-\Delta}{y+1} ; \tag{67}$$

$$T = \frac{V}{\dot{M}} \left(\frac{m_i U'}{k} + \frac{\dot{M}_o}{V_a} \left(\frac{R}{a}\right)^2 T_a \right) = \frac{m_a}{k} V_a^2 \frac{(y-\Delta)(by+\Delta)}{(y+1)^2} ; \tag{68}$$

where the last form is an explicit function of y once a solution $\Delta(y)$ of the equations has been obtained.

One consequence of the venting model and the above equations is that solutions do not exist below a minimum value of R which depends on the various parameters. Accordingly, solutions can only be obtained for finite initial values of y. For any given set of gas release parameters and a sufficiently large value of y (or R), the model allows a family of solutions corresponding to different values of $\dot{P}$ (or χ; see Eq. (61)). The range of allowed values of $\dot{R}$ (or χ) for a given value of R (or y) is determined by the energy equation. The maximum permitted value of χ is given by Eq. (66) with $\Delta=0$, or

$$\chi \leq c + (1 + c + \frac{2\gamma b}{\gamma-1}) y .$$

On the other hand, if Eq. (63) is used to eliminate q from Eq. (66), we obtain another form of the energy equation

$$\frac{\gamma+1}{\gamma-1}\,\Delta^2 - \frac{2(1-\gamma b)}{\gamma-1}\,y\Delta + c + \left(1+c+\frac{2\gamma}{\gamma-1}\,b\right) y - \chi = 0 \qquad (69)$$

which is quadratic in Δ. The requirement that Δ be real puts a lower bound on the permitted value of χ in order that the discriminant be positive for sufficiently small y.

The model equations have been integrated numerically for a variety of different allowed initial conditions. All of these families of solutions asymptotically approach the same behavior at large radius far downstream in the wake where the model assumptions are more valid. Some of the allowed values of initial conditions at small R are within reasonable ranges and some are not, but all such solution curves are less valid at small R because the model assumptions are less justified.

Before illustrating the numerical solutions we obtain the asymptotic form of the solutions and give an analytic expression for the expansion velocity that is an excellent approximation to a particular numerical solution. By direct substitution into Eqs. (63), (64), and (66) or (69), it can be verified that the following forms represent asymptotic solutions of the equations for the first

two terms in an expansion valid as $y \to \infty$ ($R \to \infty$):

$$\Delta \to \Delta_o + \frac{\Delta_o^2}{y} + O\left(\frac{1}{y^2}\right) \quad ; \tag{70}$$

$$\chi \to 2\Delta_o y + 2\Delta_o B + O\left(\frac{1}{y}\right) \quad ; \tag{71}$$

$$V \to V_a \left(1 - \frac{1+\kappa}{(1-b)y}\right) + O\left(\frac{1}{y^2}\right) \quad ; \tag{72}$$

$$T \to T_a + \frac{m}{k} V_a^2 \frac{\kappa - b}{y} + O\left(\frac{1}{y^2}\right) \quad ; \tag{73}$$

where $$\kappa = \frac{\gamma - 1}{2\gamma} (1 + c) \quad .$$

$$\Delta_o = (\kappa + b) / (1 - b) \quad . \tag{74}$$

$$B = c/2\Delta_o + \left(\frac{2\gamma}{\gamma - 1} b + 1\right) \Delta_o/2 \quad . \tag{75}$$

All solutions of the model equations have the asymptotic form given by Eqs. (70)-(73) for sufficiently large y. However, the analytic expressions obtained by keeping only the first two terms in the expression (71) and setting $\Delta = \Delta_o$ in Eqs. (67) and (68) are indistinguishable through three significant digits from a particular set of numerical solutions for $y \geq 1$. By remembering the definition

for χ, Eq. (61), we can write an explicit expression for $\dot{R}$,

$$\dot{R} = \frac{K^2}{2} V_a \frac{(R^2/a^2 + B)^{1/2}}{R^2/a^2 + 1}, \tag{76}$$

where

$$K^2/2 = (2\Delta_o/\alpha)^{1/2}. \tag{77}$$

The expression (76) for $\dot{R}(R)$ has an asymptotic expansion for $R>>a$,

$$\dot{R} \to \frac{K^2}{2} V_a \frac{a}{R} \left[1-(1-B/2)\frac{a^2}{R^2}\right] + O\left(\frac{a^5}{R^5}\right), \tag{78}$$

identical through the first two terms to the asymptotic expansion of all the solutions.

The parameter b, defined by Eq. (65), is a normalized ambient temperature and has the numerical value $b = 0.00679$ for $T_a = 1000^oK$ and $V_a = 7.8$ km/s. Hence it makes only a very small change to the value of Δ_o and B defined by Eqs. (74) and (75). However, the form of Δ_o given in Eq. (74) with the term (1-b) in the denominator indicates that this venting model cannot be used to describe the gas cloud

produced by slowly moving canisters. Indeed, it is probably inaccurate for velocities approaching the ambient thermal velocity. Thus this model must not be used to describe venting releases from sounding rockets which have velocities in this range. This breakdown in this model is associated with the compression of the atmosphere that results from our description of the atmospheric mass pick up.

The parameter c, defined by Eq. (65), is related to the stored chemical or internal energy per unit mass. For reasonable values of $\dot{E}_o/\dot{M}_o$, $c << 1$ and does not have a major affect on the solutions. The detailed analyses of barium releases from rockets[7] indicated that the best value of the initial expansion velocity of the barium vapor with a flattop distribution is $\dot{R}_o = 1.15$ km/s. This value corresponds to $E_o/M_o = 0.6\ \dot{R}_o^2/2 = 4 \times 10^5$ J/kg. We use this same value for $\dot{E}_o/\dot{M}_o$ in the case of a vented release and obtain $c = 0.0131$. With these values for b and c, the quantities Δ_o, B, and $K^2V_a/2$ have the values tabulated in Table I for the indicated values of γ.

B. Evaluation of the solutions

The equations for the venting model have been integrated numerically. The next twelve figures show examples of representative solutions for various gas release parameters and assumed initial conditions. In

TABLE I. Numerical values

Parameter	$\gamma = 1.1$	$\gamma = 1.4$	$\gamma = 5/3$
Δ_o	0.0532	0.1523	0.2108
B	0.1528	0.123	0.140
$\frac{K^2}{2} V_a$ (km/s)	3.60	6.09	7.16

order to illustrate the sensitivity of the solution to a change in the value of each of the various parameters, we have compared the solution curve produced by the changed value of a single parameter with a "nominal" case corresponding to a standard set of parameters. Table II lists the values of the parameters for which representative solutions are shown. The first column of values represent the values associated with the nominal solution. Solutions associated with the other values are illustrated in the figures.

The parameter C_o is related to the stored chemical or internal energy and is given by $C_o = \sqrt{c}\ V_a$. It is the velocity at which all the mass would travel

TABLE II. Venting model parameter values.

Parameter	Nominal Value	Other Values
C_o (km/s)	0.89	3.09
α	0.5	1.0
$\dot{R}_o$ (km/s)	3.23	2.23, 4.23, 1.93, 3.76
γ	1.4	1.1, 5/3
T_a (^oK)	1000	0

if all of the stored initial internal energy were converted into kinetic energy. The nominal value is appropriate for the specific energy associated with barium vapor of 4×10^5 J/kg. The larger value of C_o corresponds to a value of specific energy twelve times larger than for barium. If applied to hydrogen gas, it corresponds to the energy content of gaseous H_2 at 770^oK and is 8.5% greater than the mean thermal velocity.

The parameter α is the density distribution parameter defined for this cylindrical geometry case by Eq. (53). The values 0.5 and 1.0 correspond to a flattop distribution and cylindrical-shell distribution, respectively. (In the point release

case, α has the value 0.6 for a flattop distribution as discussed in Section II.).

In Fig. 9 we show the nominal solution for $\dot{R}(R)$ by a heavy curve and the solutions corresponding to the alternate values of C_o and α by lighter solid lines. In this and the subsequent eleven figures, the heavy curve always corresponds to the nominal case. The other curves represent solutions corresponding to changes in only one or two of the parameters. These curves are labeled by the non-nominal value of the parameter. At the top of the figure the nominal values of these parameters are given. The values of all parameters not shown explicitly are those given as the nominal values in Table II. Each figure thus emphasizes the sensitivity of a solution to the change in a particular parameter.

Returning to Fig. 9, the nominal curve is specified by the choice $\dot{R}_o = 3.23$ km/s at $R = R_o = a$. In this and the next eleven figures the scale length a, defined by Eq. (39), is represented by A. This value for $\dot{R}_o$ is the value produced by the expression (73) evaluated at $R = a$. The analytic expression (76) is indistinguishable from the numerically-integrated

solid curve. The two other curves behave like expression (78) for $R >> a$ (in practice, $R \gtrsim 2a$) with the appropriate evaluations for K and B given by Eqs. (77) and (75). For $C_o = 3.09$ km/s the expansion velocity is only slightly greater for a given value of R/a due to the small additional amount of initial energy available for expansion. Note that there is maximum in $\dot{R}(R)$ for $R > a$. If a larger initial value for $\dot{R}_o$ at $R_o = a$ had been chosen there would have been no maximum for $R > a$. We will illustrate the effect of the choice of $\dot{R}_o$ on the solution in the next figure. For a mass distribution more peaked towards the outer edge, the expansion velocity approaches that given by the $\alpha = 1.0$ curve corresponding to a cylindrical shell. The expansion velocity is less in this case because the energy available for expansion is distributed to all of the particles. The expansion velocity of the outer edge corresponding to a density distribution more peaked in the center with $\alpha < 0.5$ would be greater than that given by the nominal curve, varying as $\alpha^{-\frac{1}{2}}$.

Figure 10 shows solutions resulting from different choices for the initial value of $\dot{R}_o$. The values illustrated correspond to the nominal value ±1 km/s. Both curves quickly approach the nominal solution curve which is well approximated by Eq. (76). For $R \gtrsim 2a$, the solution is

fairly insensitive to the particular choice of $\dot{R}_o$ for reasonable values of this parameter. The asymptotic expansions given in Eqs. (70)-(73) and (78) depend only on the released gas parameters and are independent of $\dot{R}_o$. For the $\dot{R}_o$ = 2.23 km/s case, a smaller fraction of the total energy is contained in the kinetic energy term and a larger fraction is contained in internal energy with the result that initially the gas has a higher temperature, as we shall see below. This excess thermal energy rapidly expands the radius until the expansion velocity approaches the nominal solution.

Figure 11 illustrates the dependence of $\dot{R}(R)$ on the assumed ratio of specific heats, γ, according to the venting model equations. The two dashed curves represent solutions appropriate for the release of monatomic (γ = 5/3) and polyatomic (γ = 1.1) gases. In general, as γ decreases, the number of degrees of freedom increases with the result that more energy is stored as internal energy and less is available for kinetic energy of expansion. The initial value of $\dot{R}_o$ = 1.93 km/s for the γ = 1.1 case is the value obtained from Eq. (76) evaluated at R = a. The thin solid line with $\dot{R}_o$ = 1.93 km/s illustrates the affect of a change in γ on the resulting expansion velocity.

Equation (76) has the value 3.82 km/s at R = a with $\gamma = 5/3$. This value is below the minimum permitted value of $\dot{R}_o$ at R = a according to Eq. (69). Rather than choosing a numerical solution with a larger initial value for $\dot{R}_o$, we have shown a numerical solution beginning at $R_o = 1.1a$ with a permitted initial value for $\dot{R}_o$ of 3.76 km/s given by Eq. (76) evaluated at R = 1.1a. With this choice, the two dashed curves are indistinguishable from the analytic expression (76). Regardless of the value of γ_g associated with the released gas, when R >> a the effective value of γ of the gas mixture will tend towards γ_a associated with the ambient atmosphere as shown in Ref. 3 for the point release case. The appropriate value ranges between 1.4 and 1.67 depending upon the altitude of release.

The dependence of the temperature, T, defined by Eq. (56) in terms of the average internal energy per particle, on the gas release parameters is given by Eqs. (68) and (73). An accurate representation for the nominal case for $R \gtrsim a$ is given by Eq. (68) with $\Delta = \Delta_o$. Figure 12 shows T(R) for the nominal case and the dependence on different initial values of $\dot{R}_o$. A smaller initial kinetic energy of expansion results in a higher initial temperature. The temperature resulting from an assumed expansion into a cold atmosphere is shown by the curve labeled $T_a = 0^oK$. The presence of a warm atmosphere has only a very small effect on the dynamics

of the expansion due to the small value of the parameter b. The primary effect is to raise the temperature of the gas cloud mixed with ambient atmosphere by T_a for $R \gtrsim 2a$ as shown explicitly in Eq. (73). Figure 13 shows the effect of γ on the temperature. The greater the number of degrees of freedom, the lower the temperature.

Figure 14 shows the axial velocity of the gas plus air mixture in the frame of the canister. As the gas cloud encounters the ambient air, it comes to rest with respect to the atmosphere which streams by the canister at speed V_a = 7.8 km/s. The analytical dependence for the nominal case is given adequately by Eq. (67) with $\Delta = \Delta_o$. Figure 14 shows that the velocity is rather insensitive to the choice of $\dot{R}_o$. Equation (67) with $\Delta = \Delta_o$ indicates that the velocity of the wake with respect to the atmosphere varies as

$$V_{wake} = V_a - V \sim \frac{1 + \Delta_o}{1 + R^2/a^2} V_a \qquad \text{for} \qquad R \gtrsim a \tag{79}$$

which is rather insensitive to gas release parameters because Δ_o is small.

The shape of the plume behind the canister is obtained by recognizing that $dR/dx = \dot{R}/V$ and integrating

$$x = \int^{R} \frac{V(R')}{\dot{R}(R')}\, dR' \quad . \tag{80}$$

By using the approximate expressions (67) with $\Delta = \Delta_o$ and (76), we obtain the explicit relationship

$$x - x_o = \frac{1}{K^2}\left(R(R^2/a^2 + B)^{\frac{1}{2}} - (2\Delta_o + B)\, a\, \ell n\left[R/a + (R^2/a^2 + B)^{\frac{1}{2}}\right]\right) \tag{81}$$

where x_o is an arbitrary constant of integration. Asymptotically, for $R >> a$, the radius of the plume is found to vary as

$$R(x) \sim K(ax)^{\frac{1}{2}}\left[1 + (2\Delta_o + B)\,\frac{\ell n(R/a)}{R^2/a^2} - O\left(\frac{a^2}{R^2}\right)\right] \tag{82}$$

with K given by Eq. (77). Far in the wake $x \sim V_a t$ and the radius of the plume increases as $t^{0.5}$. This asymptotic time dependence is different from the $t^{0.4}$ dependence for the spherical point release case because of the different geometry.

Figure 15 shows the normalized plume radius as a function of normalized distance downstream of the canister for various values of the gas release parameters. The constant of integration has been chosen in each case so that $R = a$ (= 1.1a for $\gamma = 1.1$) at $x = a$. The half-power dependence of radius on distance is obvious for $R \gtrsim 2a$; the value of the y-axis intercept of the extrapolation of

the straight-line portion of the curves is equal to K. Figure 16 shows the same set of curves on a linear scale. Note that the vertical axis is expanded 9.3 times the horizontal axis. Figure 17 illustrates the sensitivity (or insensitivity) of the plume radius to assumed initial conditions.

We expect that the wake model provides an adequate description of the characteristics of the vented gas once $R \gtrsim a$. We expect that this criterion occurs within a distance of order a downstream of the canister. We have no model for the transition region from the vicinity of the canister to the cylindrical region described by the wake model. Figure 14 shows that the released gas has lost half of its orbital velocity by the time this wake model is applicable and is decelerating rapidly. The distance, L, that the released gas travels with respect to the atmosphere as it grows in radius from R_o to R is

$$L = \int (V_a - V)\, dt = \int_{R_o}^{R} \frac{V_{wake}(R')}{\dot{R}(R')}\, dR' \tag{83}$$

$$\sim a\, \frac{2(1 + \Delta_o)}{K^2}\, \ell n \left(\frac{R + (R^2 + Ba^2)^{\frac{1}{2}}}{R_o + (R_o^2 + Ba^2)^{\frac{1}{2}}} \right)$$

where we have made use of Eqs. (76) and (79) for the approximate expression. Because for large R we have $R \sim x^{0.5}$ and $R \sim t^{0.5}$, we find that this model predicts that the distance traveled is not finite but increases as ℓn t. This result is different from the spherical point release model result which has the gas cloud traveling a finite distance.

Figures 18, 19, and 20 show the normalized distance traveled by a parcel of gas located a distance x downstream in the wake for various gas release parameters and initial conditions. In these figures, L is arbitrarily assigned the value a at x = a. The three curves in Fig. 19, all drawn for the same gas release parameters, indicate that a slab of gas initially having R = a at x = a, travels 0.2a further (less) if the initial expansion velocity is 1 km/s less (greater) than the nominal value.

In summary, the wake model derived here produces quantitative estimates of the primary characteristics from a continuously venting gas release traveling at orbital velocity. All lengths scale with the characteristic scale length a. Far downstream in the wake the cylindrical plume radius expands as $t^{0.5}$, the shape of the plume as a function of distance x downstream is $R \sim K(ax)^{0.5}$, the axial velocity

falls as a^2/R^2 and the distance traveled increases indefinitely as ℓn t. At a position $x \sim 100a$ downstream, the typical plume radius is ~12a and the distance traveled with respect to the ambient atmosphere since $R = a$ is $\Delta L \sim 4a$. Close to the canister when $R \sim a$, the expansion velocity falls rapidly from ~3 km/s and the temperature rapidly cools from several thousand degrees to the ambient atmospheric temperature.

These results are dependent upon the snowplow model used to derive the appropriate equations. The most suspect assumptions are those relating to the self-similar radial density distribution and the uniformity of the axial velocity with radius. It would seem reasonable to expect that both the mass pick-up and momentum pick-up in the wake are probably more concentrated toward the outer edges than assumed by this model. Near the canister, the outer edges of the plume would be swept back more rapidly than the central portion, particularly in the lower altitude end of the intermediate altitude regime. This effect is partially modeled by the $\alpha = 1.0$ curve corresponding to the assumption that all of the released and picked-up mass is concentrated at the outer edge. The result is a small reduction in the radius of the plume. Far downstream where the axial velocity with respect to the atmosphere is small, $V_{wake} << \dot{R}$, $R >> a$, and $\rho \sim \rho_a$, the results of this model for a flattop distribution, $\alpha = 0.5$, should be more valid. Of course,

at very late time, the released gas in the plume expands by diffusion. The radial distribution can be assumed to evolve from a flattop to a Gaussian shape during the snowplow expansion as outlined in Section II-C.

V. CONDUCTIVITY ENHANCEMENTS PRODUCED BY BARIUM RELEASES

Barium releases from rockets have been conducted in the ionosphere worldwide primarily to measure ambient electric fields using small releases (< 4 kg) at high altitude (> 200 km) and to produce enhancements in the ionospheric electron concentration using large releases (16 kg to 320 kg) at lower altitudes (< 200 km). The properties of the larger releases have been studied extensively using a variety of radar, optical, propagation path, and rocket probe techniques. As a result, many characteristics of these releases, such as the time development of the scale size of the neutral cloud, peak electron concentration, and distribution of barium ions perpendicular and parallel to the magnetic field are well documented and the behavior is understood.

These large barium releases have produced major enhancements in the ionospheric field-line-integrated Pedersen (FLIP) conductivity. The ability to create such large FLIP conductivities is of interest for a variety of proposed Spacelab experiments. In this section we first briefly describe the process of creating ion clouds from released barium atom vapor. We then apply the results of Sections II and IV for the expansion of gas clouds

released in both the explosive and venting modes to the calculation of ion deposition from releases at orbital velocity. The results of these calculations are estimates of the scale size and FLIP conductivity enhancements that can be produced by barium releases from rockets and Spacelab as a function of altitude of release and amount of released vapor.

A. Ion deposition for point barium releases

In Section II we summarized the results of a snow-plow model that describes the expansion of a spherical gas cloud in an intermediate altitude regime released either at orbital or negligible velocity. A barium thermite release typically produces an expanding cloud of barium atom vapor that exits the canister in 0.1 - 0.2 seconds and thus this event can be called a point release. Our understanding of the process by which barium ion clouds are produced from the expanding vapor cloud and the resulting properties of the ion cloud comes in part from a detailed analysis[7] of the Spruce ion cloud resulting from a 48 kg barium release at 190 km altitude, and in part from observations of many barium releases ranging in size from 16 kg to 320 kg and released at various altitudes between 150 km and 255 km. The description of the ion deposition as well as the

quantitative values for important parameters for the process are taken from Ref. 7. Here we summarize this process and describe the modeling adopted to obtain quantitative estimates for other altitudes and chemical payload weights.

As the barium atom vapor expands, it encounters the ambient atmosphere. The outer radius expands initially with velocity $\dot{R}_o$. We assume that diffusion changes an initial flattop distribution into a Gaussian profile whose Gaussian scale length increases according to the snowplow model. The number of barium atoms is depleted with an exponential time constant, τ_i, by two competing processes: oxidation by ambient oxygen molecules and photoionization from excited metastable states. The cross section for the absorption of solar radiation that excites ground-state barium atoms into the metastable states is large. Photoionization commences only after a time dealy, t_i, when the barium cloud has expanded sufficiently so that the metastable exciting radiation is able to permeate the cloud.

As the barium ions are created, they become tied to the magnetic field line at their position of creation and cease their motion transverse to the magnetic field, $\vec{B}$. After the passage of several τ_i time periods, the bulk of the ionization has been created. The number of

ions on a given magnetic field line remains constant beyond this time and the distribution of this field-line content, $N_c(r)$, with radius transverse to $\vec{B}$ is a bell-shaped curve. We represent the characteristic size of the ion cloud by a scale length, $a_\perp$, which is the distance transverse to $\vec{B}$ in which N_c has fallen to e^{-1} of its central peak value.

The process described above has been modeled in detail in Ref. 7 for the Spruce ion cloud. The results of that model are the determination of appropriate values of a number of the required parameters so that the model produced results consistent with the various measurements. Table III presents a tabulation of the values of these parameters.

A popular barium thermite reaction that produces barium vapor is

$$\zeta Ba + CuO \longrightarrow BaO + Cu + (\zeta - 1)\ Ba \qquad (84)$$

where ζ is a number typically between 1.7 and 2.5. For Spruce with $\zeta = 2.5$, the 48 kg chemical payload weight produced 3.56 kg of barium atom vapor which corresponds to a vaporization efficiency of 7.4%. Quantitative determinations of this efficiency are diffuclt to obtain to much better than a factor of 2 and typical reported values range from 5% to 12%. The model value reported here is consistent with measurements of the properties of the neutral and ion clouds.

TABLE III. Parameters for the Spruce ion cloud.

Parameter	Value	Units
Inputs to Model		
1. Mass of barium vapor, M_o,	3.56	(kg)
2. Vaporization efficiency	7.4%	
3. Fraction of atoms ionized, f,	0.42	
4. Ionization time constant, τ_i,	10.0	(s)
5. Total ion inventory	6.5	($\times 10^{24}$)
6. Atmospheric density, ρ_a,	0.45	(kg/km^3)
7. Neutral diffusion coefficient, D_n,	0.052	(km^2/s)
8. Equal-mass-radius, a_o,	1.26	(km)
9. Initial expansion velocity, V_o,	1.15	(km/s)
10. Onset of photoionization, t_i,	1.9	(s)
Derived Quantities		
11. Neutral cloud radius, R, at $t = t_i$	1.59	(km)
12. Neutral cloud radius, $\bar{a}$, at $t = t_i + \tau_i$	3.8	(km)
13. Transverse scale size, $a_\perp$,	2.7	(km)
14. Field-line content, N_c,	2.4	($10^{17} m^{-2}$)
15. Peak ion density at 100 s	1.7	($10^{13} m^{-3}$)
16. Ion cloud length at 100 s	7.8	(km)
17. Initial Pedersen conductivity	27	(mho)

The fraction, f, of the atoms that are ionized is equal to the ratio of the photoionization rate, ν, to the total loss rate of barium atoms. The photoionization time, $1/\nu$, has been consistently reported by Haerendel et al.[8] of the Max-Planck Institute to be of order 19 s. Rosenberg et al.[9] of AFCRL report a time closer to 30 s. We choose $1/\nu = 24$ s as being within 20% of the correct value. The oxidation rate is proportional to the molecular oxygen concentration, $\tilde{k}n_{O_2}$, and was estimated by Rosenberg et al.[9] from observations of a series of barium releases at different altitudes. Because n_{O_2} is considerably lower in the 1972 CIRA atmosphere model than in the U.S. Standard Atmosphere used by Rosenberg et al., we have had to use a relatively large value for the rate constant, $\tilde{k} = 1.25 \times 10^{-16}$ m^3/s, in order to match their observed loss rates. The fraction ionized is

$$f = \frac{\nu}{\nu + \tilde{k}n_{O_2}} = \frac{1}{1 + 3 \times 10^{-15} n_{O_2}} \tag{85}$$

and has the value for Spruce given as entry 3 in Table III. The time constant for the loss rate of barium atoms is

$$\tau_i = \frac{1}{\nu + \tilde{k}n_{O_2}} = \frac{f}{\nu} = \frac{24}{1 + 3 \times 10^{-15} n_{O_2}} \text{ s} \tag{86}$$

and has the value given as entry 4 for Spruce. The total number of barium atoms is $N_T = M_o/m_{Ba}$ where m_{Ba} is the atomic weight of barium. The total ion inventory given as entry 5 for Spruce is fN_T.

If we neglect transport of barium ions perpendicular to the magnetic field, the conservation equation for the ions can be written

$$\frac{\partial n_i}{\partial t} + \frac{\partial}{\partial z} n_i v_{iz} = \nu n_b(r,z,t) \tag{87}$$

where v_{iz} is the velocity in the z-direction assumed to be along $\vec{B}$, $n_b(r,z,t)$ is the concentration of barium atoms, and r is the radial coordinate perpendicular to $\vec{B}$. Based on the discussion in Sec. II, we take the distribution of barium atoms to be an expanding Gaussian of the form

$$n_b(r,z,t) = \frac{N_T}{[\pi R^2(t)]^{3/2}} \exp[-(r^2 + z^2)/R^2(t)]\, e^{-t^*/\tau_i}. \tag{88}$$

where t^* is the length of time that the barium atoms have been exposed to ionizing radiation. By integrating Eq. (87) along the magnetic field we obtain an equation for the time dependence of the radial distribution of the field-line content $N_c(r,t) = \int n_i dz$

$$\frac{\partial N_c(r,t)}{\partial t} = \frac{\nu N_T}{\pi R^2(t)} \exp[-r^2/R^2(t)]\, e^{-t^*/\tau_i} \tag{89}$$

If we start the ionization process at time, t_i, after release we can integrate Eq. (89) in order to determine the radial profile of the field-line content of the ion cloud,

$$N_c(r,t) = \nu N_T \int_{t_i}^{t} \frac{\exp[-r^2/R^2(t')]}{\pi R^2(t')} e^{-(t' - t_i)/\tau_i} dt'. \quad (90)$$

Entries 6-9 in Table III are related to the neutral cloud expansion. The first two are atmospheric numbers for 190 km altitude and determine the equal-mass radius. As discussed previously, it is appropriate to delay the start of photoionization until the neutral cloud has expanded sufficiently so that the metastable exciting radiation can permeate the neutral cloud. For the Spruce ion cloud, this delay time was considered a free parameter and adjusted until the time-dependent characteristics of the ion cloud matched the available data as described in detail in Ref. 7. The radius of the Spruce neutral cloud at the delay time t_i was $1.26\ a_o = 1.59$ km as given in entry 11.

If we define $\bar{a}$ as the size of the Gaussian radius of the neutral cloud at the time $t = t_i + \tau_i$ after release, i.e., at one ionization time constant after ionization has been assumed to begin, we may write the field-line content as

$$N_c(r,t) = \frac{fN_T}{\pi \bar{a}^2} I(r,t) \tag{91}$$

where

$$I(r,t) = \frac{\bar{a}^2}{\tau_i} \int_{\tau_i}^{t} \frac{\exp[-r^2/R^2(t')]}{R^2(t')} e^{-(t' - t_i)/\tau_i} dt' . \tag{92}$$

I(r,t) represents a normalized field-line content. The normalization is chosen so that

$$\frac{1}{\pi \bar{a}^2} \int_0^{\infty} I(r,t)\, 2\pi r dr = \left(1 - \exp[-(t - t_i)/\tau_i]\right) . \tag{93}$$

which approaches one as $t \to \infty$.

The result of the integration in Eq. (92) combined with Eq. (91) is the field-line content as a function of radius transverse to the magnetic field. From the profile we determine that for Spruce the radius at which the content has a value e^{-1} of its central peak value is $a_\perp = 2.66$ km. The value of $I(0,\infty)$ is 1.65 which when combined with Eq. (91) determines the peak field-line content through the center of the cloud as given by entry 14 in Table III.

For a point release at orbital velocity, we neglect the translation of the neutral cloud and use the

approximation that the ions are deposited as though the neutral cloud were stationary. As pointed out in Sec. II, the distance that the neutral cloud travels is finite and quickly becomes small compared to the rapidly expanding spherical cloud. Hence the same procedure outlined above can be applied for this case with an appropriate specification for R(t) as is discussed in Sec. V-C.

B. Ion deposition for venting-mode barium thermite releases

Thermite reactions have been successfully used in order to produce lithium atom vapor trails released in a venting mode from both rockets and satellites.[10] To date, there have been no releases of barium atom vapor via a thermite reaction in the venting mode. Thus, we have no data regarding the nature of the ionization enhancement that can be produced by such a release. In this section we calculate porperties of such an enhancement by adapting the ion-deposition procedures applicable to the Spruce ion cloud to the trail-like neutral-cloud expansion model resulting from a venting-mode release.

In principle, the procedures are similar but the details of the calculations are different due to the cylindrical geometry and the motion of the neutral cloud in the axial, x', direction. We assume that there is a

critical radius, R_i, to which the cloud must expand before photoionization and loss of barium atoms commences. (We will discuss the criteria for determining this critical value as a function of altitude and mass-venting-rate, $\dot{M}_o$, in the next section.) In the rest-frame of the shuttle, the venting-mode model presents a steady-state shape for the cloud-wake, R(x') with the origin chosen so that R(0) = R_i, in which the gas has an axial flow velocity V[R(x')] = V'(x') which approaches V_a as $x' \to \infty$. In the (x,y,z) rest-frames of the atmosphere, the shuttle travels in the negative x-direction, which we shall assume to be perpendicular to $\vec{B}$, with velocity $V_s = -V_a$. At time $t = t_i$, we choose the origin of the x-axis to be located at the position where $R = R_i$. Due to the coordinate transformation

$$x' = x + V_a(t - t_i) \quad ,$$

the cloud radius, R_c, in the rest frame of the atmosphere is

$$R_c(x,t) = R(x') \equiv R[x + V_a(t - t_i)] \quad . \tag{94}$$

After the passage of many τ_i time periods, the bulk of the ionization has been deposited and is uniform in x. Henceforth, we will concentrate only on the x = 0 position and examine the time dependence of the ion deposition on field lines as the expanding neutral trail sweeps by that position. The cloud radius at x = 0 becomes

a function of time only;

$$R_c(t) = R[V_a(t - t_i)] \quad . \tag{95}$$

Note that in this steady-state problem, the time t_i represents a critical time such that at $x = 0$, $R_c = R_i$ at $t = t_i$; it does not represent a time delay since release as in the point release problem.

During the ion deposition we model the barium cloud trail as having a Gaussian density profile in the radial direction with a Gaussian scale length $R_c(t) = R(x')$ given by our self-similar snowplow expansion for the reasons discussed in Sec. II-C. The barium atom concentration that enters Eq. (87) at $x = 0$ for $t > t_i$ is now written

$$n_b(y,z,t) = \frac{\dot{N}_T}{V\pi R_c^2} \exp[-(y^2 + z^2)/R_c^2] e^{-t^*/\tau_i} \tag{96}$$

where $\dot{N}_T = \dot{M}_0/m_{Ba}$ is the rate at which barium atoms are being emitted from the source, $\vec{z}$ is parallel to $\vec{B}$, and $\vec{y}$ is perpendicular to $\vec{x}$ and $\vec{B}$. This expression is the cylindrical equivalent of the expression given in Eq. (88) for the spherical case. With the expression (96) for n_b, Eq. (87) can be integrated along the magnetic field to get the rate of change of the transverse distribution in y of the field-line ion content.

$$\frac{\partial N_c(y,t)}{\partial t} = \frac{\nu \dot{N}_T}{\sqrt{\pi}\, V(R_c) R_c(t)} \exp[-y^2/R_c^2(t)] e^{-t^*/\tau_i} \quad . \tag{97}$$

In this equation, the length of time, t*, that the barium atoms have been exposed to ionizing radiation is not equal to $t - t_i$ as in the point-release case, but is equal to the time that it has taken the cloud to grow from radius R_i to radius R_c,

$$t^*(t) = \int_{R_i}^{R_c(t)} \frac{dR'}{\dot{R}(R')} \quad , \tag{98}$$

where $\dot{R}(R) \equiv (dR/dx')V$ is given by the venting model results discussed in Sec. IV.

The uniform-in-x transverse profile of the field-line ion content, $N_c(y)$, is obtained by integrating Eq. (97). It is convenient to change variables and integrate with respect to t* by making use of the relations

$$\frac{dt^*}{dt} = \frac{1}{\dot{R}(R_c)} \frac{dR_c}{dt} = \frac{1}{V} \frac{dx'}{dR} \frac{dR_c}{dt} = \frac{V_a}{V(R_c)} \tag{99}$$

where the first, second, and third equalities follow from Eq. (98), the definition of $\dot{R}(R)$, and Eq. (95), respectively. With this substitution, we obtain

$$N_c(y) = \frac{f\dot{N}_T}{\sqrt{\pi}\, V_a} \int_0^\infty \frac{\exp[-y^2/R'^2(t^*) - t^*/\tau_i]}{R'(t^*)} \frac{dt^*}{\tau_i} \qquad (100)$$

where $R'(t) = R[x'(t)]$ and $x'(t) = \int_0^t V dt'$ is the axial position of a slab of released gas at time t after $R = R_i$.

If we define $\bar{a}'$ as the radius of the wake at one time period τ_i after being exposed to ionizing radiation.

$$\bar{a}' = R'(\tau_i) \,, \qquad (101)$$

we may write Eq. (100) as

$$N_c(y) = \frac{f\dot{N}_T}{V_a \sqrt{\pi}\, \bar{a}'} I'(y) \qquad (102)$$

where $I'(y)$ is a normalized field-line content;

$$I'(y) = \bar{a}' \int_0^\infty \frac{\exp -[y^2/R'^2(t') - t'/\tau_i]}{R'(t')} dt' \,. \qquad (103)$$

The normalization is chosen so that

$$\int_0^\infty I'(y)\, dy = \sqrt{\pi}\, \bar{a}'$$

which is the same value that would result if $I'(y)$ were $\exp(-y^2/\bar{a}'^2)$.

In order to determine the properties of such a release we need to carry out the integral in Eq. (103). The venting-mode model determines the function $R'(t')$

once a specification of $\dot{M}_o$ (which determines the characteristic length a) and R_i is made. For the Spruce ion cloud, the detailed modeling[7] resulted in a value for the radius of the neutral cloud of 1.59 km = 1.26 a_o when photoionization began. For this venting mode model, we take R_i = 1.59 km. For the spherical point release with a flattop distribution, a cloud radius equal to 1.26 a_o implies that the barium atom density, $M_o/(4\pi R_i^3/3)$ = $\rho_a/2$, was one-half the ambient atmospheric density. We apply this same criterion in the venting-mode model case,

$$\dot{M}_o/V\pi R_i^2 = \rho_a/2 \ ,$$

which reduces to

$$VR_i^2 = 2V_a a^2 \ . \qquad (104)$$

Examination of the numerical integration of the venting mode equations indicates that criterion (104) for the nominal case occurs at R_i = 1.69 a. Thus, for the venting-mode equivalent of a Spruce-like point release at 190 km altitude with R_i = 1.59 km, we have a = 0.94 km which corresponds to $\dot{M}_o$ = 9.7 kg/s. For these same conditions we find that $\bar{a}' = R'(\tau_i)$ = 10.9 km.

We have carried out the integral in Eq. (103) using these values, and have found that I'(y) is a bell-

shaped curve that has a peak value $I'(0) = 1.56$ and has fallen to $0.57 = (1/e)I'(0)$ at $y = 0.57\ \bar{a}'$. Hence, a venting-mode release that produces barium atoms at the rate of 9.7 kg/s at 190 km altitude is calculated to produce a cylindrical trail of barium ions having a characteristic scale of $a_\perp = 0.57\ \bar{a}' = 6.2$ km in the transverse direction and a maximum field-line content of $1.56\ f\dot{N}_T/(V_a\sqrt{\pi}\ \bar{a}') = 1.84 \times 10^{17}\ m^{-2}$.

C. Scale size and magnitude of conductivity enhancements from rockets and Spacelab

In Secs. II, III, and IV we have discussed models that describe the expansion of neutral gas clouds released in an intermediate altitude regime in both a point release mode at both negligible and orbital velocity and a venting-mode at orbital velocity. In Secs. V-A and V-B we have described the application of the results of the neutral cloud modeling to the calculation of the deposition of ionization on magnetic field lines resulting from: a) a point 48-kg barium thermite release ($M_o = 3.56$ kg) from a rocket at 190 km altitude; and b) a venting-mode barium thermite release ($\dot{M}_o = 9.7$ kg/s) at orbital velocity at 190 km altitude. The procedures described for the former case produce results consistent with various detailed measurements made of such a release as

described in Ref. 7. The procedures described for the venting-mode case are derived from criteria established in the point-release case, but there are no data available for comparison.

In this section we derive the field-line-integrated Pedersen (FLIP) conductivity that results from the ionization enhancements that are created and describe how we model the characteristics of the conductivity modifications produced by releases of different magnitudes at different altitudes.

The FLIP conductivity enhancement due to the deposition of ionization from barium thermite releases is defined by

$$\Sigma_p(h) = \frac{e}{B} \int \frac{\varepsilon(z) n_i(z)}{1 + \varepsilon^2(z)} \, dz \qquad (105)$$

where z is the coordinate along $\vec{B}$, $n_i(z)$ is the distribution of ion concentration along the magnetic field line that passes through the peak value of $n_i(z)$, $\varepsilon(z) = [\Omega\tau(z)]^{-1}$ where $\Omega = eB/m_{Ba}$ is the barium ion gyrofrequency and $\tau(z)$ is the altitude-dependent ion-neutral collision time, and h is the altitude of the peak in the ion concentration. Henceforth we will adopt a nominal value of $\Omega = 35\ s^{-1}$ appropriate for a 5×10^{-5} T magnetic field.

The ion-neutral collision time can be obtained from measurements of the mobility of barium ions in nitrogen gas[11] resulting in

$$\tau = \frac{8.6 \times 10^{15}}{\bar{n}_n} \text{ s} \tag{106}$$

where $\bar{n}_n$ is an effective neutral concentration in particles/m^3,

$$\bar{n}_n = n_{N_2} + n_{O_2} + 0.8\, n_O \quad . \tag{107}$$

In deriving Eq. (106) it has been assumed that the collision cross section varies inversely as the square root of the temperature and that the collision cross section for oxygen molecules and atoms is the same as it is for nitrogen molecules. The fact that the lighter oxygen atoms are less efficient in stopping a heavier barium ion is expressed by the appropriate Langevin factor,

$$(1 + m_{Ba}/m_{N_2})^{\frac{1}{2}} (1 + m_{Ba}/m_O)^{-\frac{1}{2}} \sim 0.8 \quad ,$$

where m_{N_2} and m_O are the masses of the nitrogen molecules and oxygen atom respectively.

The distribution of ionization along the magnetic field through the peak value is governed by Eq. (87) with the right-hand-side evaluated at r = 0. As discussed in

Sec. V-A, after the passage of several τ_i time periods (typically of order 1 minute after release) most of the ionization has been deposited on field lines. The extent of the distribution of ionization along field lines is still small at that time compared to the atmospheric neutral-density scale-height H_n. Hence, the value of the FLIP conductivity in Eq. (105) resulting from the deposition of ionization on field lines can be approximated by

$$\Sigma_p(h_r) = \frac{e}{B} \frac{\varepsilon_r}{1 + \varepsilon_r^2} N_c \sim 3.2 \times 10^{-15} \frac{\varepsilon}{1 + \varepsilon^2} N_c \quad \text{mho} \tag{108}$$

where ε_r is evaluated at the altitude of release, h_r, and N_c is the peak field-line content in m^{-2} through the center of the cloud given by

$$N_c = N_c(0,\infty) = 1.65 \frac{fN_T}{\pi \bar{a}^2} \tag{109}$$

for point releases where $N_c(r,t)$ is defined by Eq. (91), and

$$N_c = N_c(0) = 1.56 \frac{f\dot{N}_T}{V_a \sqrt{\pi}\ \bar{a}'} \tag{110}$$

for venting-mode releases where $N_c(y)$ is defined by Eq. (102). Note that $\dot{N}_T/V_a$ is the number of barium atoms that the source emits per unit length and f is the fraction of

these atoms that are photoionized.

The numerical coefficients in Eqs. (109) and (110) were derived on the basis of calculations appropriate for the nominal 190 km altitude releases described earlier (M_o = 3.56 kg and $\dot{M}_o$ = 9.7 kg/s, respectively). We have not carried out the detailed ion deposition calculations indicated by Eqs. (92) and (103) for releases of different amounts of barium vapor at different altitudes. Instead, we approximate the field-line content produced by other releases by the expressions (109) and (110). In these expressions, N_T and $\dot{N}_T$ depend directly on the amount of released vapor or the rate of vapor release, respectively, and f, given by Eq. (85), depends on the altitude of release. The scale sizes of the neutral clouds one time period τ_i after photoionization, $\bar{a}$ and $\bar{a}'$, depend in a complicated way on both factors as described below.

By combining Eqs. (109) and (110) with Eq. (108), we obtain expressions for the FLIP conductivity as a function of amount of released gas and altitude,

$$\Sigma_p(u_r) = 1.68 \times 10^{-21} \frac{\epsilon_r}{1 + \epsilon_r^2} \frac{fN_T}{\bar{a}^2} \text{ mho} \quad , \qquad (111)$$

$$\Sigma_p(n_r) = 2.82 \times 10^{-21} \frac{\epsilon_r}{1 + \epsilon_r^2} \frac{f\dot{N}_T}{V_a \bar{a}'} \text{ mho} \quad , \tag{112}$$

for the cases of point releases, and venting-mode releases, respectively, with $\bar{a}$, $\bar{a}'$, and V_a expressed in km, km, and km/s, respectively. N_T and $\dot{N}_T$ are the number of barium atoms and number of barium atoms per second, respectively.

Equation (27) in Sec. II-B provides an excellent analytic approximation to the neutral cloud radius, R(t) for $R > a_o$. For the case of stationary point releases, we take for the characteristic size of the neutral cloud at one time period, τ_i, after photoionization commences, the expression

$$\bar{a} = 1.2\ a_o \left[\left(\frac{1.15\ \tau_i}{a_o} + S_i \right)^{0.8} - 0.44 \right]^{1/2} \text{ km} \tag{113}$$

where a_o is in km, τ_i is given by Eq. (86), and S_i is a parameter reflecting the time delay before the onset of photoionization. We assume that photoionization commences when the optical depth of the cloud to the metastable-exciting radiation approaches one. This assumption is equivalent to a critical value for the product of the barium density times the cloud radius or

$$\rho_i R_i = \frac{3M_o}{4\pi R_i^2} = 0.34 \text{ kg/km}^2 \qquad (114)$$

where the numerical value was obtained from the Spruce case. If we use Eq. (27) with $S_i = \dot{R}_o t_i / a_o$ in order to evaluate Eq. (114), we obtain

$$S_i = (0.44 + 2\rho_a a_o)^{1.25} \qquad (115)$$

where $\rho_a a_o$ is expressed in kg/km^2. This value used in Eq. (113) determines the dependence of $\bar{a}$ on mass of released gas and altitude.

For the case of a point release at orbital velocity, we take

$$\bar{a} = 2.68\, a_o \left[\left(\frac{1.15\, \tau_i}{a_o} + S_i \right)^{0.8} - 0.44 \right]^{1/2} \text{ km} \qquad (116)$$

which is larger than Eq. (113) by about a factor of 2.3 . Again by applying the criterion (114), we obtain

$$S_i = (0.44 + 0.4\, \rho_a a_o)^{1.25} . \qquad (117)$$

The expressions (115) and (117) are not accurate whenever the corresponding critical radius $R_i < a_o$. This condition occurs only above a critical altitude depending on M_o when $S_i < 0.6$ and is much smaller than the term $1.15\, \tau_i / a_o$ to which it is added. Hence this approximation to $\bar{a}$ does not lead to significant error.

In the case of a venting-mode release, Eq. (76) can be integrated in order to obtain time as a function of wake radius which provides an implicit R(t):

$$K^2V_a(t - t_o) = R(R^2/a^2 + B)^{\frac{1}{2}} + a(2 - B)\ell n[R/a + (R^2/a^2 + B)^{\frac{1}{2}}] \quad (113)$$

where t_o is an arbitrary constant of integration. This equation cannot be inverted to obtain R(t) implicitly but we have found that the expression

$$R(t) = a\left[\frac{K^2V_a}{a}\,t + S_i + 0.2 - \ell n\left(\frac{K^2V_a}{a}\,t + S_i\right)\right]^{1/2} \quad (119)$$

with a in km and K^2V_a = 12.2 km/s provides an adequate representation for the radius for the nominal case for $R \gtrsim 1.2$ a with S_i = 1.24. Because S_i and t are additive, the time t in this equation can be interpreted as the time lapse after photoionization commences if we scale S_i properly with $\rho_a a$ in order to reflect the critical time to reach a critical radius R_i. The criterion (114) in this case reduces to

$$\rho_i R_i = \frac{\dot{M}_o}{V_i \pi R_i} = 0.34 \text{ kg/km}^2 \quad (120)$$

or

$$\frac{V_i R_i}{V_a a} \sim \frac{R_i^2/a}{(R_i^2 + 2.8\ a^2)^{\frac{1}{2}}} = 3\rho_a a \quad (121)$$

with $\rho_a a$ expressed in kg/km^2. The middle expression is an approximate expression which is reasonably accurate for $R_i > 1.2\ a$. By solving this quadratic equation for $(R_i/a)^2$ in terms of $\rho_a a$, using this value in Eq. (118) and adjusting t_o so that $S_i = 4.05$ when $R_i/a = 1.69$ as for Spruce, we obtain the following expression for S_i for the venting mode case,

$$S_i = \frac{R_i}{a}\left(\frac{R_i^2}{a^2} + B\right)^{1/2} + (2 - B)\ell n\left[\frac{R_i}{a} + \left(\frac{R_i^2}{a^2} + B\right)^{\frac{1}{2}}\right] - 1.17 \quad . \qquad (122)$$

Equation (119) then defines the characteristic size of the neutral cloud wake as $\bar{a}' = R(\tau_i)$.

As discussed in Sec. V-A, the transverse scale size of the ion cloud field-line content defined as the half-width at (1/e) of the maximum value is given as

$$a_\perp = 0.7\ \bar{a} \qquad (123)$$

in the case of point releases and

$$a_\perp = 0.57\ \bar{a} \qquad (124)$$

in the case of venting-mode releases.

Figures 21-26 show contours of constant values of the transverse scale size, $a_\perp$, and FLIP conductivity, Σ_p, for the three release mode cases. The shaded portions

of these figures represent regions in which the snowplow models used, applicable only to the intermediate altitude regime, are not valid. The contours should not be used in the shaded regions because their actual form is qualitatively different from those shown. Fortunately, the allowed regions correspond to regions of many interesting suggested experiments.

As a typical result, a 48 kg barium release at 190 km altitude will produce a FLIP conductivity of approximately 30 mho, several times the ambient ionospheric conductivity, and will have a transverse scale size just less than 3 km. The extra energy available in the shuttle release causes the gas to expand faster resulting in the barium ionization being spread over a larger area. The correspondingly lower density of ionization results in lower conductivity. If the same amount of chemical payload is released from shuttle, the resulting conductivity is lower by a factor of 5 from that produced by a release from a rocket and the transverse size of the ion cloud is increased by a factor of approximately 2.3.

As time passes, the conditions envisioned by this modeling change and the distribution of ionization both parallel and perpendicular to $\vec{B}$ chang.. After about a minute following release the ionization clouds

that are produced have the characteristics that we have described. Beyond this time, the distribution of ionization along the magnetic field is governed by Eq. (87) with the right-hand side equal to zero. The z-component of the ionization velocity is given by

$$v_{iz} = v_{nz} + g_z\tau + k(T_e + T_i)\tau \frac{\partial}{\partial z} \ln(n_i) \qquad (125)$$

where v_{nz} and g_z are the components of the neutral wind velocity and gravity parallel to $\vec{B}$, respectively, T_e and T_i are the electron and ion temperatures, respectively, and τ is the ion-neutral collision time given by Eq. (106). The resulting evolution of the distribution parallel to $\vec{B}$ as a result of neutral wind, gravity and pressure gradients in an exponentially varying atmosphere whose effective number density, $\bar{n}$, defined in Eq. (107), varies as

$$\bar{n}(h) = \bar{n}(h_r) \exp[-(h - h_r)/H_n] \qquad (126)$$

has been discussed in detail in Sec. 4 of Ref. 7. Initially the distribution is Gaussian, then the peak density descends in altitude and the distribution in altitude evolves into a Chapman-like layer with the density falling off rapidly on the underside and exponentially on the top side. An analytical solution of Eq. (87) for $n_i(z,t)$ with v_{iz} given by Eq. (125) has been obtained

that describes the evolution as a function of time for various models of altitude-dependent neutral winds. By analytically integrating the solution, the remarkable result was obtained that at a later time when the peak in the ionization density has descended to altitude h, the FLIP conductivity has the simple value

$$\Sigma_p(h) = \Sigma_p(h_r)\exp[-(h - h_r)/H_n] \ . \qquad (127)$$

We remark that this fully-time-dependent result obtained in Ref. 7 does not require that z be in the vertical direction, and that the winds can be either constant or altitude dependent with an exponential profile.

In the direction transverse to the magnetic field, the situation is far more complex. A neutral wind blowing across a plasma gradient leads to the well-known gradient-drift instability.[12] The result is that the coherent picture of a conductivity modification no longer applies because the ionization striates. The typical time scale for point releases from rockets between 150 and 250 km for striations to onset is 5 to 20 minutes. Simple theoretical modeling indicates that this onset time scales with $\zeta a / v_n$ where ζ is a factor that depends on the magnitude of the conductivity enhancement and typically lies between 5 and 20. Hence, concepts to affect ionospheric and magnetospheric current flows by

conductivity enhancements such as we have been describing can probably only be planned for the first 10 minutes following release.

References

[1] L. M. Linson, "AMPS Experiments Involving Gas Releases", AAS Advances in the Astronautical Sciences, 32, Part 2, 501 (1977).

[2] J. Nogl, ed., "Experiment Summary Document", TRW No. 33476-6001-RV-00, Appendix to Chemical Release Module, A Multi-user Facility for Shuttle Spacelab, AMPS Chemical Release Facility Definition Team, J. Heppner, Leader, Goddard Space Flight Center, Greenbelt, Maryland (1978).

[3] D. C. Baxter and L. M. Linson, "Dynamics of Gas Clouds Released from Spacelab", Science Applications, Inc., La Jolla, California, in preparation (1979).

[4] D. C. Baxter and L. M. Linson, "Dynamics of Gas Clouds Released at Satellite Orbital Velocity", in Rarefied Gas Dynamics, ed. J. L. Potter, American Institute of Aeronautics and Astronautics, New York, New York, 51, 477 (1977).

[5] G. W. Stuart, "Explosions in Rarefied Atmospheres," Phys. Fluids, 8, 603 (1965).

[6]P. A. Bernhardt, "High Altitude Vapor Releases from the Space Shuttle", EOS, Trans. AGU, 59, 1162 (1978), to be published in J. Geophys. Res.

[7]L. M. Linson and D. C. Baxter, "Ion Cloud Modeling", DNA 4455F, (SAI-77-918-LJ), Science Applications, Inc., La Jolla, California, (November 1977).

[8]G. Haerendel, R. Lüst, and B. Meyer, "MPI Analysis of Observations," in Barium Releases at Altitudes Between 200 and 1000 Kilometers," NASA SP-264, pp. 15-46, 1971.

[9]N. W. Rosenberg, G. T. Best, F. P. Delgreco, M. M. Klein, M. A. Macleod, T. M. Noel, W. K. Vickery, "AFCRL Barium Release Studies 1967," reissued as Special Report #4, pp. 1-48, Standford Research Institute, Menlo Park, Calif. 94025, January 1969.

[10]J. Heppner, private communication (1978).

[11]J. H. Mitchell and K. E. W. Ridler, "The Speed of Positive Ions in Nitrogen," Proc. Roy. Soc., (London), A146, 911, 1934.

[12]L. M. Linson and J. B. Workman, "Formation of Striations in Ionospheric Plasma Clouds," J. Geophys. Res., Vol. 75, p. 3211 (1970).

Figure Captions

FIG. 1. Cloud radius vs. time for various values of the ratio of specific heats, γ, and density profile parameter, α. Translational velocity at release is 7.8 km/s except for the curve u=0.

FIG. 2. Temperature, radius, and distance traveled vs. time for a 100 kg gas release at orbital velocity at 200 km altitude.

FIG. 3. The evolution of the normalized density distribution, $g(z, \tau_D)$, from an initial flat-top to a Gaussian as a result of diffusion for several values of the diffusion parameter τ_D.

FIG. 4. The evolution of the normalized density distribution, $g(z, \tau_D)$, from an initial shell to a Gaussian as a result of diffusion for several values of the diffusion parameter τ_D.

FIG. 5. Normalized diffusion function $\bar{\tau}$ (s) for a gas with γ=5/3 in terms of which the diffusion parameter τ_D is defined according to Eq. (38). The dashed curves

show the values of $\bar{\tau}(s)$ if the snowplow were stopped at s=18 and 46 respectively.

FIG. 6. Number density, n, mass density, ρ_a, and mean-free-path, λ, as a function of altitude based on the CIRA 1972 model atmosphere. Note the logarithmic altitude scale. The solid curves correspond to an exospheric temperature $T_{ex} = 1200^{\circ}$; the dashed curves correspond to $T_{ex} = 700^{\circ}$ and 2000°.

FIG. 7. Contours of constant characteristic length, a, for a CIRA 1972 model atmosphere with $T_{ex} = 1200^{\circ}$ in the altitude versus mass-venting-rate plane. The dashed curves show the shape of the contours for $T_{ex} = 700^{\circ}$ and 2000°.

FIG. 8. Contours of constant a/λ in the altitude versus mass-venting-rate plane. The dashed curves show the shape of the contours for $T_{ex} = 700^{\circ}$ and 2000°.

FIG. 9. Radial expansion velocity as a function of normalized radius for different density profiles and specific internal energies.

FIG. 10. Radial expansion velocity as a function of normalized radius for different assumed initial velocities.

FIG. 11. Radial expansion velocity as a function of normalized radius for different values of the ratio of specific heats.

FIG. 12. Temperature, defined according to Eq. (56), as a function of normalized radius for different assumed initial expansion velocities and ambient atmospheric temperature.

FIG. 13. Temperature, defined according to Eq. (56), as a function of normalized radius for different values of the ratio of specific heats.

FIG. 14. Axial velocity in the rest frame of the canister as a function of normalized radius for different assumed initial expansion velocities.

FIG. 15. Normalized radius versus normalized axial position for various values of gas release parameters plotted on a logarithmic scale.

FIG. 16. Normalized radius versus normalized axial position for various values of gas release parameters plotted on a linear scale.

FIG. 17. Normalized radius versus normalized axial position for different assumed initial expansion velocities plotted on a logarithmic scale.

FIG. 18. Normalized travel distance versus normalized axial position for different density profiles and specific internal energies.

FIG. 19. Normalized travel distance versus normalized axial position for different assumed initial expansion velocities.

FIG. 20. Normalized travel distance versus normalized axial position for different values of the ratio of specific heats.

FIG. 21. Contours of constant transverse scale size of the conductivity modification in the altitude versus chemical payload weight plane for point barium releases from rockets. In this and the next 5 figures the model is invalid in the shaded regions.

FIG. 22. Contours of constant field-line-integrated Pedersen conductivity in the altitude versus chemical payload weight plane for point barium releases from rockets.

FIG. 23. Contours of constant transverse scale size of the conductivity modification in the altitude versus chemical payload weight plane for point barium releases at orbital velocity.

FIG. 24. Contours of constant field-line-integrated Pedersen conductivity in the altitude versus chemical payload weight plane for point barium releases at orbital velocity.

FIG. 25. Contours of constant transverse scale size of the conductivity modification in the altitude versus chemical payload release-rate plane for venting mode releases at orbital velocity.

FIG. 26. Contours of constant field-line-integrated Pedersen conductivity in the altitude versus chemical payload release-rate plane for venting mode releases at orbital velocity.

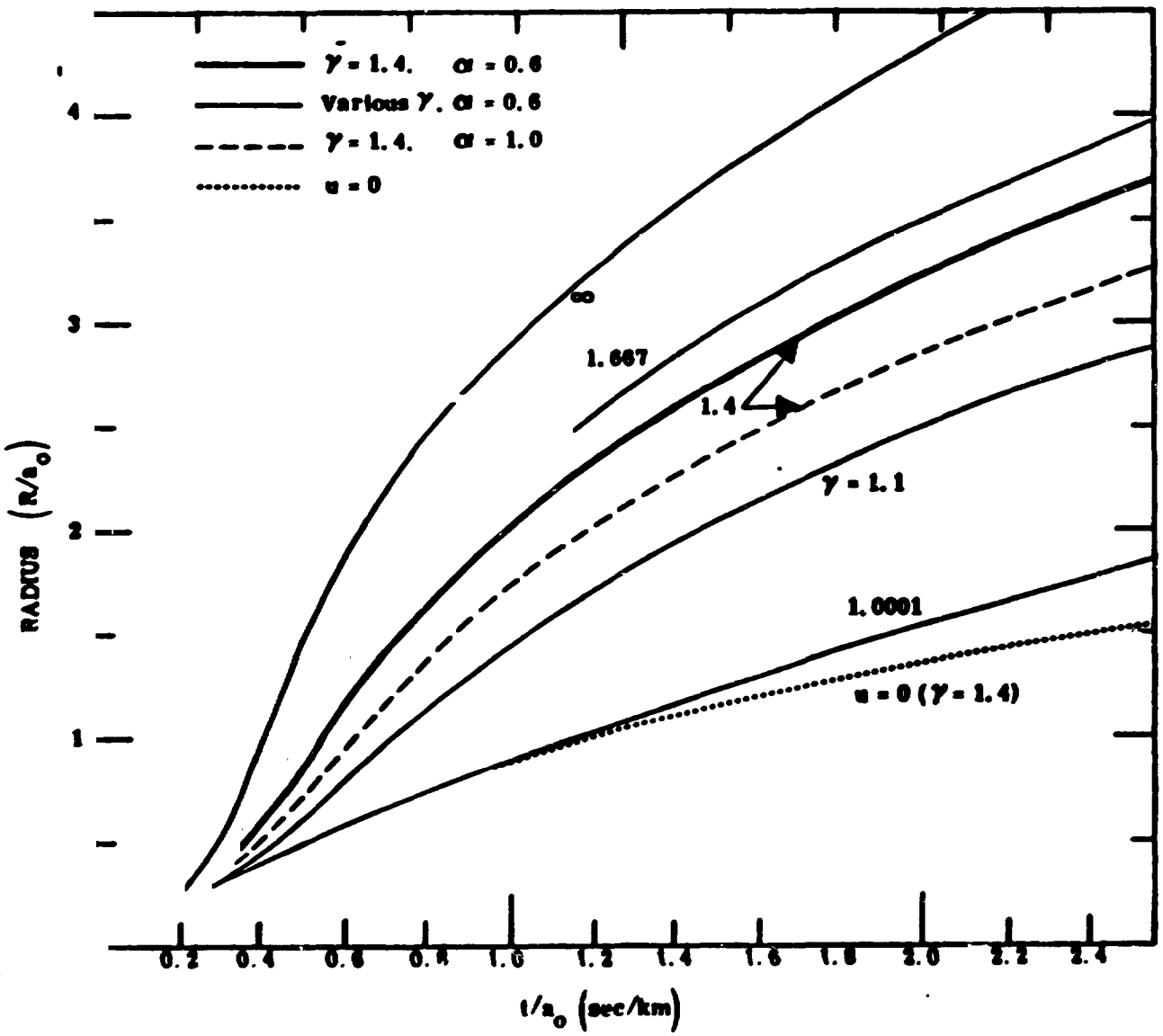

FIG. 1. Cloud radius vs. time for various values of the ratio of specific heats, γ, and density profile parameter, α. Translational velocity at release is 7.8 km/s except for the curve u = 0.

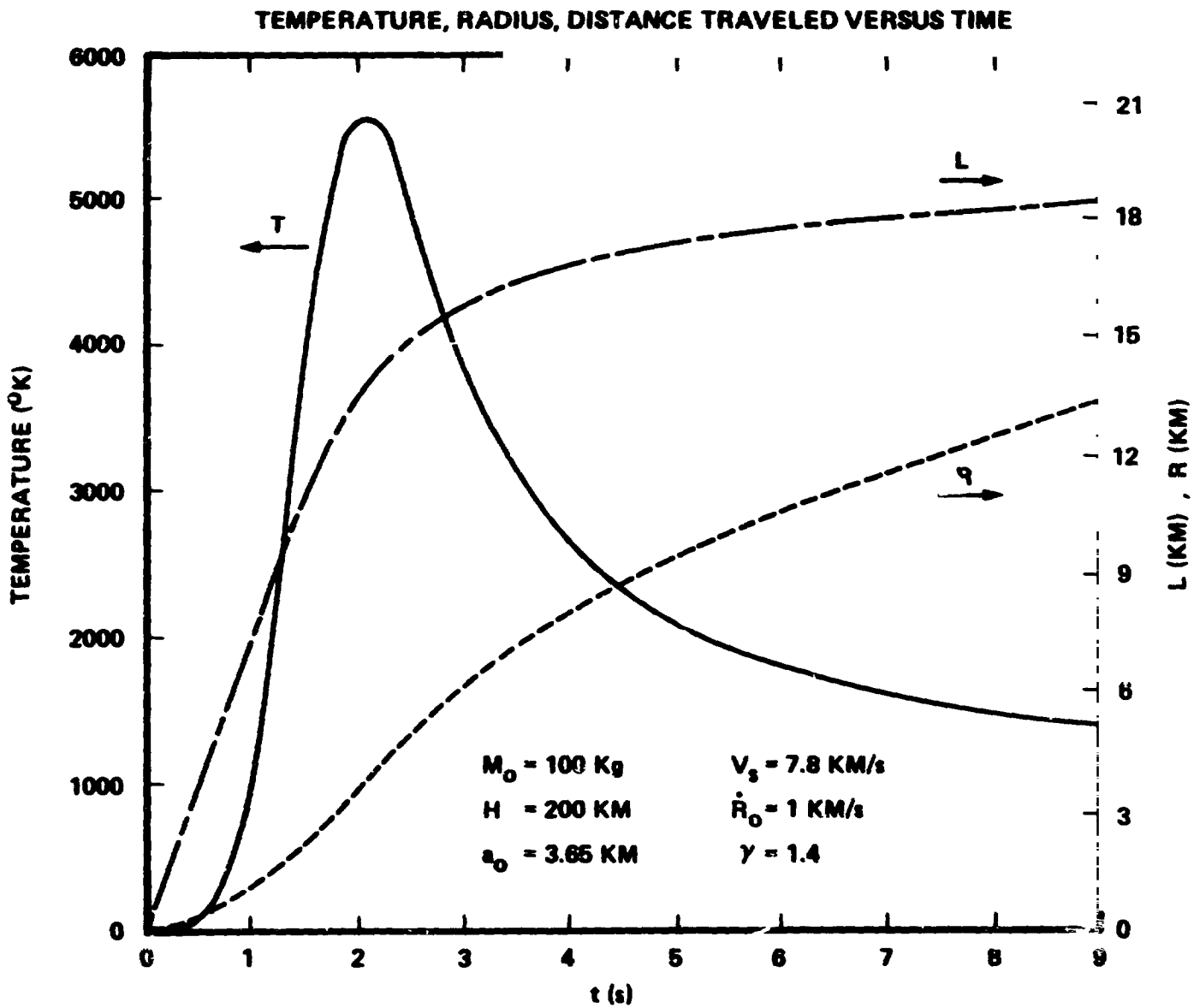

FIG. 2. Temperature, radius, and distance traveled vs. time for a 100 kg gas release at orbital velocity at 200 km altitude.

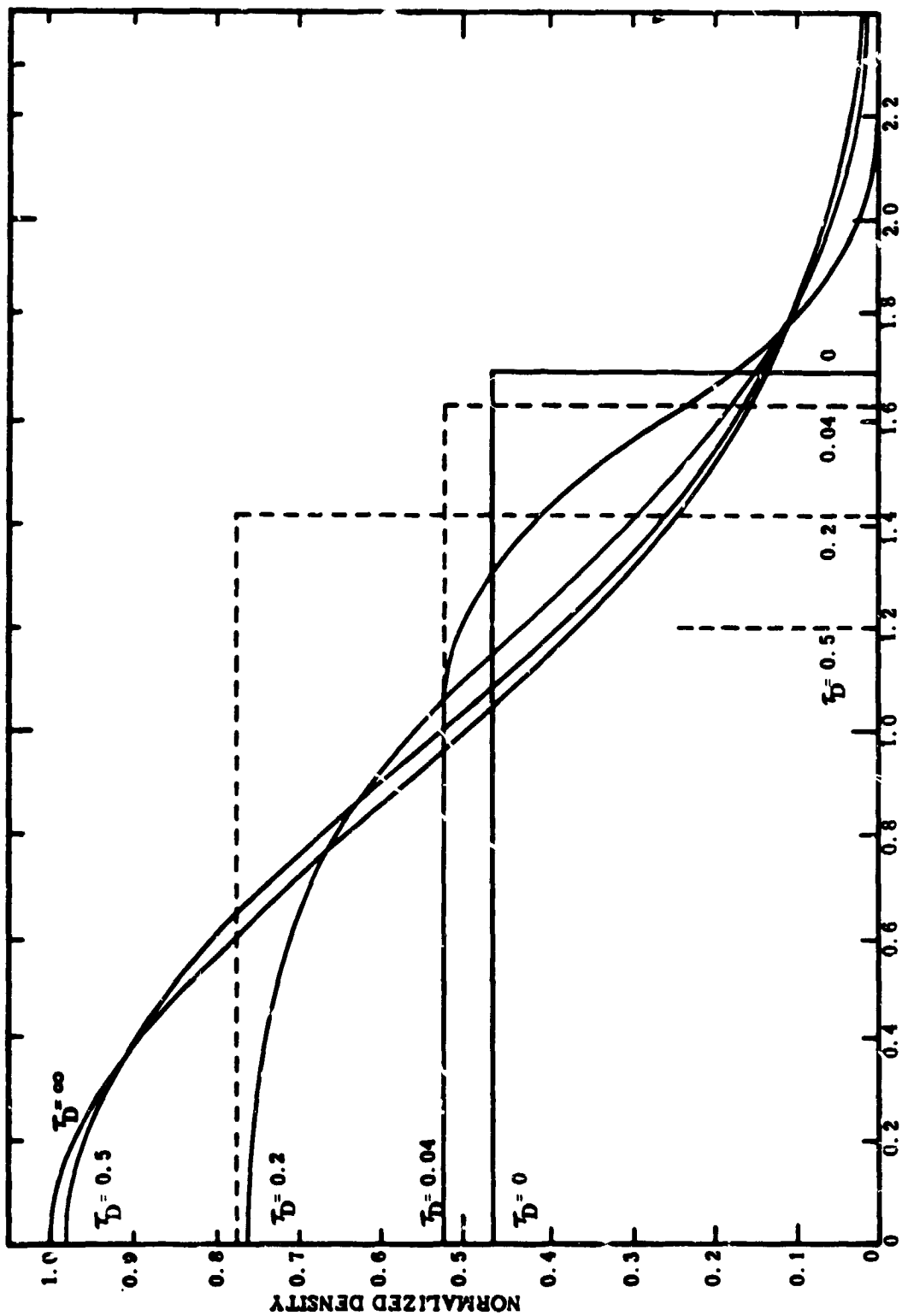

FIG. 3. The evolution of the normalized density distribution, $g(z, \tau_D)$, from an initial flat-top to a Gaussian as a result of diffusion for several values of the diffusion parameter τ_D.

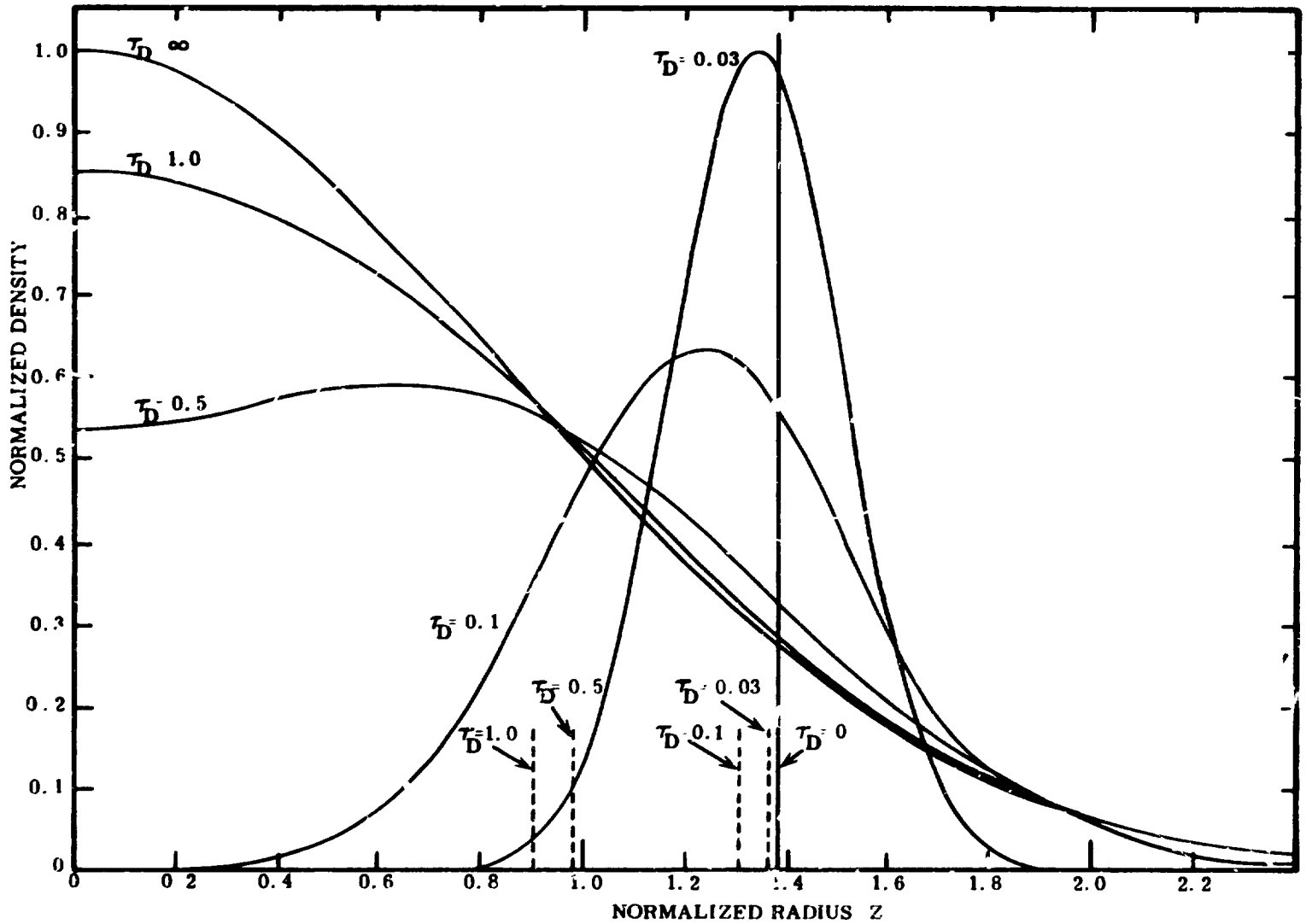

FIG. 4. The evolution of the normalized density distribution, $g(z, \tau_D)$, from an initial shell to a Gaussian as a result of diffusion for several values of the diffusion parameter τ_D.

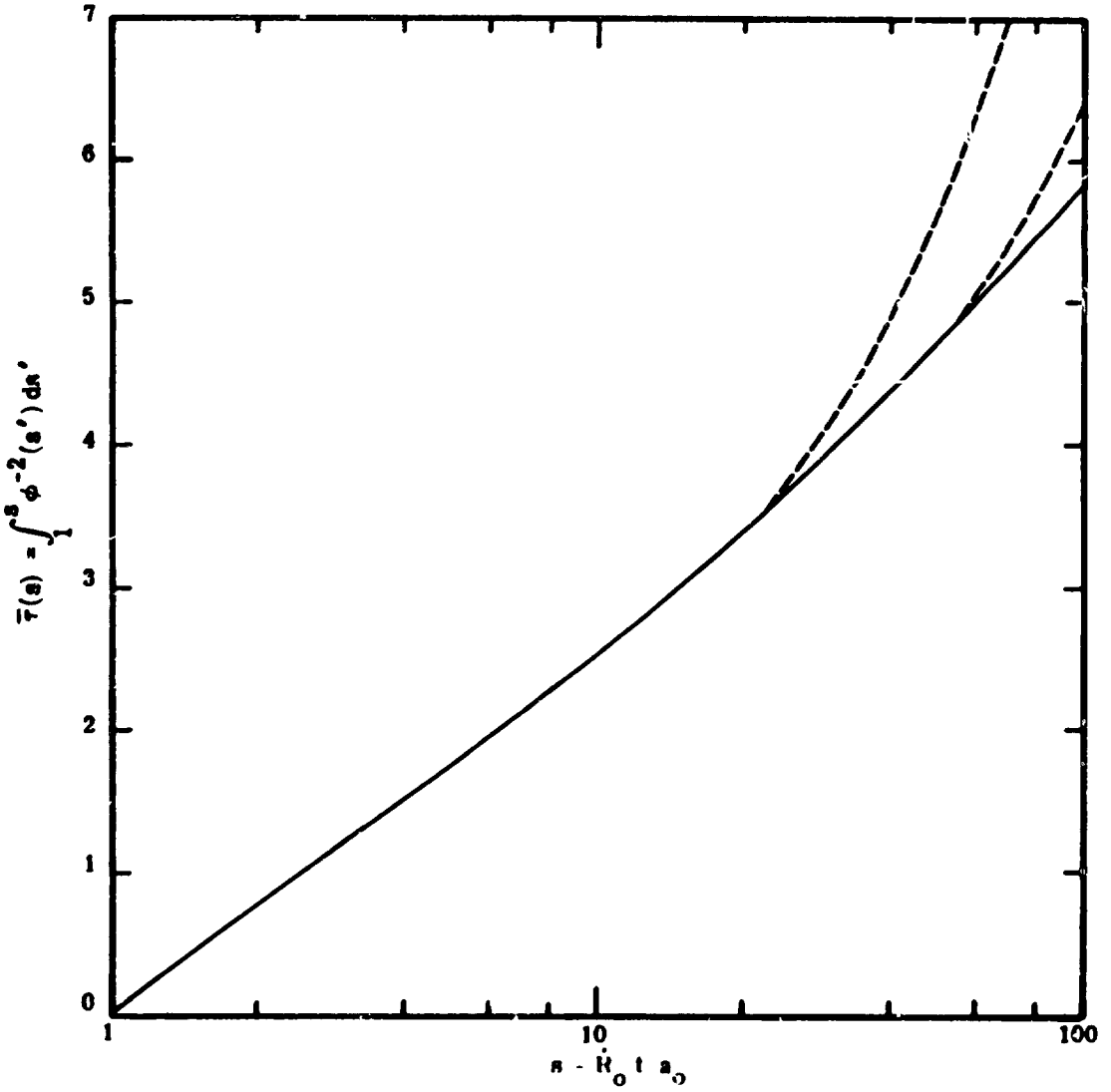

FIG. 5. Normalized diffusion function $\bar{\tau}$ (s) for a gas with $\gamma = 5/3$ in terms of which the diffusion parameter τ_D is defined according to Eq. (38). The dashed curves show the values of $\bar{\tau}$ (s) if the snowplow were stopped at s = 18 and 46 respectively.

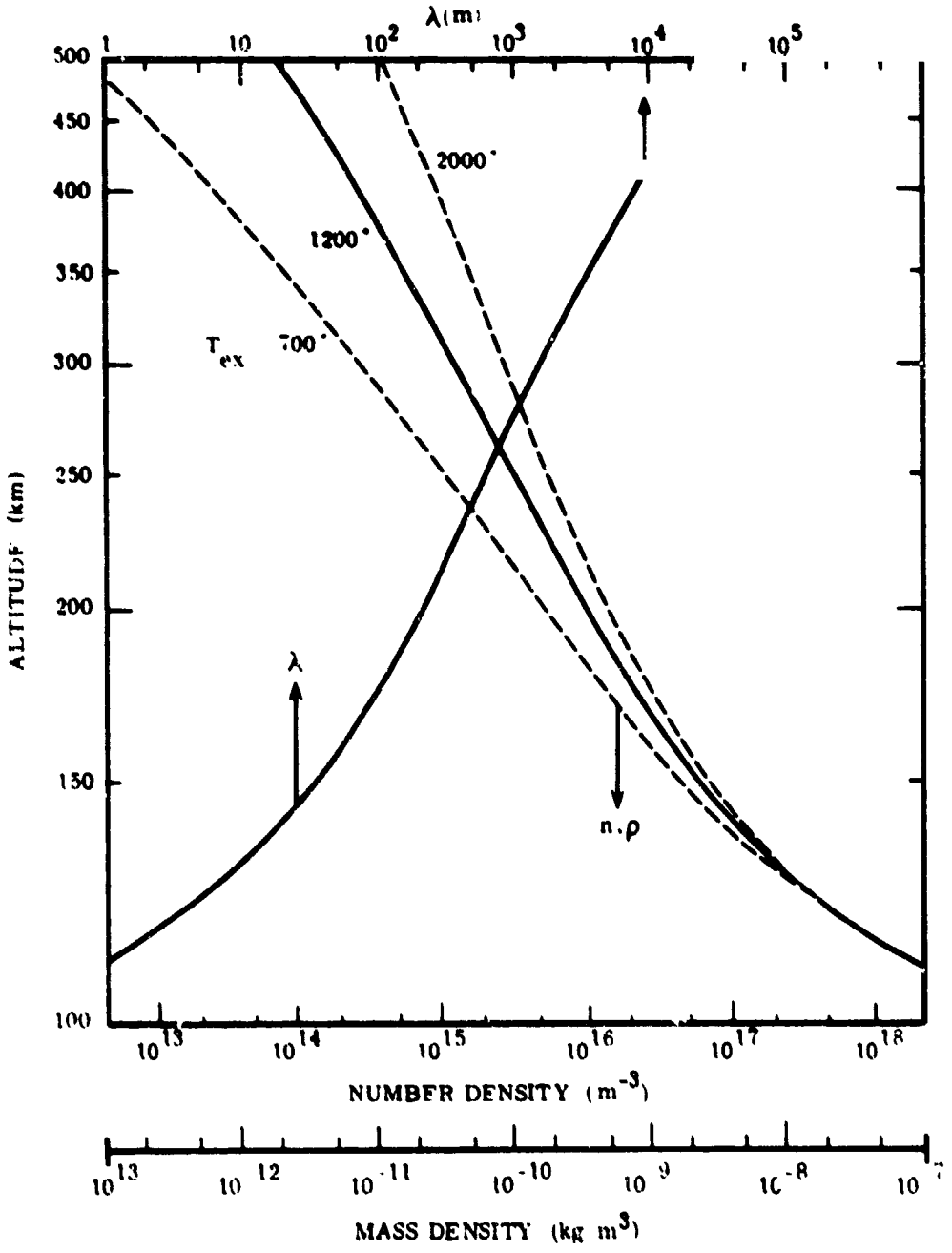

FIG. 6. Number density, n, mass density, ρ_g, and mean-free-path, λ, as a function of altitude based on the CIRA 1972 model atmosphere. Note the logarithmic altitude scale. The solid curves correspond to an exospheric temperature T_{ex} = 1200°; the dashed curves correspond to T_{ex} = 700° and 2000°.

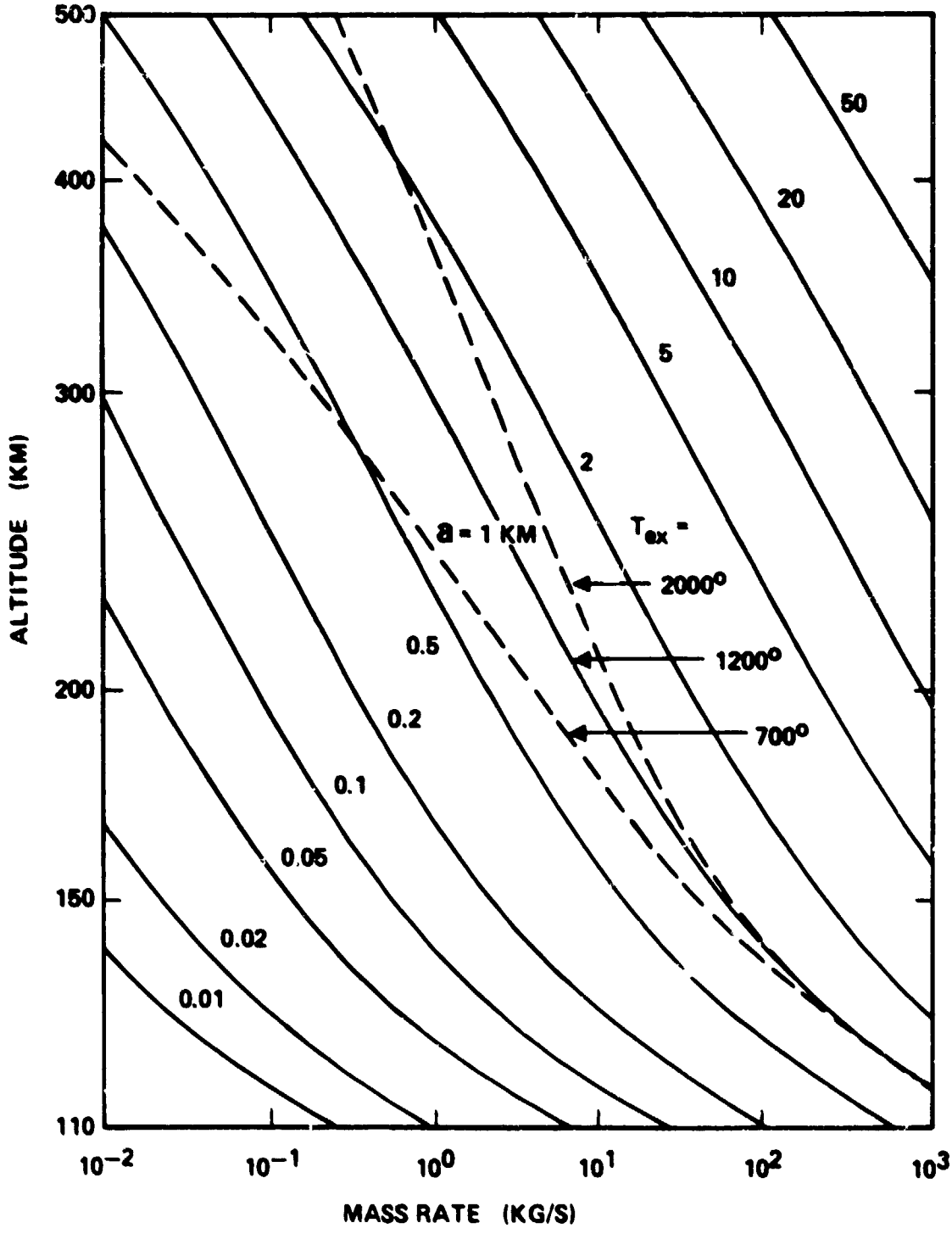

FIG. 7. Contours of constant characteristic length, a, for a CIRA 1972 model atmosphere with $T_{ex} = 1200^{o}$ in the altitude versus mass-venting-rate plane. The dashed curves show the shape of the contours for $T_{ex} = 700^{o}$ and 2000^{o}.

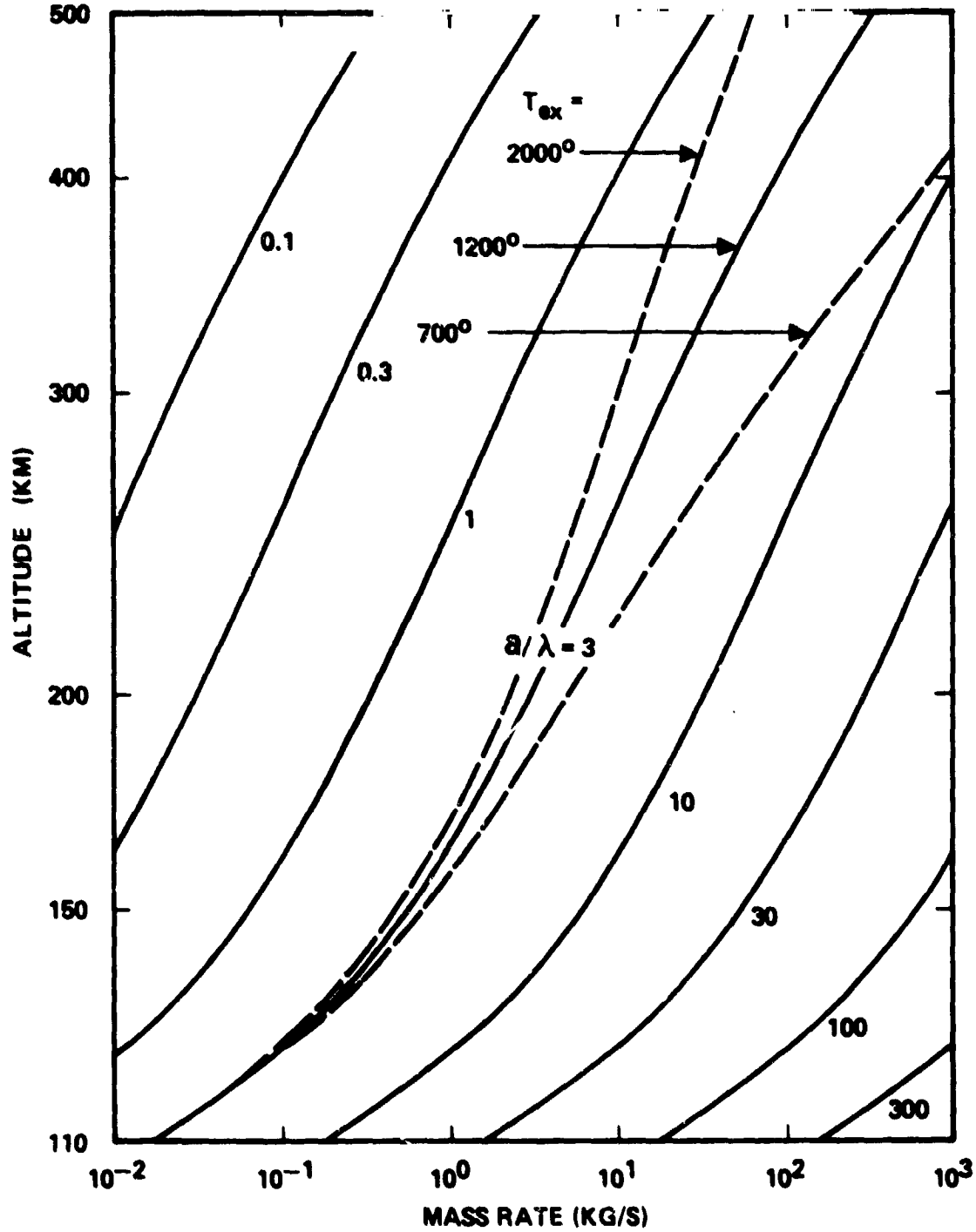

FIG. 8. Contours of constant a/λ in the altitude versus mass-venting-rate plane. The dashed curves show the shape of the contours for T_{ex} = 700° and 2000°.

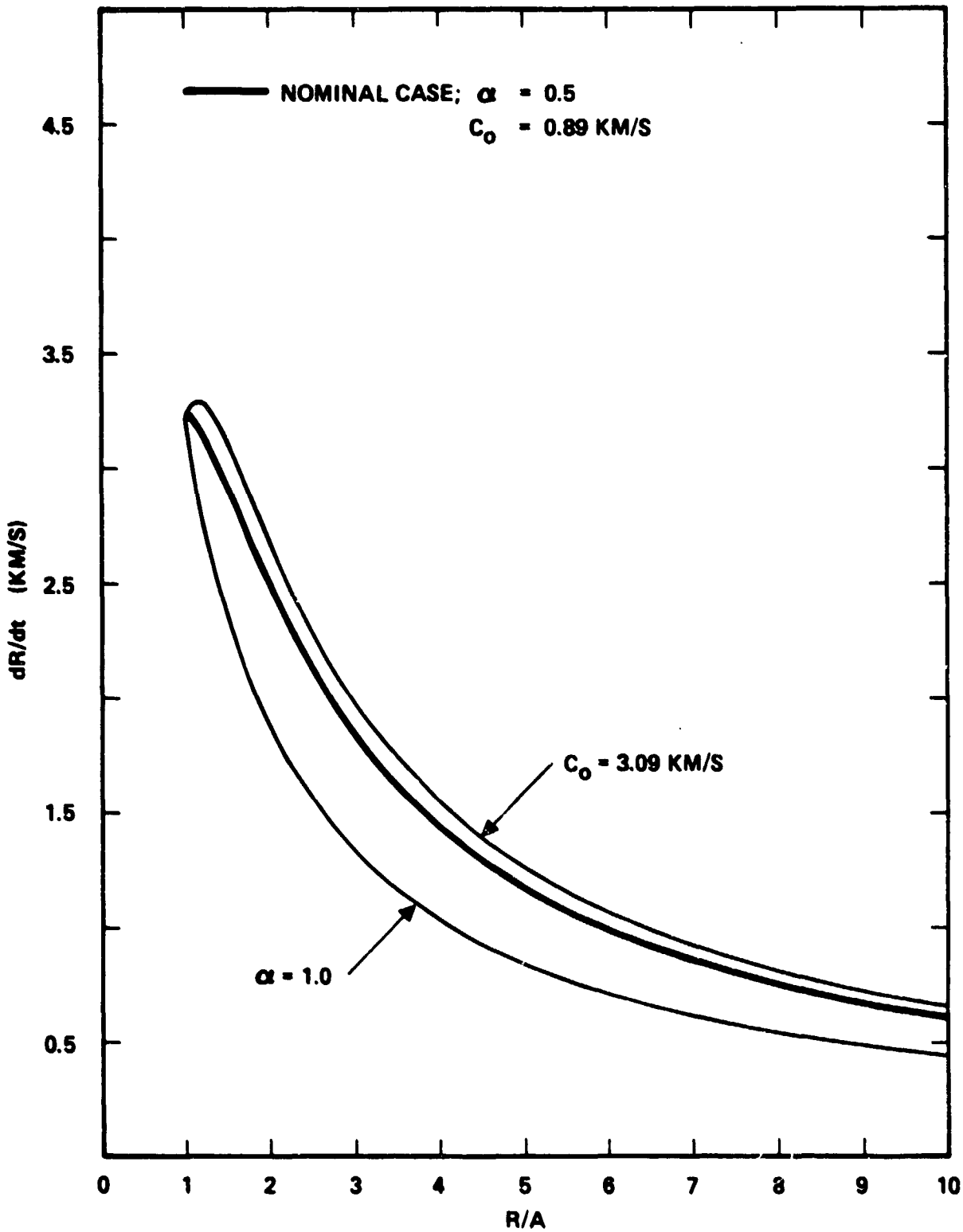

FIG. 9. Radial expansion velocity as a function of normalized radius for different density profiles and specific internal energies.

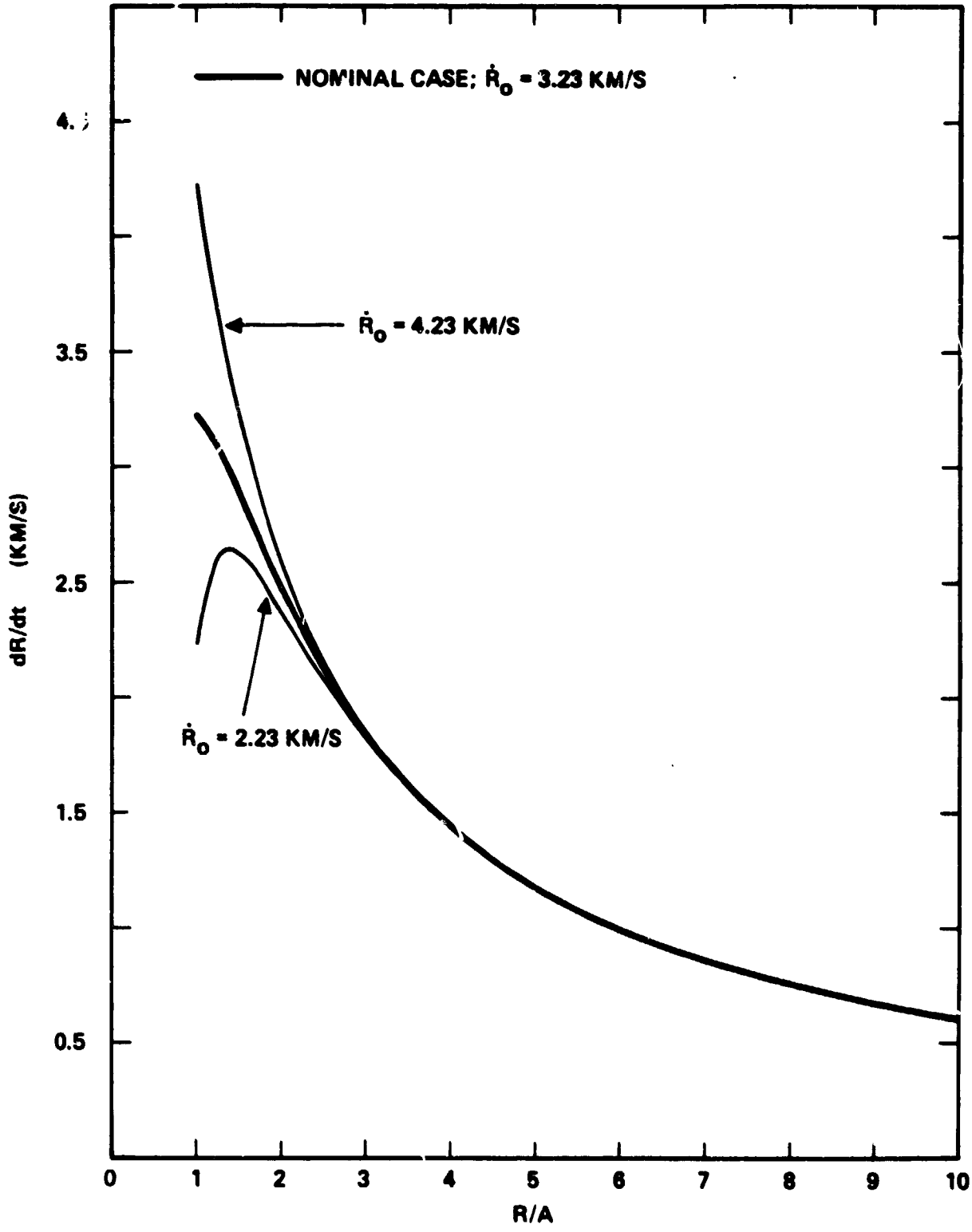

FIG. 10. Radial expansion velocity as a function of normalized radius for different assumed initial velocities.

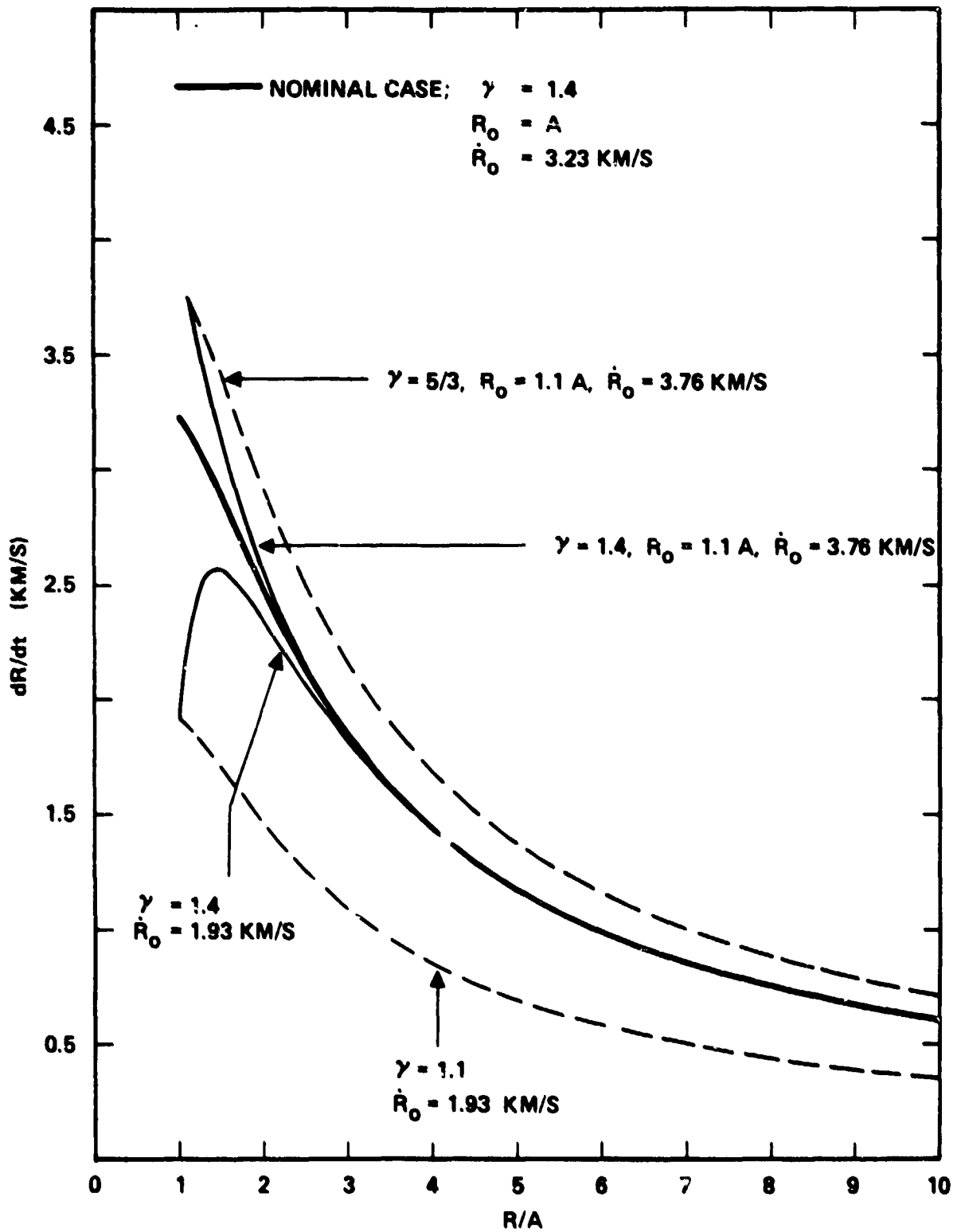

FIG. 11. Radial expansion velocity as a function of normalized radius for different values of the ratio of specific heats.

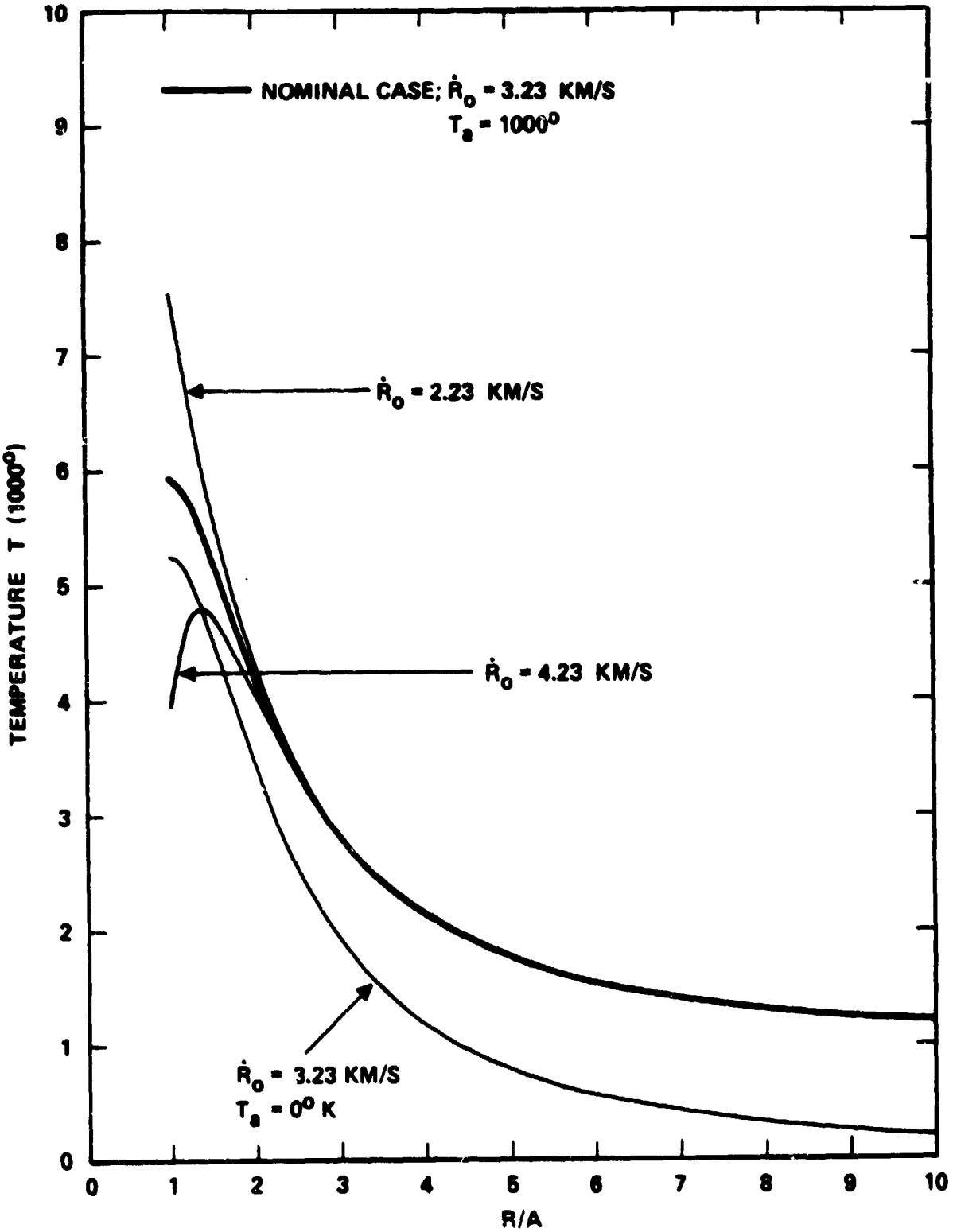

FIG. 12. Temperature, defined according to Eq. (56), as a function of normalized radius for different assumed initial expansion velocities and ambient atmospheric temperature.

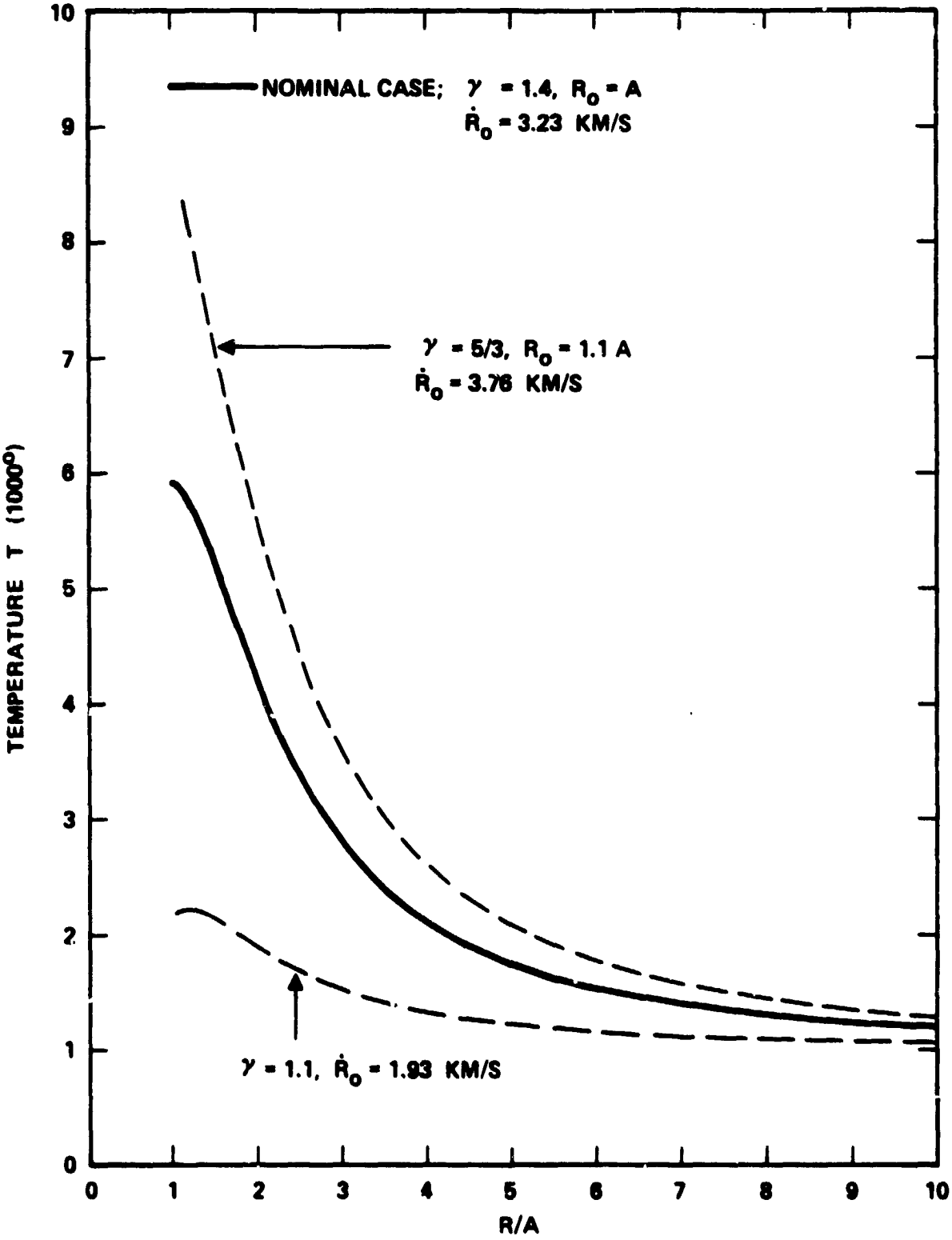

FIG. 13. Temperature, defined according to Eq. (56), as a function of normalized radius for different values of the ratio of specific heats.

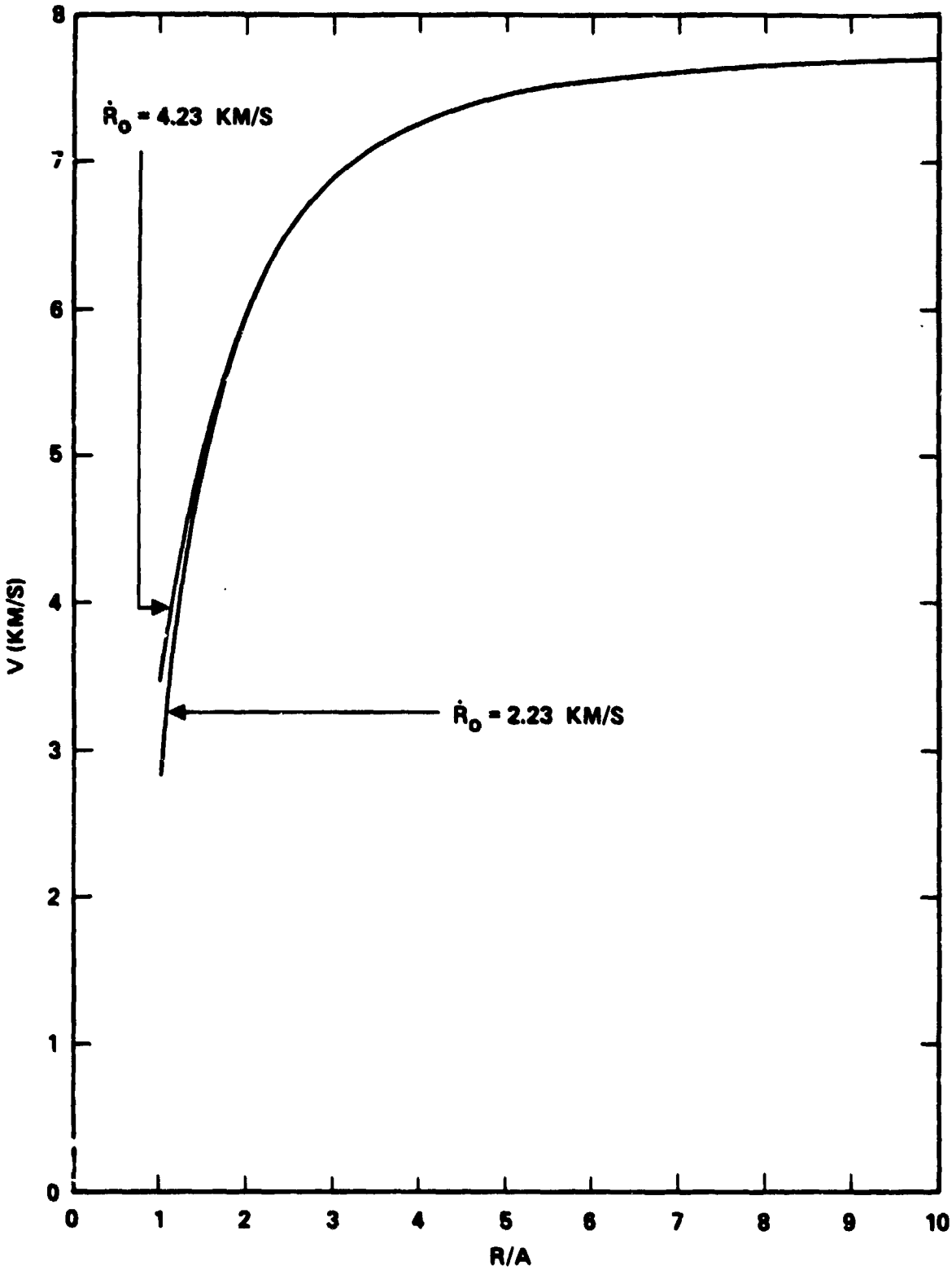

FIG. 14. Axial velocity in the rest frame of the canister as a function of normalized radius for different assumed initial expansion velocities.

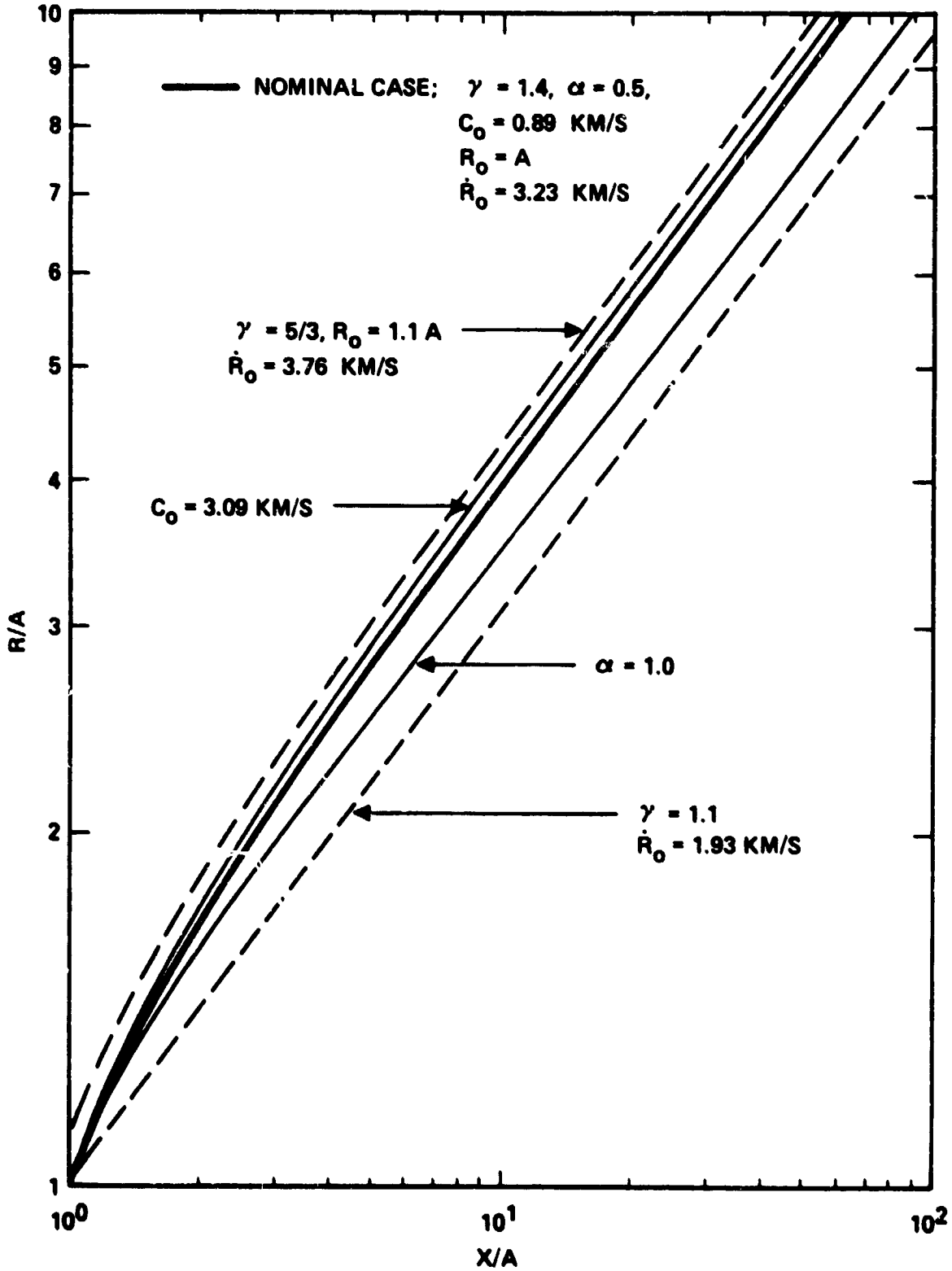

FIG. 15. Normalized radius versus normalized axial position for various values of gas release parameters plotted on a logarithmic scale.

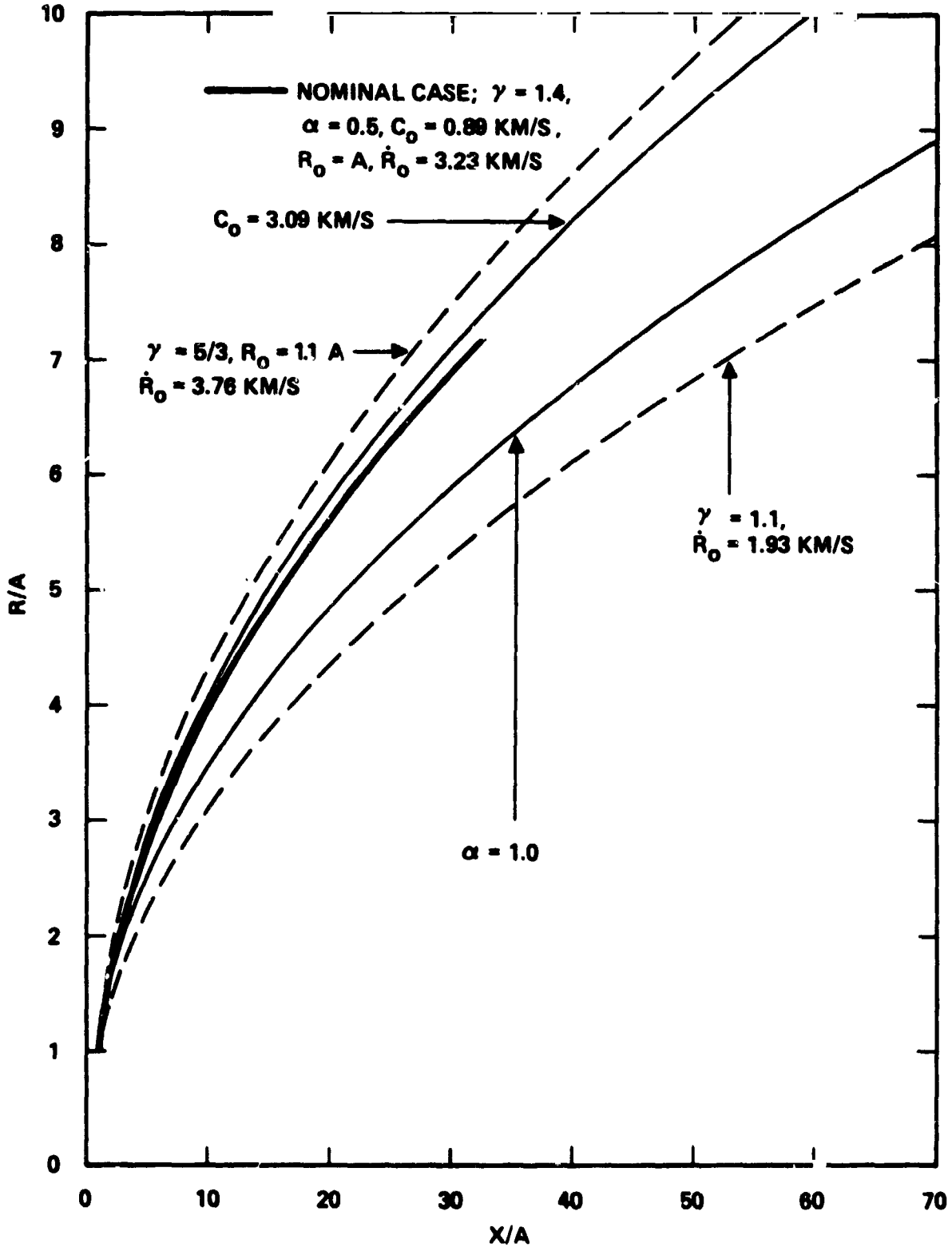

FIG. 16. Normalized radius versus normalized axial position for various values of gas release parameters plotted on a linear scale.

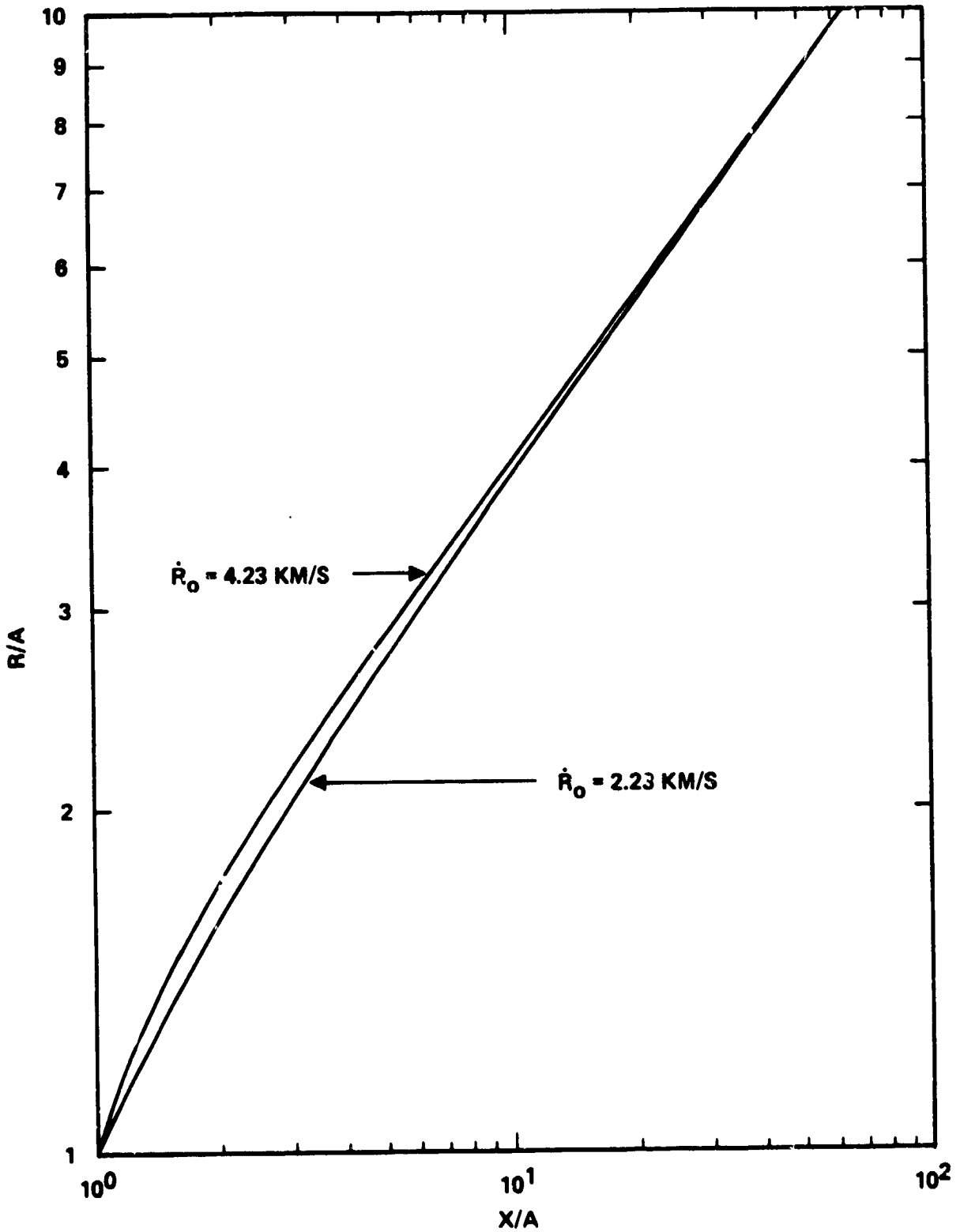

FIG. 17. Normalized radius versus normalized axial position for different assumed initial expansion velocities plotted on a logarithmic scale.

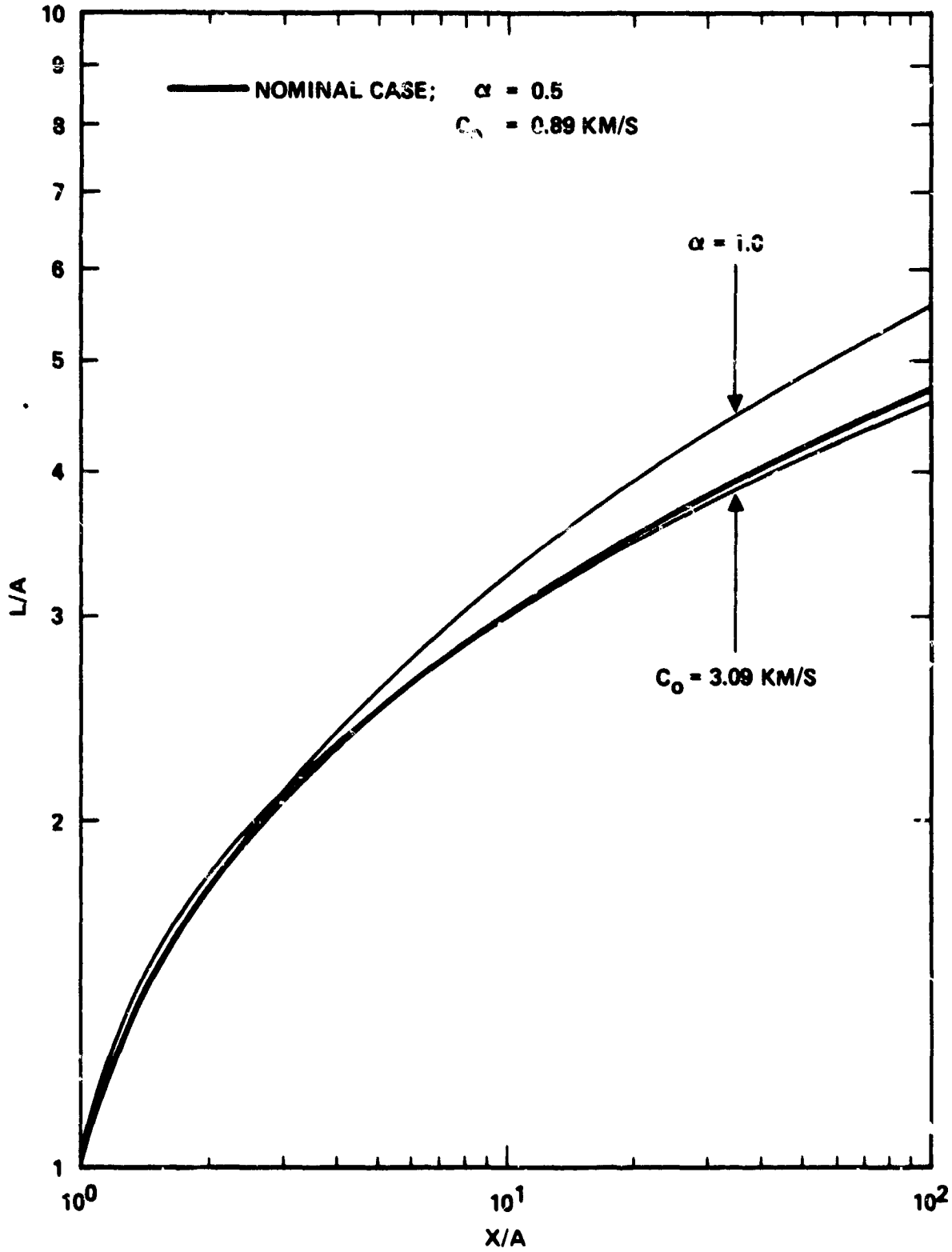

FIG. 18. Normalized travel distance versus normalized axial position for different density profiles and specific internal energies.

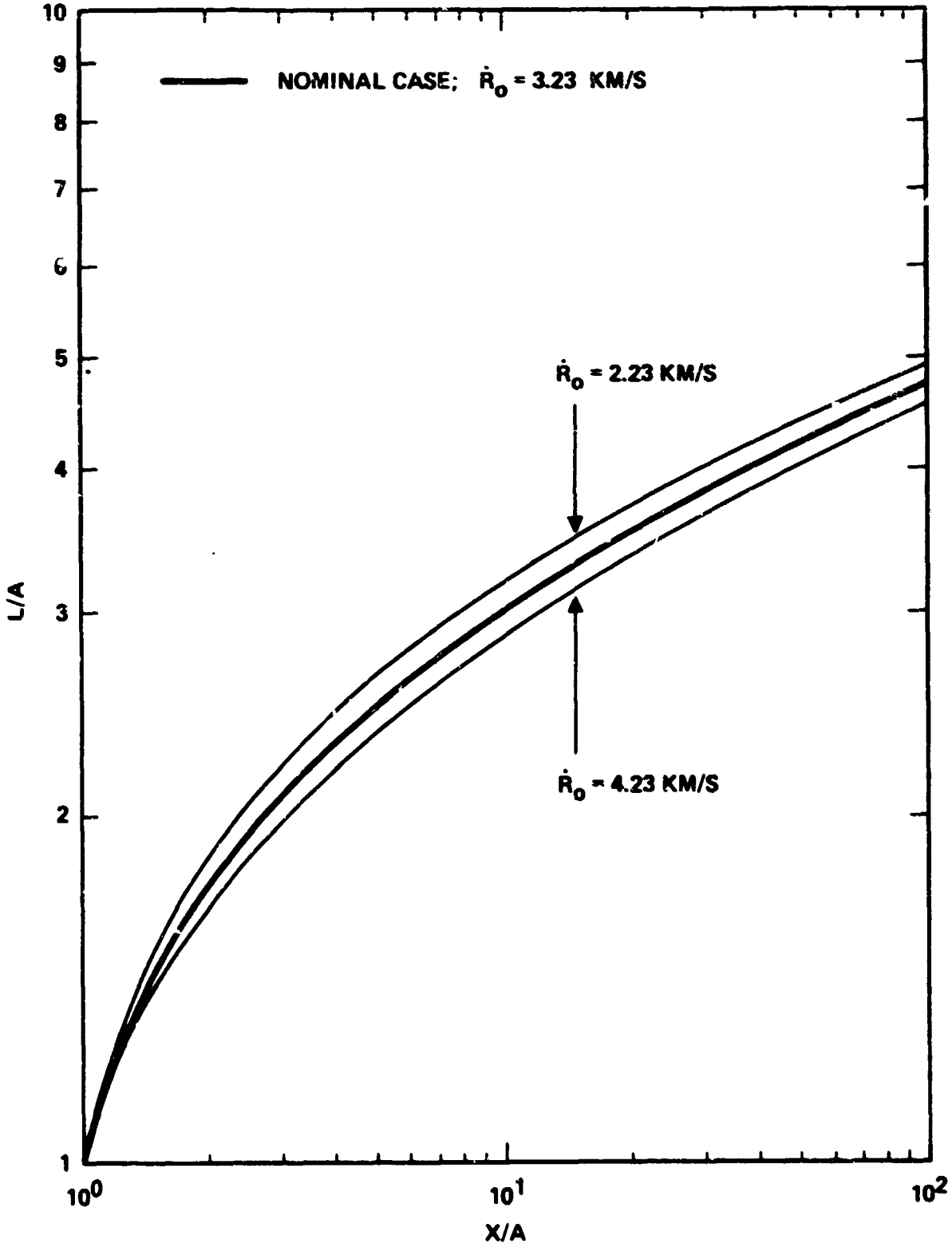

FIG. 19. Normalized travel distance versus normalized axial position for different assumed initial expansion velocities.

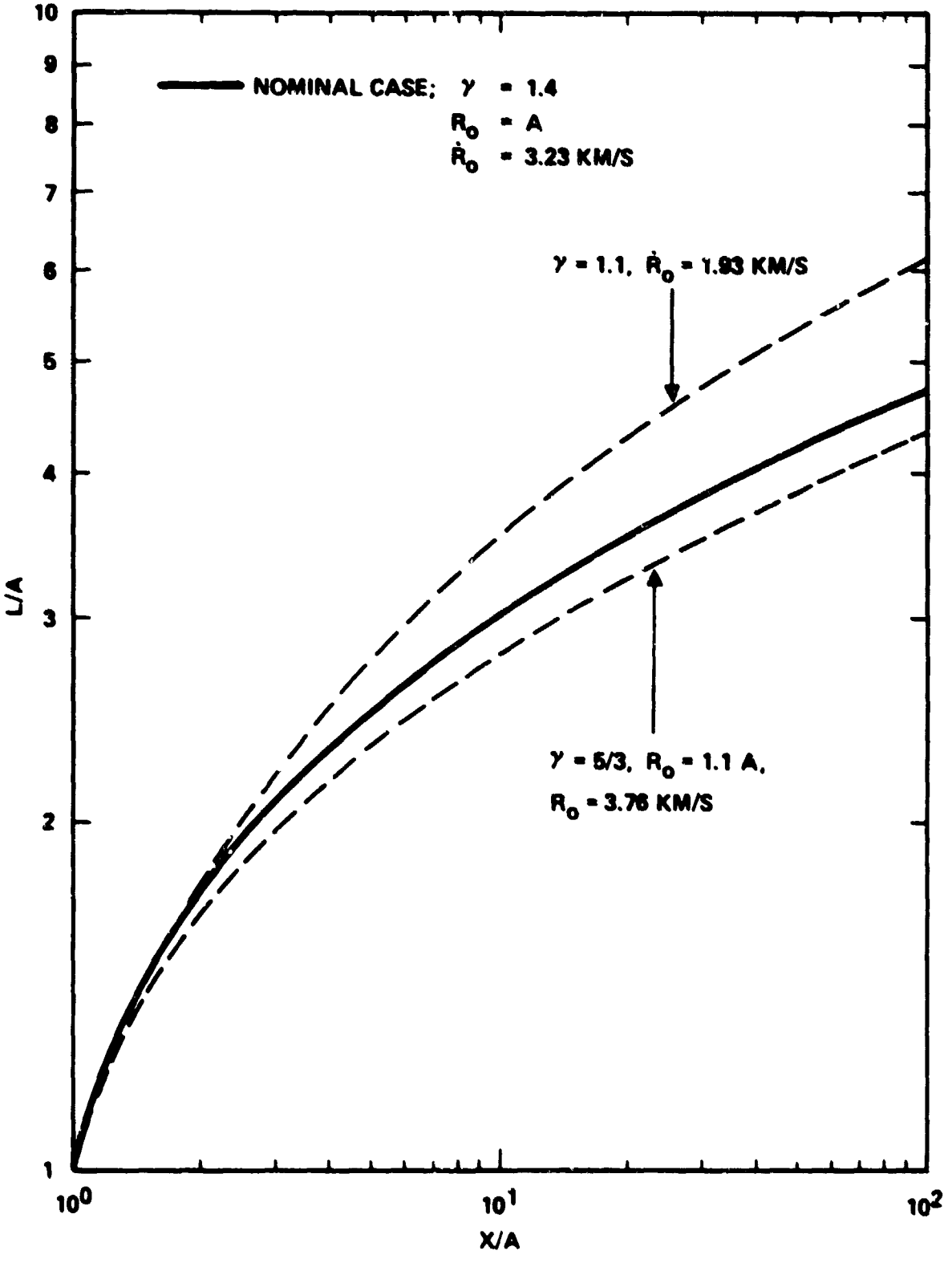

FIG. 20. Normalized travel distance versus normalized axial position for different values of the ratio of specific heats.

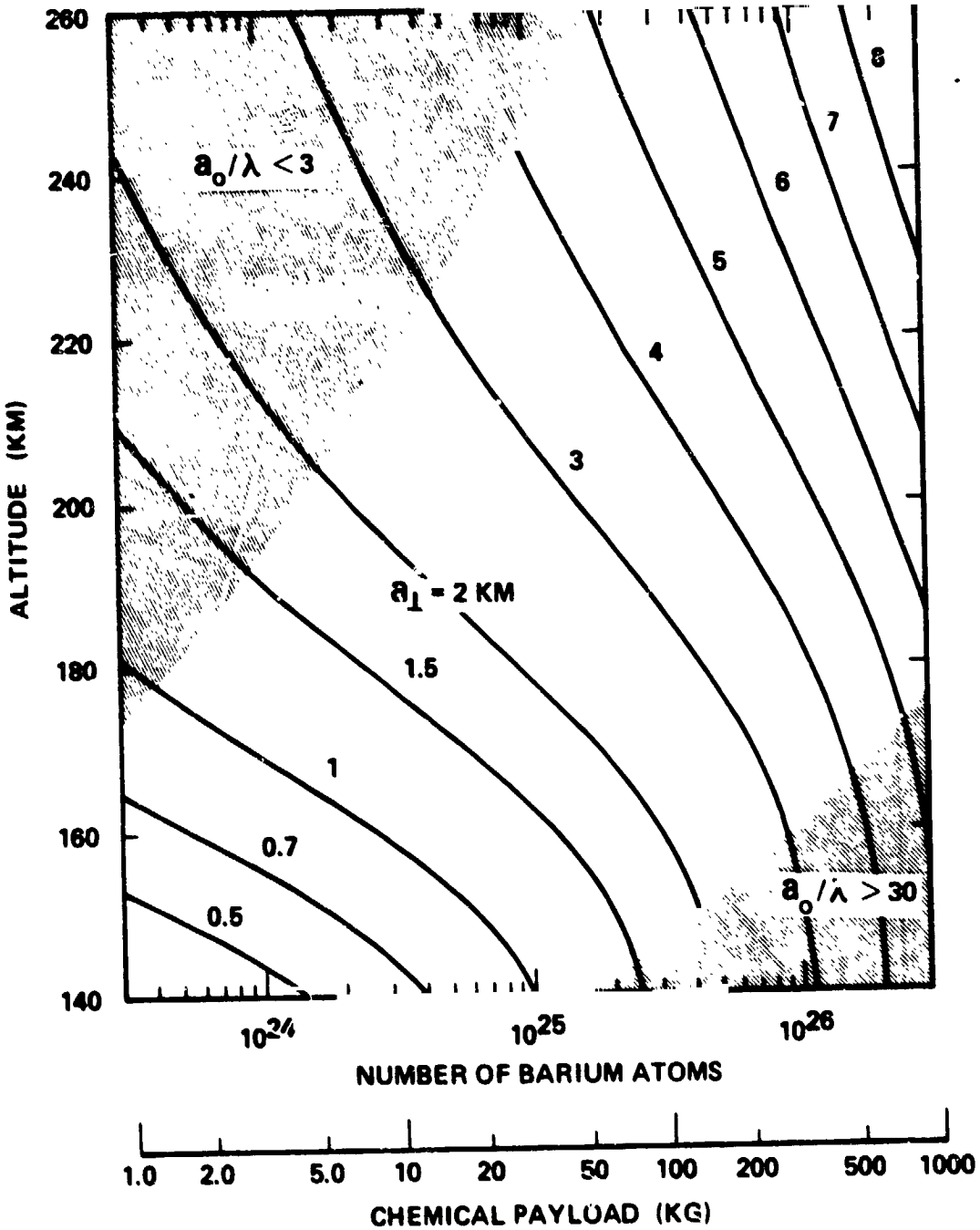

FIG. 21. Contours of constant transverse scale size of the conductivity modification in the altitude versus chemical payload weight plane for point barium releases from rockets. In this and the next 5 figures the model is invalid in the shaded regions.

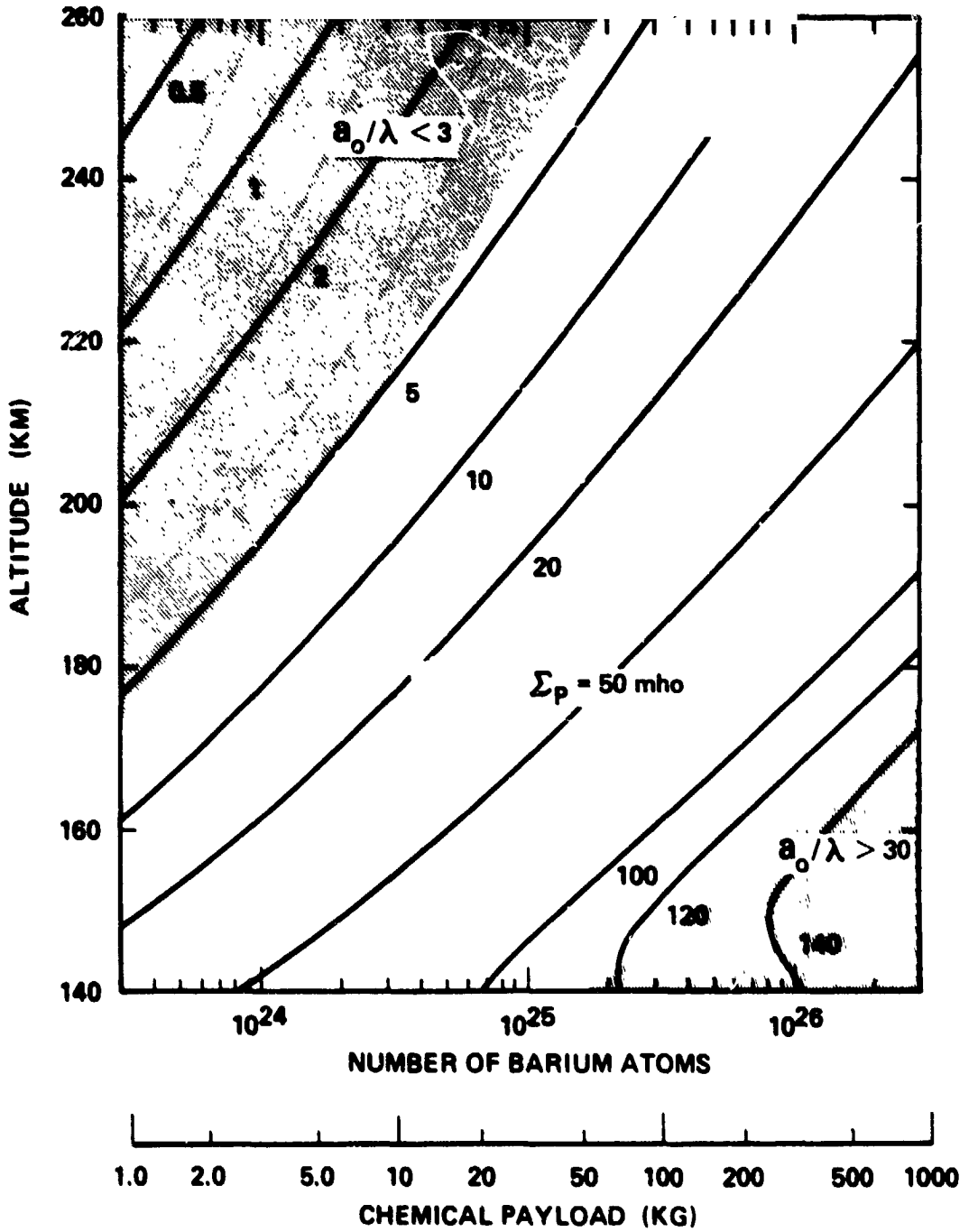

FIG. 22. Contours of constant field-line-integrated Pedersen conductivity in the altitude versus chemical payload weight plane for point barium releases from rockets.

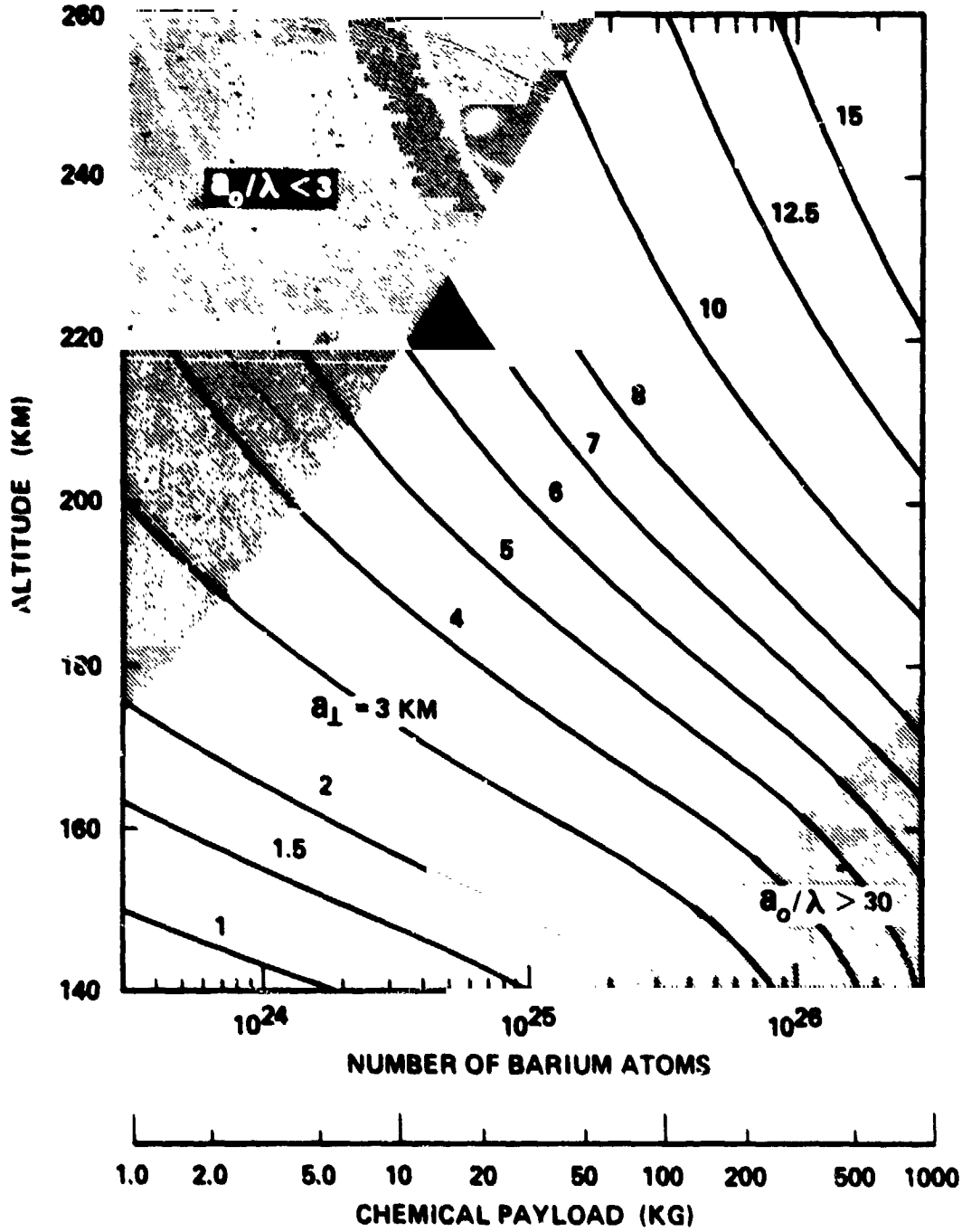

FIG. 23. Contours of constant transverse scale size of the conductivity modification in the altitude versus chemical payload weight plane for point barium releases at orbital velocity.

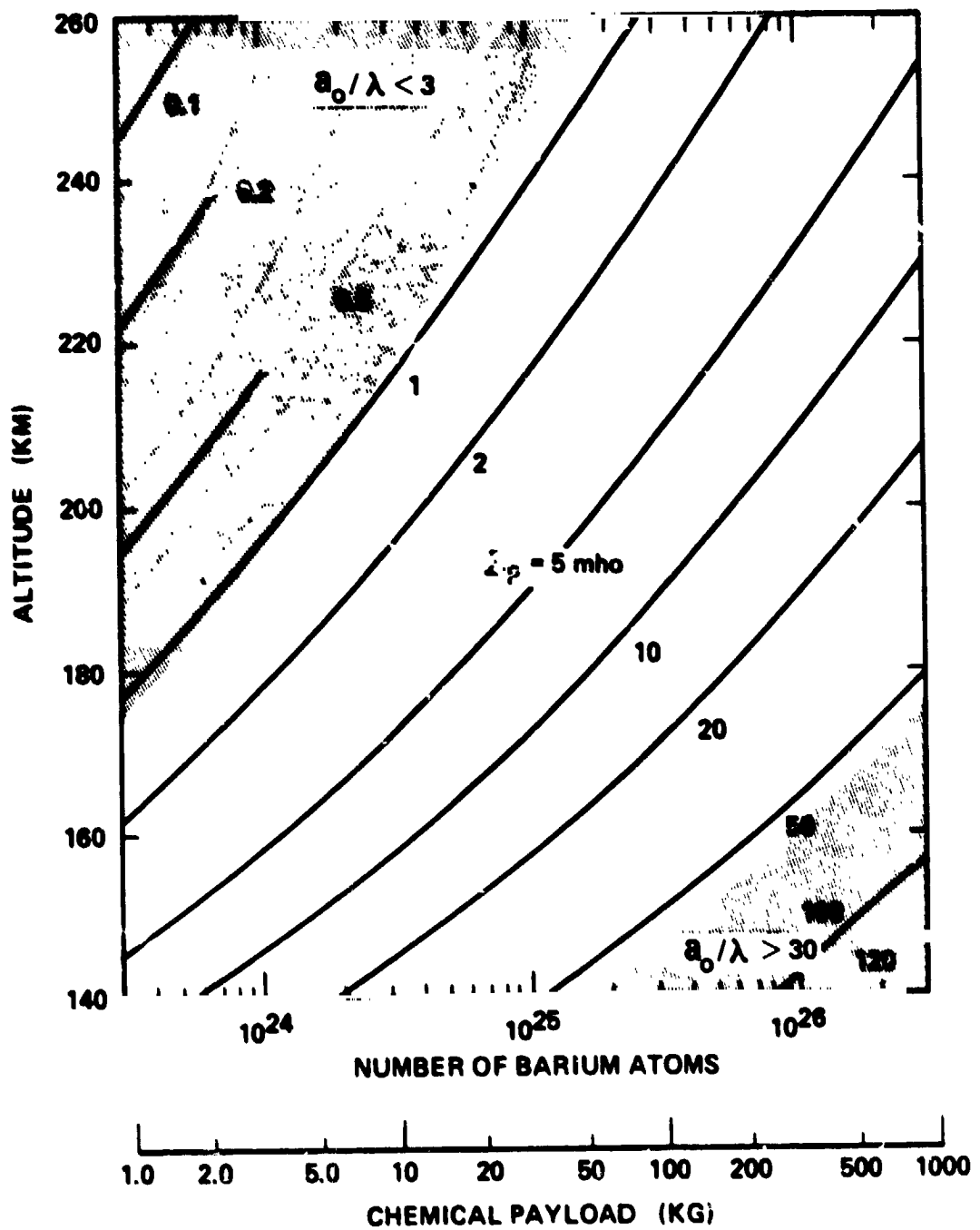

FIG. 24. Contours of constant field-line-integrated Pedersen conductivity in the altitude versus chemical payload weight plane for point barium releases at orbital velocity.

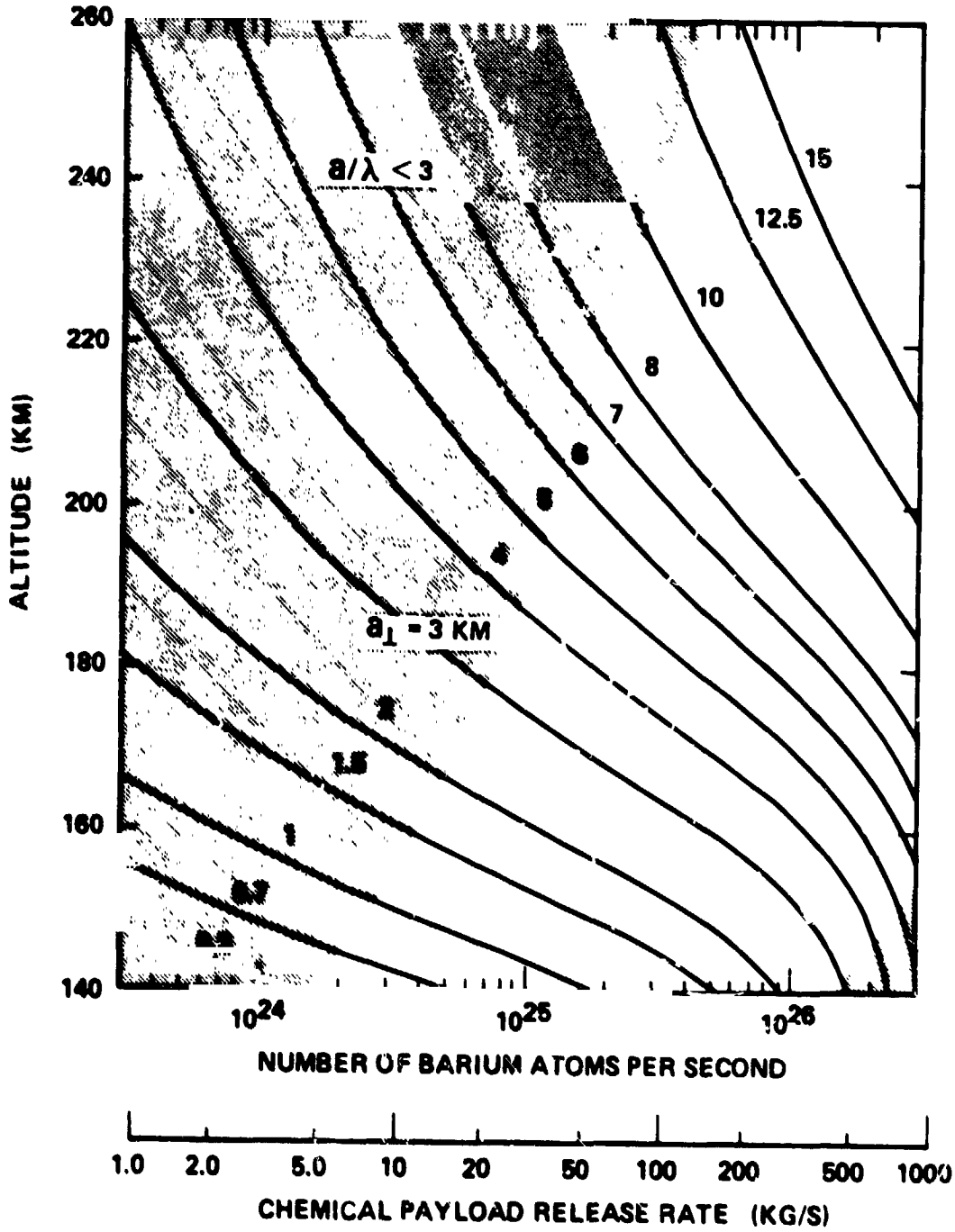

FIG. 25. Contours of constant transverse scale size of the conductivity modification in the altitude versus chemical payload release-rate plane for venting mode releases at orbital velocity.

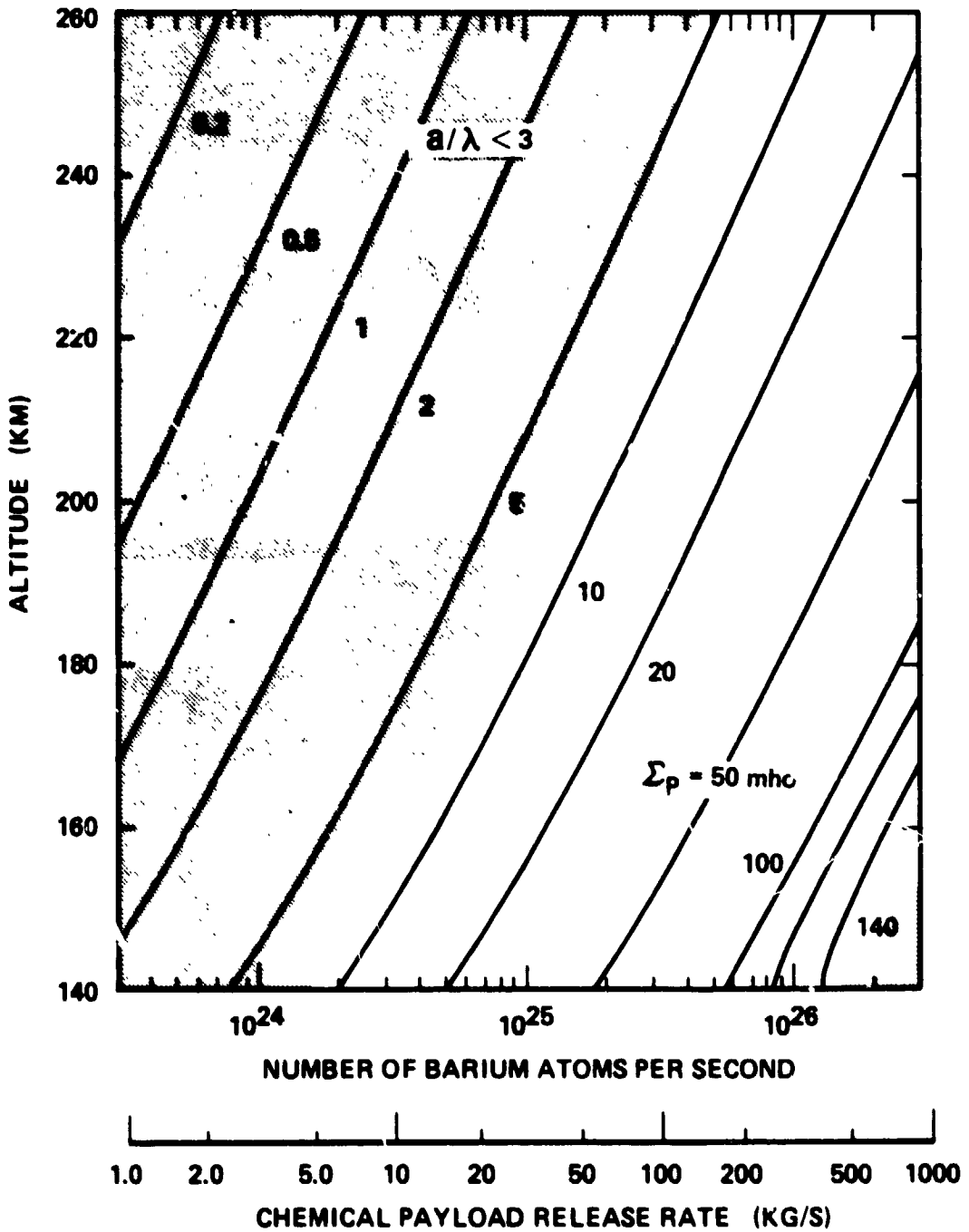

FIG. 26. Contours of constant field-line-integrated Pedersen conductivity in the altitude versus chemical payload release-rate plane for venting mode releases at orbital velocity.